Development of computer-vision system based on smartphone image and artificial neural network for postharvest management of agricultural products

(農産物の収穫後の管理のための
スマートフォンのイメージとニューラルネットワークを
基盤としたコンピュータービジョンシステムの開発

Hokkaido University
Graduate School of Agriculture

Division of Bio-systems Sustainability
Doctor Course

Byeong-Hyo Cho

Acknowledgements

I am grateful to so many people who guided and supported me during the completion of this research. Especially, I deeply thank Professor Shigenobu Koseki, my advisor, for his superior guidance and trust throughout the period of my doctor's course. I also thank Professor Chung-Su Han and Professor Hyun-Kwon Noh, my former advisors, who always led me with encouragement and advice. I would also like to thank the members of my dissertation committee, Professor Kazunori Iwawbuchi, Dr. Hiroshi Okamoto, and Dr. Kento Koyama for providing constructive comments and suggestions. And thanks to Dr. Jung-Hyun Lee for his encouragement and advice.

Thanks to all members of the agricultural and food process engineering laboratory. I would also like to thank my friends who live in Korea.

Finally, I deeply thank encouragement, support, and devotion of my family and dedicate this research to my family.

Table of Contents

List of Tables

List of Figures

Chapter 1 Introduction

1.1. Quality management after harvest

Postharvest technology refers to the handling, sorting, storage, transportation, marketing, and management of biological products from harvest until final consumption (Studman, 2001). The quality management of agricultural commodities is the most important type of management for modern food industries, because high product quality is the basis for success in today's highly competitive market (Du and Sun, 2006). However, most biological products (e.g., cereals, fruits, vegetables, and nuts) are living organisms that continue to respire after harvest. Their degeneration causes quality changes and losses over time. In particular, temperature and humidity are the most important environmental factors affecting changes in their physical and chemical properties. Although low-temperature (i.e., chilled) conditions generally inhibit microbial growth and suppress metabolic changes to maintain fruit quality (Wang and Wang, 2009), such conditions may also lead to chilling injuries, including peel-browning and ripening problems (Oliveira et al., 2016). High temperatures cause produce to ripen or spoil more quickly. Furthermore, relative humidity (RH) is inversely related to the water loss of agricultural products and can affect the occurrence of physiological disorders and nonuniformities in ripening (Ahmad et al., 2006). For this reason, improved quality postharvest management technology is required.

Ripening and overall quality of agricultural products are evaluated via the application of destructive and nondestructive methods. However, destructive methods are time consuming and expensive, and the results are tied to the specific produce evaluated (Magwaza and Tesfay, 2015). Therefore, many studies have focused on the development and application of various non-destructive techniques to evaluate ripening and quality on a

real-time basis (Zude-Sasse et al., 2016).

There have been several attempts to predict quality using environmental data, such as temperature and RH (Li and Zhang, 2010; Xie et al., 2017). Li and Zhang (2010) developed a real-time tracking system using environmental data for the loss of agricultural products during transportation. However, their methods required sensors to measure environmental data and dedicated devices to store them. Additionally, there remained the possibility that someone could tamper with or destroy the data during collection (Xie et al., 2017). Furthermore, there have been attempts to predict the remaining shelf life of agricultural products using time–temperature indicators (TTI), which record the thermal history of the produce based on the irreversible color changes caused by the cumulative effects of time and temperature (Wang et al., 2015). However, there are several problems related to TTIs, such as the migration of toxic substances, the inaccuracy of temperature monitoring, and the high costs of commercial application (Lee, 2018). Therefore, a postharvest management system is urgently needed to safely and quantitatively predict the ripening stages and quality of agricultural products after harvest.

1.2. Computer-vision system (CVS)

A CVS acquires and analyzes a visual image of a real scene to obtain information or to apply control processes. Computer vision has experienced rapid growth both in theory and application since the 1970s (Brosnan and Sun, 2002). CVSs have proven to be highly flexible, accurate, repeatable, and cost-efficient, and these advantages have encouraged manufacturers to apply a variety of CVS methods (Sylla, 2002). Moreover, over the past few decades, CVSs have increasingly been used in agricultural and food industries, corresponding to the rapid development of information science, image processing, pattern

recognition, and their respective computer hardware and software advancements (Kılıç et al., 2007; Zhang et al., 2014). CVSs based on camera–computer interaction have often been used as scientific inspection tools for safety and quality of a variety of agricultural products and have provided objective and nondestructive quality evaluations thereof (Du and Sun, 2006; Kılıç et al., 2007).

Girolami et al. (2013) compared a CVS's results with that of a colorimeter to assess the color of beef, pork, and chicken, reporting that the CVS method seemed to provide valid measurements that reproduced colors very similar to the real ones. Sun et al. (2009) utilized a CVS to determine and analyze the color parameters of lean beef using several color classes to investigate the relationship between the features and color scores of beef. The lean color features were significantly different from the color scores of beef ($p < 0.001$), and there were high correlations between the total of red, green, blue (RGB), hue, saturation, intensity, L^* value (i.e., lightness or brightness), a^* value (i.e., redness or greenness), and b^* value (i.e., yellowness or blueness) color features and scores. Zhang et al. (2014) proposed a fruit-classification system that used both computer vision and feedforward neural networks to recognize 18 types of fruits, reporting that the system classified 1,653 color fruit images into 18 categories with a classification accuracy of 89.1%. Arakeri and Lakshmana (2016) proposed an automatic and effective tomato-grading system based on computer vision, and the proposed method showed a 96.47% accuracy in evaluation quality.

Most external quality attributes (e.g., color, texture, size, shape, and defect) can be inspected and graded using CVSs. However, owing to the lack of spectral and multi-constituent information in digital images, some external quality characteristics (e.g., rottenness, bruising, and other problems) remain extremely difficult to detect when using only a CVS. Meanwhile, hyperspectral and multispectral images are sometimes used to

detect inconspicuous external quality characteristics. The greatest advantage of hyperspectral images is the extensive information provided by the hundreds of thousands of monochromatic images in the spectral domain. However, this extensive information comes with some drawbacks, such as the time consumption of image acquisition and the computing complexity of image processing and analysis. Multispectral images involve two or more waveband monochromatic images from the visible spectrum. The greatest advantage of a multispectral image is that the wavelengths of a monochromatic image can be chosen freely using narrowband filters. However, a disadvantage is that the experimental system must be built according to the specific task (Zhang et al., 2014). Therefore, in this study, the CVS advantages (e.g., simple image processing, fast analysis, low cost, and ease of use) are leveraged to predict the ripening stage and quality of agricultural products.

In recent years, smartphones with their high-quality cameras have increasingly become available. Hence, high-quality images of agricultural products can be easily obtained using those systems (Li et al., 2020). The use of smartphones for their camera capabilities has become very important to CVS imaging (Song et al., 2020). Cruz-Fernández et al. (2017) developed a method to determine fat content in cold meat products using smartphone image processing, reporting that the method could determine the fat content with an error of less than 20%. They suggested that further experiments should compare their results with those of fixed cameras and scanning devices. Cubero et al. (2018) developed a portable smartphone CVS that allowed the color indices of citrus fruits to be measured automatically. The color index was compared with estimates from an expert panel, and R^2 values of 0.881 and 0.854 were obtained for indoor and outdoor conditions, respectively. The results demonstrated the feasibility of a smartphone-integrated CVS for inspecting the colors of citrus fruits in real time under outdoor

conditions.

CVSs have often been used to acquire agricultural images, and there have been many successful cases. Therefore, with this research, I investigate the utility of the smartphone as a CVS camera device for the nondestructive analysis of agriculture products.

1.3. Artificial neural networks (ANN)

Machine learning (ML) has emerged alongside high-performance computing and big-data technologies to create new opportunities for unraveling, quantifying, and understanding data-intensive processes. Typically, ML involves a learning process having the objective to learn from training data to make predictions or decisions (Liakos et al., 2018). There are various ML models (e.g., decision trees, support vector machines (SVM), and ANNs) that require training data methods (e.g., regression, Bayesian models, and instance-based). ANNs reflect a relatively new area of ML research that uses computational modeling tools to understand complex real-world problems (Basheer and Hajmeer, 2000; Alden et al., 2019). In particular, ANNs allow arbitrary non-linear relationships between independent and dependent variables and all possible interactions among them. Other ML techniques require additional modeling to allow this flexibility (Sargent, 2001). However, ANNs have distinct disadvantages, such as hardware dependence, unexplained network functionality, the need of a proper network structure, and more. Moreover, unexplained network functionality is the most important. When an ANN provides a curious solution, it is difficult to interpret and understand the produced weights, owing to the black-box nature of neural networks. As such, inappropriate solutions can reduce the trustworthiness of an ANN. Nevertheless, they have various advantages, such as organic learning, non-linear data processing, and fault tolerance.

Furthermore, they have been successfully applied in agriculture-related fields (Liakos et al., 2018). Thus, an ANN was applied to data training in this study.

ANNs are special types of ML algorithms inspired by the biological neurons of the human brain (Tran, 2020). They use artificial neurons as central processing units to perform mathematical operations to generate an output from a set of inputs via regression or classification. As shown in Fig. 1-1, a directed network diagram describes the relationship between input data (*X* variables) and output data (*Y* variable). Weights (*w* values) and biases are randomized prior to learning. As training proceeds, both parameters are adjusted toward the desired values and the correct output. Then, input data are summed and passed via an activation function.

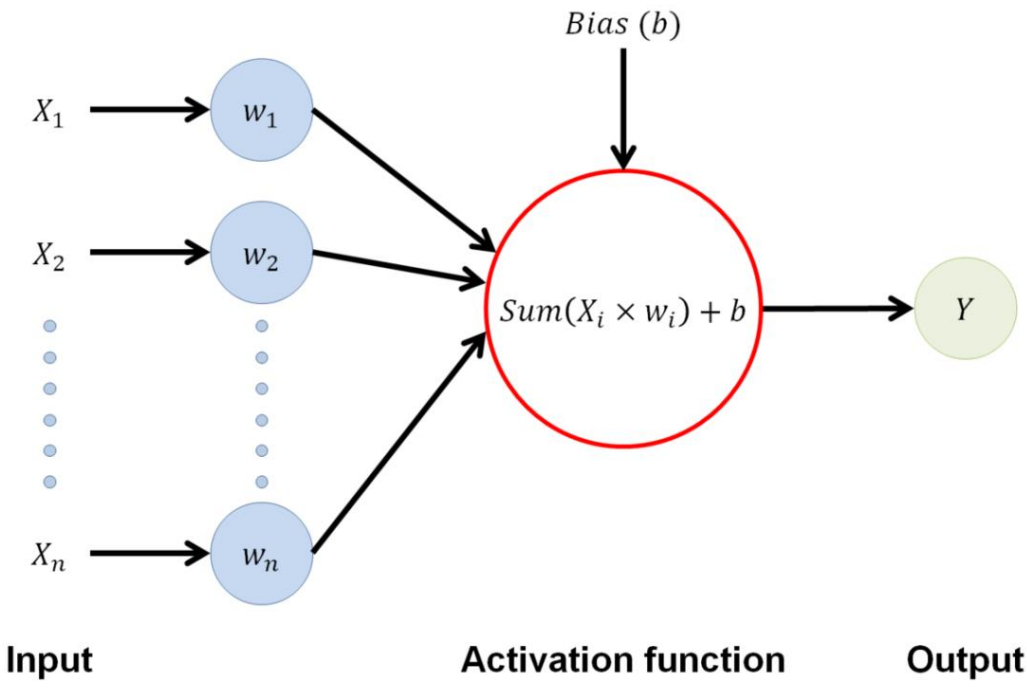

Fig. 1-1. Structure of neuron.

ANNs comprise a set of neurons having internal connections with an input layer, hidden layers, and an output layer (Fig. 1-2). The input layer is the first layer of the ANN

that receives the input data. In the hidden layers, the weight is adjusted so that the network attempts produce the desired output data. If a satisfactory level is reached, training stops, and the ANN uses the weights to make further decisions, identify new patterns, or define fresh associations. The results are then obtained and output via the output layer (Satish and Setty, 2005; Mohebbi et al., 2010; Menlik et al., 2010; Tran et al., 2020).

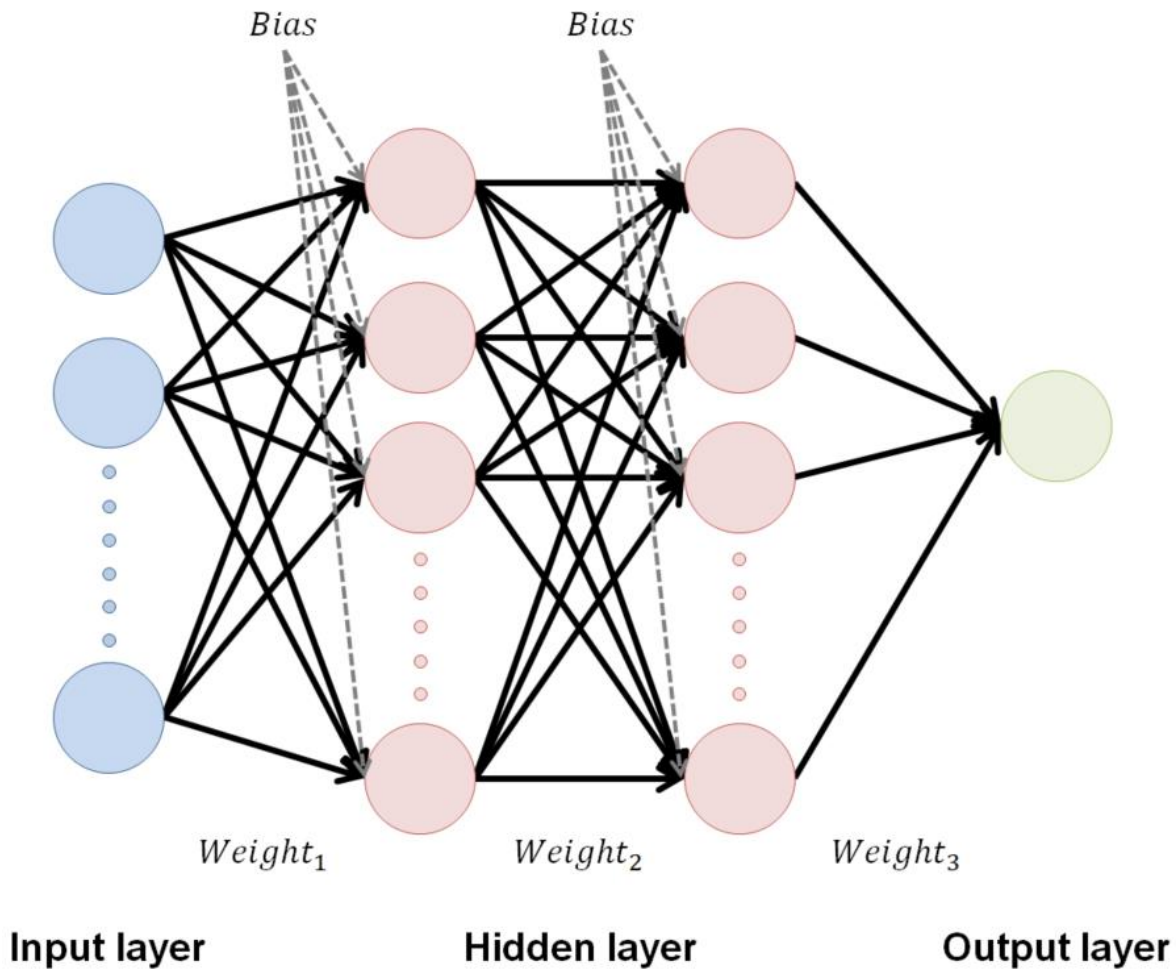

Fig. 1-2. Artificial neural network architecture.

The ANN is a very popular tool that is used to accomplish a variety of classification and prediction tasks in the broadly defined field of agriculture. Sant'Anna et al. (2015) compared the performance of an ANN with Fisher's classical multivariate statistical

technique and Anderson's discriminant function to assess the genetic diversity classification of 10 plant populations, reporting that ANNs were better than the classical methods, because fewer wrongly classified individuals were output. Azizi et al. (2016) applied linear discriminant analysis and nonlinear ANN methods to identify and discriminate 10 potato cultivars using morphological data obtained from image processing, reporting that the correctness of the ANN classification was 100%. Additionally, it was found that ANNs can be applied to predict yield component analyses of agriculture products. ANNs are more accurate and robust than multiple linear regressions (MLR) for the prediction of seed yields and essential oil contents of the ajowan caraway plant (Niazian et al., 2018a; Niazian et al., 2018b). Sharma et al. (2007) compared the performance of an ANN with conventional MLRs to predict the first-lactation 305-day milk yield for Karan Fries dairy cattle, reporting that the ANN attained more than 92% prediction accuracy, which is relatively higher than that of conventional MLRs.

ANNs can also be used to classify the ripening stages of fresh fruits and vegetables or to predict their quality indices. Sidehabi et al. (2018) used both K-means clustering and ANNs to classify the ripeness levels (i.e., ripe, nearly ripe, or unripe) of passion fruits, reporting an accuracy of 90%. Yossy et al. (2017) developed a mango-fruit sorting system using both neural networks and CVSs and detected ripe or unripe mangos with 94% accuracy. Lan et al. (2020) predicted the soluble solid content (SSC) of Korla fragrant pears based on electrical properties and ANNs, showing that the ANN could predict the SSC with a coefficient of determination (R^2) of 0.97 and a root mean-square error (RMSE) of 0.26.

Accordingly, ANNs have been applied to various fields of agriculture, and there have been many successful cases. Therefore, the ANN is used as the computational modeling tool for this study to predict the quality indices of fresh fruits and vegetables.

1.4. Research objectives

I aim to develop a smartphone-based CVS to predict the ripening stages and quality indices of agricultural products. The specific objectives of this study include the following.

First, I investigate the utility of the smartphone as a CVS camera device by comparing the color features obtained using the smartphone and a colorimeter, and I develop a CVS for the nondestructive analysis of agriculture products. The study focuses on image processing and data modeling.

Second, I use the Hass avocado and the Cavendish banana to investigate the changes of physical and chemical properties during ripening under various temperatures and RH combinations to understand the effects of these environmental factors on quality. The study focuses on data collection via digital images and quality indices for model development to predict the ripening stages and quality indices of the fruit under various storage conditions.

Third, I apply the developed smartphone CVS to predict the ripening stages and/or quality indices of the fruits during their ripening processes at different conditions. The study focuses on the suitability of using the developed smartphone CVS for predicting the ripening stages and/or quality indices of the fruit during ripening under various conditions.

Chapter 2 CVS development

2.1. Introduction

The application of computer vision in agriculture has increased considerably over the past few decades. CVS-based pattern recognition and image processing are mature techniques used for safety and quality analysis in several agricultural applications, including crop monitoring, precision agriculture, robotics, nondestructive inspection of product properties, and quality control and classification along processing lines (Cubero et al., 2010; Bhargava and Bansal, 2018). There have been many efforts to build fruit classification and internal quality prediction systems using computer vision. If workers apply internal quality factors and do not destroy the fruit during measurement, the methods are *nondestructive* (Ohali, 2011).

However, owing to the lack of spectral and multi-constituent information in CVSs, prediction of internal quality remains extremely difficult via CVSs alone. Thus, some spectroscopic techniques (e.g., hyperspectral and multispectral imaging) are utilized to nondestructively predict the internal quality indices of agricultural products, because they provide better predicting power than simply reviewing digital images (Polder et al., 2000). Recently, advances in hardware, software, image technologies, and pattern recognition have led to many CVS-related food-industry studies.

Yahaya et al. (2014) measured fruit quality using an optical fiber sensor connected to RGB light-emitting diodes (LED) and reported that it was possible to classify the ripening stages of mangoes into six levels with a coefficient of determination (R^2) of 0.879. Sanaeifar et al. (2016) used both digital images and support vector regression to predict the quality indices of bananas during their ripening process, including firmness, total soluble solids (TSS), pH, and titratable acidity (TA). Predictions were made with R^2>0.99. Pereira

et al. (2018) predicted the ripening of the papaya fruit using digital imaging and random-forest techniques, reporting that it was possible to classify ripening into three levels with an accuracy of 94.3%. As mentioned, SVCs are now used to predict ripening stages and quality indices. Therefore, I have chosen to do the same for the agricultural products in this study. Recently, smartphones have actively been used for the nondestructive analysis of fruits, owing to their ease of use, portability, and variable functionality. Intaravanne et al. (2012) proposed a 2D spectral-analysis concept based on smartphone imagery for banana-ripeness estimation. Yahaya et al. (2015) used RGB images captured by a smartphone camera to determine Sala mango qualities. Nasiri et al. (2019) used both smartphone images and convolutional neural networks to classify defective dates (*Phoenix dactylifera* L.) from healthy ones and to predict their ripening stages.

However, only a few studies have used smartphone-based CVSs to quantitatively predict quality indices and ripening. Therefore, I aim to investigate the utility of the smartphone as a CVS device by comparing the color features obtained using the smartphone to those of a colorimeter and to develop a smartphone CVS for the nondestructive analysis of agriculture products.

2.2. Materials and methods

2.2.1. CVS

Figure 2-1 shows the CVS developed for this study. It consists of four main components: an imaging and lighting system; an illumination chamber; a copy stand; and a computer.

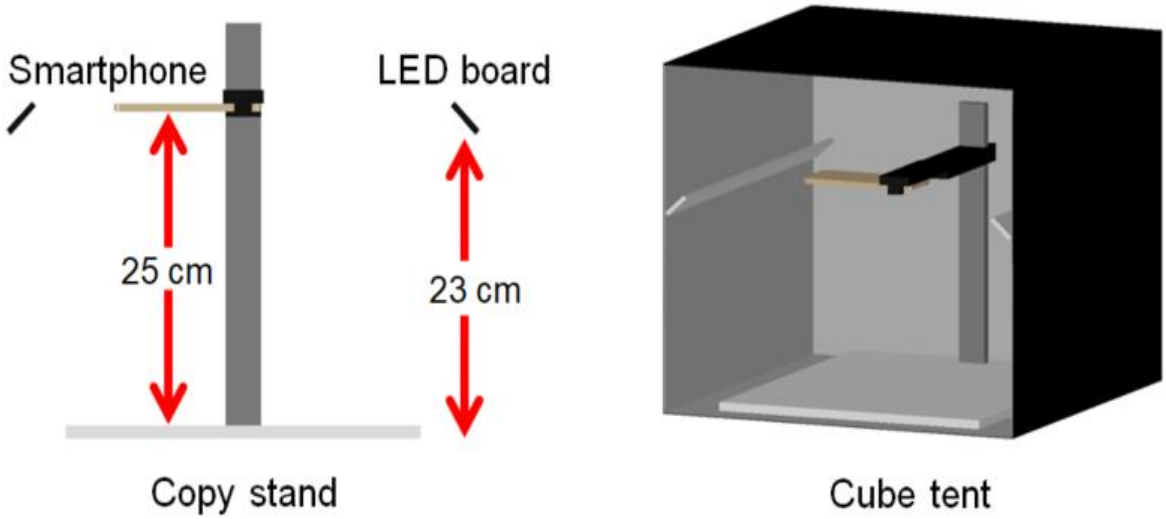

Fig. 2-1. The schematic diagram of a computer vision system (CVS).

An iPhone5s smartphone (Apple, Cupertino, USA) was used in this study. The specifications are summarized in Table 2-1. The spatial resolution was 3,264×2,448 pixels with a lens aperture of f/2.2. The camera's autofocus system was used to obtain an optimized image. The camera was fixed at a vertical distance of 25 cm above the bottom of the copy stand.

A nylon cube tent (F40, SAMTIAN, Shenzhen, China) was used as the illumination chamber. An LED board (110 V/30 W) having a color reproduction index of up to 95% and a color temperature of 5,500±200 K was used as the light source. Two LED boards were placed on the left and right sides of the chamber and were fixed at a vertical distance of 23

cm above the bottom of the copy stand. LED boards illuminated the given object at an angle of 45° with respect to the vertical, which is most effective when illuminating plane objects (Saldaña et al., 2013).

Table 2-1. Smartphone camera specifications.

Variable	Specification
Image size	3,264 × 2,448 pixels
Zoom	No zoom
Flash mode	No flash
Sensitivity	Auto
White balance	Auto
Operation mode	Auto
Aperture	f/2.2
Exposure time	Auto
Image type	JPEG
Focal length	4 mm
Resolution	72 dpi

2.2.2. Colorimeter

A colorimeter (CR-400, KONICA MINOLTA, Tokyo, Japan) was used to verify the CVS and was calibrated using a standard white plate (Y = 85.4, x = 0.3173, and y = 0.3240). The colorimeter provided three color values: L^*, a^*, and b^*. The color values ranged from 0 to 100 (L^*) and from -127 to 127 (a^* and b^*). The aperture diameter of the colorimeter was 8 mm.

2.2.3. Color paint

Four paints having colors of black, gray, silver-gray, and white were used to verify the

CVS. The reflectance of each color is listed in Table 2-2.

Each paint color was captured 10 times every 30 min in the CVS, and the LED boards were turned 1 h before image capturing to achieve a stable lightning (Dowlati et al., 2013). RGB reflectances were extracted from the obtained images using the CVS and were used to verify light-source stability. The *L*a*b** values of each paint color were determined using both the CVS and the colorimeter. These values were used to verify the usability of the smartphone CVS.

Table 2-2. Specifications of the color paints.

	Paint 1	Paint 2	Paint 3	Paint 4
Paint color	Black	Gray	Silver-gray	White
				
Reflectance value (by measurement)	20%	46%	60%	86%

2.2.4. Color changes

Total color difference (ΔE) was determined by the Eq. 2-1:

$$\Delta \boldsymbol{E} = \sqrt{(\boldsymbol{L}_{\boldsymbol{C}}^{*} - \boldsymbol{L}^{*})^{\boldsymbol{2}} + (\boldsymbol{a}_{\boldsymbol{C}}^{*} - \boldsymbol{a}^{*})^{\boldsymbol{2}} + (\boldsymbol{b}_{\boldsymbol{C}}^{*} - \boldsymbol{b}^{*})^{\boldsymbol{2}}}, \qquad \text{(Eq. 2-1)}$$

where $\boldsymbol{L}_{\boldsymbol{C}}^{*}$, $\boldsymbol{a}_{\boldsymbol{C}}^{*}$, and $\boldsymbol{b}_{\boldsymbol{C}}^{*}$ values were obtained using the CVS, and values of $\boldsymbol{L}^{*}$, $\boldsymbol{a}^{*}$, and $\boldsymbol{b}^{*}$ were obtained using the colorimeter.

Hue angle and chroma (C*) were calculated using Eqs. 2-2 and 2-3, respectively (Fernández-Vázquez et al., 2013; Girolami et al., 2013).

$$\boldsymbol{Hue\ angle = tan^{-1}(b^*/a^*)}, \quad \text{(Eq. 2-2)}$$

$$\boldsymbol{C^* = \sqrt{a^2 + b^2}}, \quad \text{(Eq. 2-3)}$$

The differences in chroma (ΔC) and lightness (ΔL) were calculated using Eqs. 2-4 and 2-5.

$$\boldsymbol{\Delta C = C_C^* - C^*}, \quad \text{(Eq. 2-4)}$$

$$\boldsymbol{\Delta L = L_C^* - L^*}, \quad \text{(Eq. 2-5)}$$

where $\boldsymbol{C_C^*}$ and $\boldsymbol{L_C^*}$ are chroma and lightness values, respectively, obtained using the CVS, and $\boldsymbol{C^*}$ and $\boldsymbol{L^*}$ are those obtained using the colorimeter.

Hue difference (ΔH) was calculated using Eq. 2-6 (Yakushev and Kanash, 2016).

$$\boldsymbol{\Delta H = \sqrt{\Delta E^2 - \Delta L^2 + \Delta C^2}}, \quad \text{(Eq. 2-6)}$$

2.2.5. Statistical analysis

The correlation coefficients between the color values obtained using the CVS and the colorimeter were evaluated using the Pearson correlation. IBM's SPSS statistical package (v.20.0, IBM, Armonk, USA) was used for statistical analysis in this study.

RMSE was chosen to assess the differences among color values (i.e., *L**, *a**, *b**, chroma, and hue angle) obtained using the CVS and the colorimeter. This was calculated using Eq. 2.7:

$$\boldsymbol{RMSE = \sqrt{\frac{1}{n}\sum_{i=1}^{n}(Color_c - Color_{cvs})^2}}, \quad \text{(Eq. 2-7)}$$

where $\boldsymbol{Color_c}$ and $\boldsymbol{Color_{cvs}}$ are color values obtained using both devices.

2.3. Results and discussion

2.3.1. Light-source test

A good lightning system will provide uniform radiation across the scene while avoiding shines or shadows. The light must be spectrally uniform and stable over time. Otherwise, image uncertainty will increase (Saldaña et al., 2013).

Figures 2-2, 2-3, and 2-4 show the reflectances for red, green, and blue channels, respectively. As seen, the reflectance of each channel does not show a large difference based on image acquisition. This result indicates that the LED board was a reliable lighting source for my CVS.

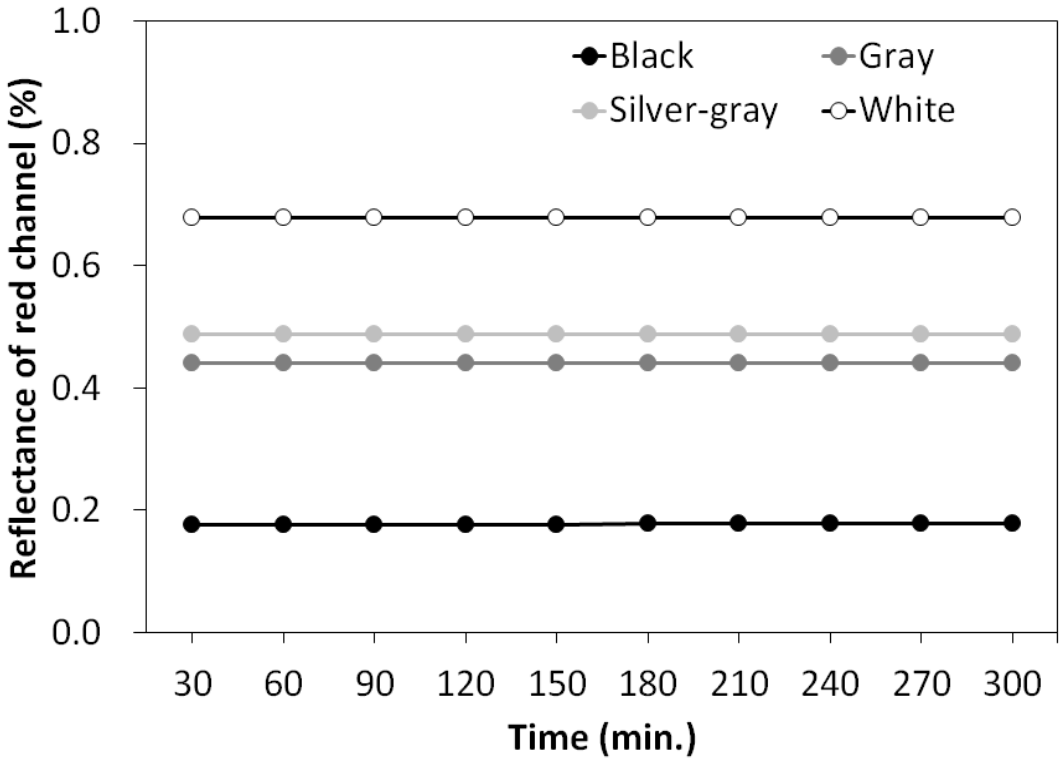

Fig. 2-2. The reflectance of each paint in red channel during image acquisition.

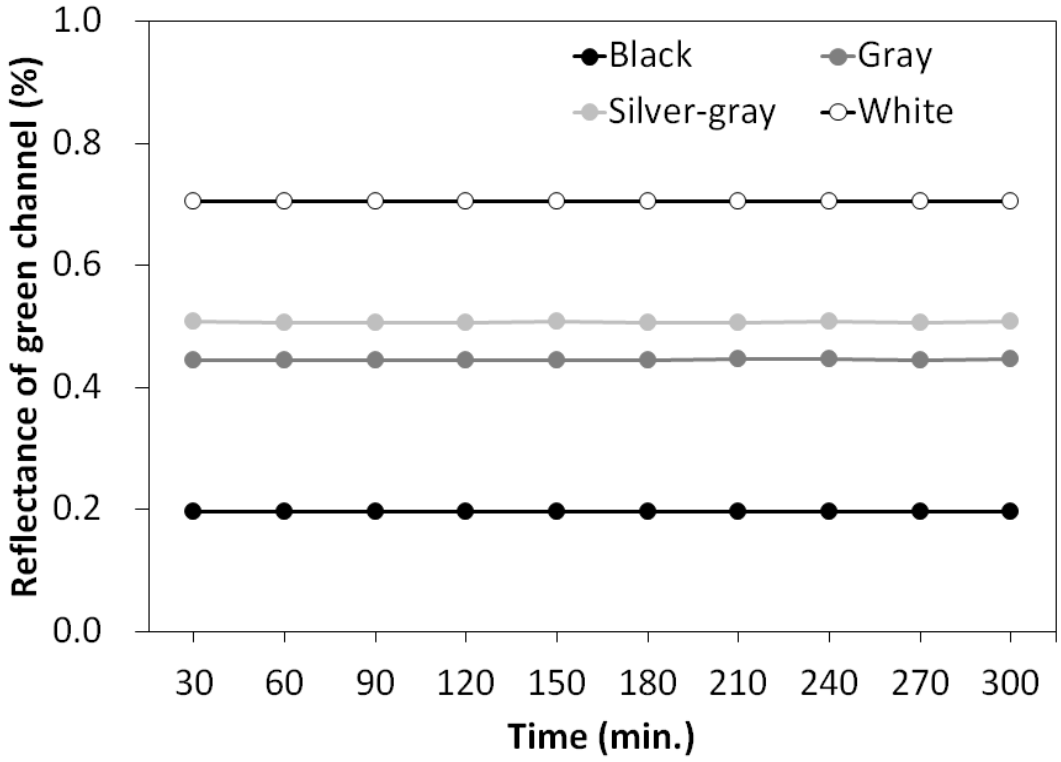

Fig. 2-3. The reflectance of each paint in green channel during image acquisition.

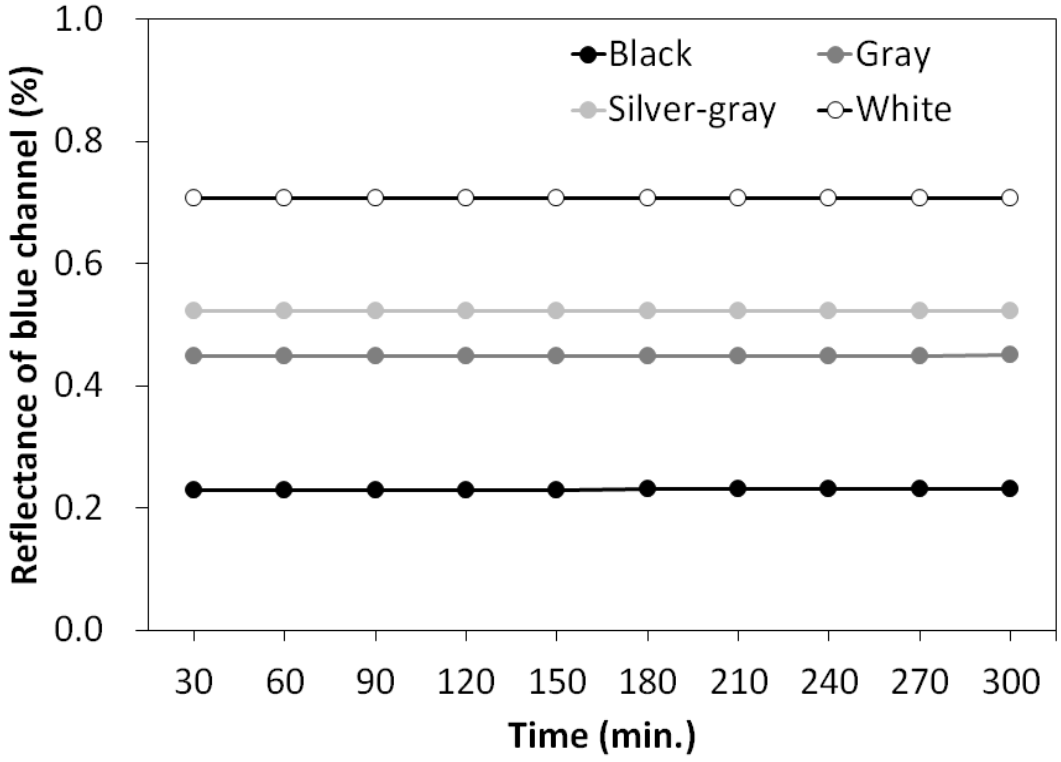

Fig. 2-4. The reflectance of each paint in blue channel during image acquisition.

2.3.2. Comparison of color values determined by CVS and colorimeter

When black and gray paints were evaluated, the *b** and chroma values obtained using the CVS and the colorimeter were significantly different. However, the *L**, *a**, and hue-angle values did not show significant differences. When silver-gray paint was evaluated, the *a**, chroma, and hue-angle values obtained using the CVS and the colorimeter did not show significant differences. However, the *L** and *b** values differed by 6.21 and 5.55, respectively. In the case of white paint, all color values, except for *L**, did not show significant differences.

The color differences between the two methods are best represented by the total color difference value (ΔE). The ΔE values were 6.85, 4.73, 8.33, and 13.76 for black, gray, silver-gray, and white, respectively. ΔE values in the range of 2–10 indicate that the difference in color can be detected at a glance. If it is greater than 10, the colors are considered to be more opposite than similar (Tomasevic et al., 2019). These findings are similar to those of previous studies (Goñi and Salvadori, 2017; Tomasevic et al., 2019). The ΔL values were 0.62, 2.18, -6.21, and -13.43 for black, gray, silver-gray, and white paints, respectively. Positive ΔL values indicate that the color obtained using the CVS was lighter than the color obtained using the colorimeter (Tomasevic et al., 2019). The positive difference in chroma (ΔC) means that the CVS color had greater intensity or was more saturated than the color obtained using the colorimeter.

As revealed, there were difference between the color values obtained using the CVS and the colorimeter. These results were caused by differences in measurement-area size: an aperture diameter of 8 mm for the colorimeter and 40×40 pixels for the CVS. Nevertheless, because the RMSE of most color values exhibited relatively small variety in the range of 0.06–2.62, the smartphone camera could, therefore, be used as my CVS imaging system.

Table 2-3. Comparison of color values (mean ± SD, n = 10) between obtained at several paints using CVS and colorimeter.

Parameter	CVS	Colorimeter	Significance *p*	RMSE	CVS	Colorimeter	Significance *p*	RMSE
	Black				Gray			
*L**	20.69±0.03	20.07±0.02	**	0.62	47.81±0.03	45.63±0.31	**	2.20
*a**	0.22±0.10	-0.05±0.03	*	0.28	-0.29±0.01	0.45±0.02	*	0.74
*b**	-6.18±0.04	0.63±0.02	**	6.82	-0.74±0.02	3.39±0.02	**	4.13
Chroma	6.19±0.04	0.63±0.03	**	5.56	0.80±0.02	3.42±0.02	**	2.62
Hue angle	-1.54±0.02	-1.50±0.04	**	0.05	1.19±0.02	1.44±0.01	**	0.25
ΔE	6.85±0.05				4.73±0.14			
ΔL	0.62±0.04				2.18±0.30			
ΔC	5.55±0.04				-2.62±0.04			
ΔH	8.80±0.06				4.94±0.02			
	Silver-gray				White			
*L**	53.80±0.01	60.02±0.23	**	6.22	72.73±0.02	86.15±0.19	**	13.43
*a**	-1.09±0.03	-1.19±0.01	*	0.12	-2.20±0.02	-0.24±0.02	*	1.96
*b**	-2.77±0.01	2.78±0.03	**	5.55	-1.11±0.02	1.16±0.02	**	2.27
Chroma	2.97±0.01	3.02±0.03	**	0.06	2.46±0.02	1.19±0.03	**	1.28
Hue angle	1.20±0.01	-1.17±0.01	**	2.36	0.47±0.01	-1.36±0.01	**	1.83
ΔE	8.33±0.19				13.76±0.19			
ΔL	-6.21±0.23				-13.43±0.19			
ΔC	-0.05±0.04				1.28±0.03			
ΔH	5.55±0.04				3.26±0.02			

CVS: computer vision system, RMSE: root mean square error, *: $p < 0.05$, **: $p < 0.01$.

2.4. Conclusion

To develop the CVS for this study, lighting and imaging systems were investigated with respect to four different paint colors: black, gray, silver-gray, and white. The RGB reflectances did not show large differences during image acquisition, regardless of paint color. This means that the LED board used in this study can be used as the lighting source for the CVS. Several color variables (i.e., L^*, a^*, b^*, chroma, hue angle, ΔE, ΔL, ΔC, and ΔH) obtained using the CVS and the colorimeter were compared, and because the small RMSE of most color values ranged from 0.06–2.62, I assessed that the smartphone camera could be used as the imaging system for my CVS. Therefore, the CVS developed in this study can be applied for the nondestructive analysis of fruits and vegetables.

Chapter 3 Development of a prediction model for Hass avocado quality indices and ripening stages using ANN

3.1. Introduction

The avocado (*Persea americana* Mill.), botanically classified as a one-seeded berry, has been cultivated for 4,000–6,500 years and one of the most economically important fruit in subtropical and tropical horticulture (Galindo-Tovar et al., 2008; Quiñones-Islas et al., 2013). The avocado has gained popularity because of its good flavor and high dietary value. In particular, as its health benefits (e.g., anti-vascular disease and reduced diabetes) have become known, global avocado production reached 6.4 million tons in 2018 (Ding et al., 2007; Ding et al., 2009; FAO STAT, 2020).

However, the avocado is a climacteric fruit, and it continues to ripen after harvesting while undergoing physiological changes (Maftoonazad and Ramaswamy, 2005; Pinto et al., 2019). As with many other fruits, storage temperatures affect ripening and subsequent quality (Arpaia et al., 2019). Hopkirk et al. (1994) reported that avocados do not properly ripen at 30℃ and that ripening at 25℃ negatively affected quality by enhancing the abundance of storage disorders, compared with 15 and 20℃ temperatures (Hopkirk et al., 1994). Arpaia et al. (2019) investigated the impact on avocado quality of short-term exposures to elevated temperatures that can sometimes occur following harvesting and prior to ripening. They reported that avocados that ripened at temperatures above 20℃ had an increased incidence of pink pulp discoloration. Consequently, a postharvest management methodology is required to determine avocado quality during storage and ripening in order to prevent fruit loss caused by quality deterioration.

In avocados, firmness, oil content, dry matter (DM), and moisture of the fresh pulp are the key variables used to reliably test ripeness (Lewis, 1978; Wedding et al., 2013;

Blakey, 2016). In particular, pulp firmness is one of the main indices of maturity (Mizrach, 2000). The peel colors of Hass and Gem avocados change from green to purple/black during ripening (Cox et al., 2004). Hence, these changes are indicators of ripeness. Arzate-Vázquez et al. (2011) applied image processing to classify Hass avocados and reported that the color and texture features evaluated from the digital images showed an adequate correlation with pulp firmness. Jaramillo-Acevede et al. (2020) developed a ripeness classification model for Hass avocados based on digital image processing (DIP) and ANNs, reporting that the model showed 88% accuracy in the classification of the analyzed dataset. Nevertheless, only a few studies have determined the ripeness of Hass avocados using changes of peel color during the ripening process at different storage temperatures.

I aim to investigate the quality changes of the Hass avocado during the ripening process at four different temperatures (10, 15, 20, and 25℃) and to develop a prediction model of ripening stages based on DIP and ANN models.

3.2. Materials and methods

3.2.1. Avocado sampling

A total of 600 unripe Hass avocados imported from Mexico by a Japanese company were used in this study. Avocados lacking damage were selected and stored at four different temperatures (i.e., 10, 15, 20, and 25℃), and the RH was fixed at 95%, as suggested in previous works (Woolf et al., 2003; Tesfay et al., 2017; Arpaia et al., 2018). The avocados were divided into 8–23 groups from each storage period reflecting 23, 18, 11, and 8 storage days at temperatures of 10, 15, 20, and 25℃. Each group consisted of 10 avocados.

Fig. 3-1. Hass avocado used in this study.

3.2.2. Weight loss

The weight loss of whole avocados was determined by comparing the initial weights to those after ripening. The weight loss was calculated as the percentage loss of initial weight (Eq. 3-1).

$$\boldsymbol{Weight\ loss}\ (\%) = \frac{\boldsymbol{W_i} - \boldsymbol{W_f}}{\boldsymbol{Wi}} \times \mathbf{100}, \qquad \text{(Eq. 3-1)}$$

where $\boldsymbol{W_i}$ and $\boldsymbol{W_f}$ denote the initial weight and that after storage and ripening, respectively.

3.2.3. Peel color

Peel-color characteristics of Hass avocados were assessed using a portable colorimeter (CR-400, KONICA MINOLTA, Tokyo, Japan), calibrated using a standard white plate (Y = 85.4, x = 0.3173, and y = 0.3240). Each sample was measured three times, and the color values of each were averaged. The color values were expressed as *L*a*b** ranging from 0 to 100 (*L**) and from -127 to 127 (*a** and *b**) (Cho et al., 2016).

3.2.4. Firmness

Firmness of the avocado pulp was performed by blunt puncturing until tissue failure and was measured using a tabletop universal testing instrument (EZ-SX, SHIMADZU, Kyoto, Japan) that employed a cylindrical probe of 5 mm diameter with a 50 mm/min loading rate of the crosshead (Mizrach and Flitsanov, 1999). Each avocado sample was measured three times and averaged. The firmness of the pulp was expressed as the maximum force (kPa).

3.2.5. pH value

The pH value was determined using a pH meter (D-51, HORIBA, Kyoto, Japan), as

suggested previously (Saucedo-Pompa et al., 2009). Each avocado sample was measured three times, and the pH value of each sample was averaged.

3.3.6. DM

The DM content was determined by 5 g sample at 70℃ at 24 h. The DM was calculated with Eq. 3-2. Each sample was measured three times, and the average value was calculated.

$$\boldsymbol{Dry\ matter}\ (\%) = \frac{\boldsymbol{W_d}}{\boldsymbol{W_f}} \times \mathbf{100}, \qquad \text{(Eq. 3-2)}$$

where $\boldsymbol{W_f}$ is the fresh weight of the sample, and $\boldsymbol{W_d}$ is the dry weight of the sample.

3.3. Image processing

Figure 3-2 shows the flow diagram of image processing for extracting several features from Hass avocado images. Scikit-image and OpenCV Python libraries were used in this study (Van der Walt et al., 2014; Mustaffa and Khairul, 2017). Before processing, all images were rescaled to an 816×612-pixel size (maintaining aspect ratio) using the Scikit-image library.

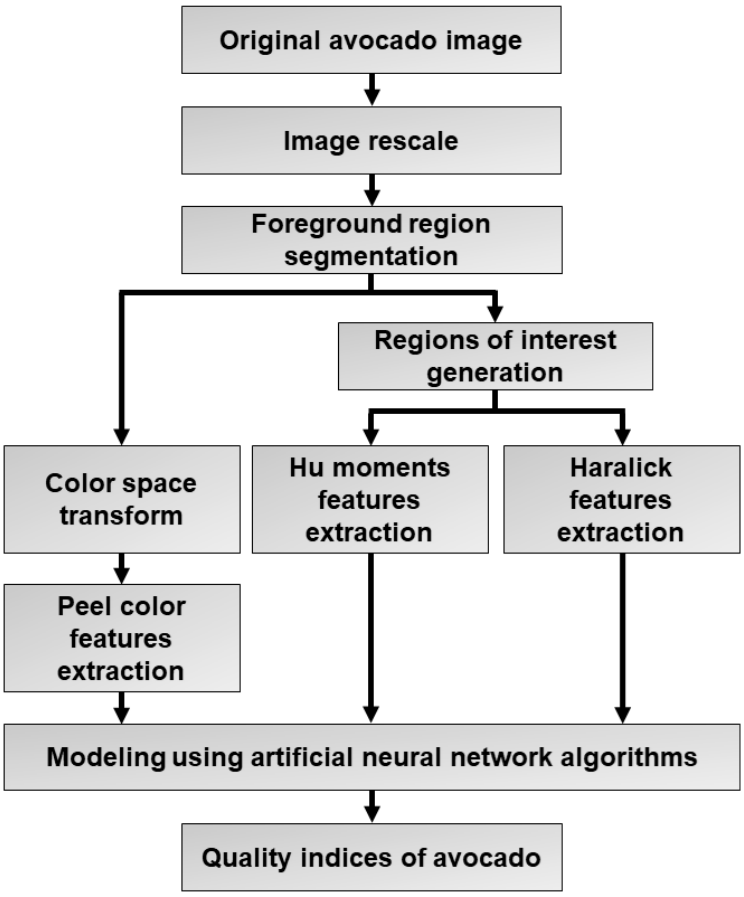

Fig. 3-2. Flow diagram of the image processing for Hass avocado.

3.3.1. Sample segmentation

The avocado samples were separated from the background using K-means clustering (Fig. 3-3), the most classical partition method and one of the 10 classical data-mining algorithms. The basic idea of K-means clustering is to cluster the objects closest to the target by clustering the K points in the space (Zheng et al., 2018). In this study, the number of the cluster was equal to two, because the avocado images were divided into two parts: sample and background. A blue-channel image was extracted and was chosen as the initial clustering sample, because the contrast between the sample and the white background was highest. The initial clustering centers were then determined from the color histogram of the

blue channel image using the K-means clustering algorithm (Aravind et al., 2010). The Euclidean distance was adopted as the distance criterion, which finds the optimal classification of an initial cluster center vector. The clustering centers are constantly updated by minimizing the objective function via multiple iterations. If the cluster centers are no longer updated, then the process is complete (Hu et al., 2014; Li et al., 2015). The binary images obtained from the above processing underwent a color-inverse transition, which made background and avocado sample pixels equal to 0 and 1, respectively. Additionally, holes in the sample were removed. A binary image without a background and the original RGB image were superimposed using the logical AND operator. As a result, the avocado sample and background formed an RGB image with color values and zeros, respectively.

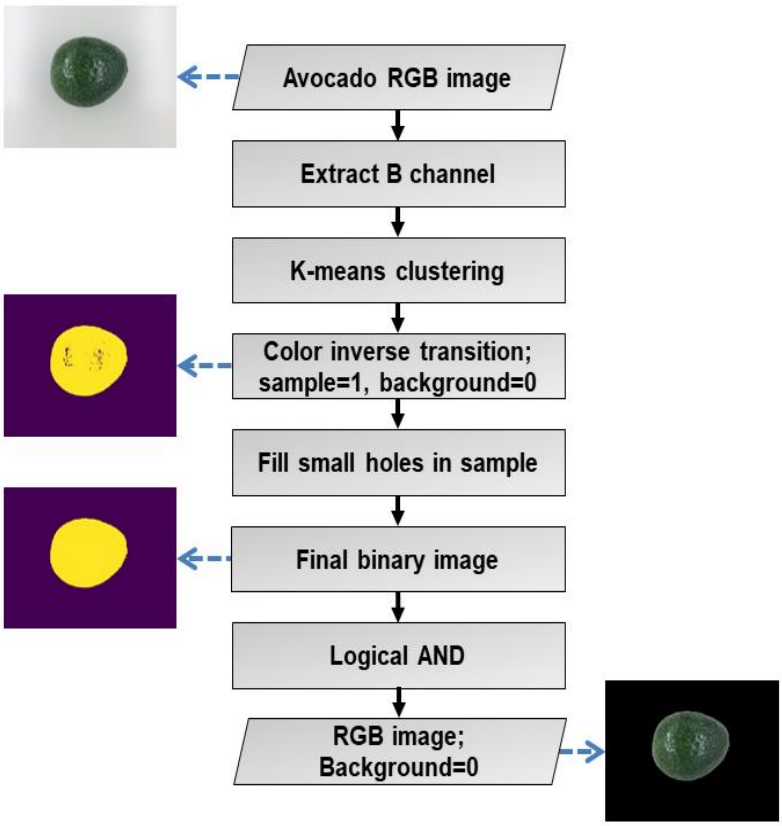

Fig. 3-3. Flow diagram of the algorithm employed for foreground region segmentation for Hass avocado.

3.3.2. Feature extraction

The external optical characteristics of avocados, including color, shape, and texture, observed from samples belonging to various ripening stages are potential criteria for identifying different ripening stages (Zhuang et al., 2019). Hence, I used those features from the avocado images as input data.

Three regions of interest (ROI) were sampled and extracted from the avocado sample. The sizes of each ROI were assigned to a 48×48-pixel size to simplify the feature extraction process. The location of ROI2 was calculated based on the center coordinate of the avocado sample, and the locations of ROI1 and ROI3 were calculated by the following:

$$\boldsymbol{ROI1} = \boldsymbol{P_{Center}} - \frac{\boldsymbol{Y_v}}{\boldsymbol{3}}, \quad \text{(Eq. 3-3)}$$

$$\boldsymbol{ROI3} = \boldsymbol{P_{Center}} + \frac{\boldsymbol{Y_v}}{\boldsymbol{3}}, \quad \text{(Eq. 3-4)}$$

where $\boldsymbol{P_{center}}$ is the center coordinate of the avocado sample, and $\boldsymbol{Y_v}$ is the vertical length from center coordinate.

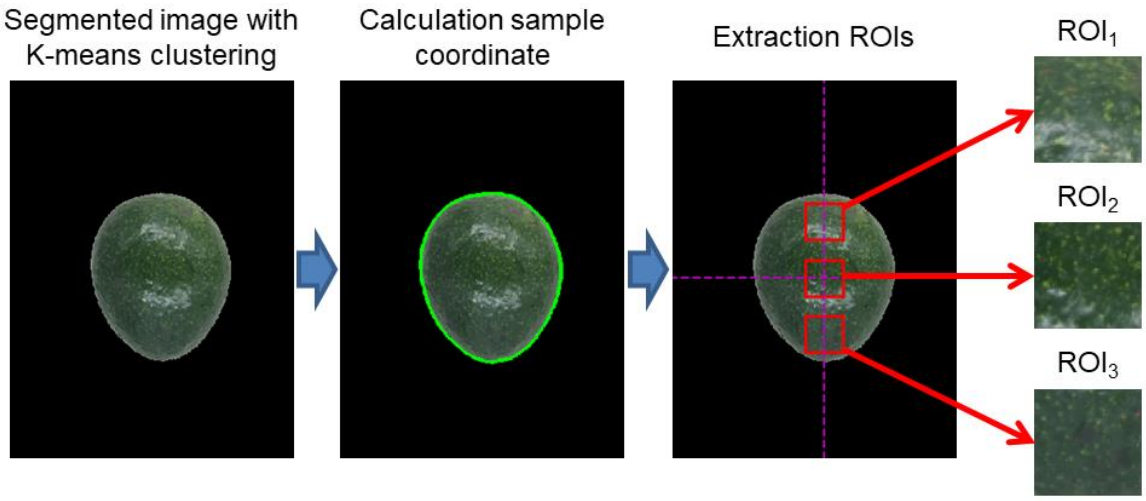

Fig. 3-4. Location of three ROIs from the segmented avocado region.

3.3.2.1. Color feature extraction

All images were converted from RGB to several color spaces (i.e., *L*a*b**, HSV, LUV, YUV, XYZ) using the Scikit-image library function (Bell et al., 2009). The HSV color space provides the pure hue, saturation, and value color representation, respectively (Zhuang et al., 2019). In LUV color space describes luminance and chromaticity values. Negative values of U and V indicate the prominence of a red component and green over blue (Kekre and Thepade, 2009). YUV refers to luminance and the same two chrominance components as in LUV. Y describes the intensity of light (Podpora et al., 2014). XYZ color space has a linear relationship with the non-gamma-corrected RGB and is the foundation of the *L*a*b**, LUV, and LCH color spaces (Asmare et al., 2009). *L*a*b**, HSV, LUV, YUV, and XYZ color features were extracted from entire avocado sample, and the average intensities of all pixels in each color space were calculated. All feature values obtained from the various color spaces were also analyzed to find correlations to quality indices (e.g., firmness, pH value, and DM).

3.3.2.2. Hu-moment feature extraction

The Hu-moment feature provides pattern information as outlined or silhouetted features in a gray image and is useful, because their computations are algorithmically simple and uniquely defined for any image function. Hu moments are described by using statistical and central moments, defined by Eqs. 3-5 and 3-6, respectively (Muñoz-Rodríguez et al., 2005):

$$\boldsymbol{m_{pq}} = \sum \boldsymbol{i} = \mathbf{0u} - \mathbf{1} \sum \boldsymbol{j} = \mathbf{0v} - \mathbf{1} \boldsymbol{x_i^p y_j^q f}(\mathbf{x}, \mathbf{y}), \qquad \text{(Eq. 3-5)}$$

$$\boldsymbol{\mu_{pq} = \sum i = 0m - 1 \sum j = 0n - 1 (x_i - \bar{x})^p (y - \bar{y})^q f(x, y)},$$ (Eq. 3-6)

where ***f*(x, y)** is the pixel intensity, and **(x, y)** is the pixel coordinate. $\boldsymbol{\bar{x} = m_{10} m_{00}}$, and $\boldsymbol{\bar{y} = m_{10} m_{00}}$.

Normalized moments are defined by Eq. 3-7:

$$\boldsymbol{\eta_{pq} = \mu_{pq} \mu_{00}^{\gamma}},$$ (Eq. 3-7)

where $\boldsymbol{\gamma = p + q2 + 1}$.

Hu moments are invariant to scale, rotation, and translation and are defined by Eqs. 8–14 (Muñoz-Rodríguez et al., 2005; Leiva-Valenzuela and Aguilera, 2013).

$$\boldsymbol{HU_1 = \eta_{20} - \eta_{02}},$$ (Eq. 3-8)

$$\boldsymbol{HU_2 = (\eta_{20} - \eta_{02})^2 + (2\eta_{11})^2},$$ (Eq. 3-9)

$$\boldsymbol{HU_3 = (\eta_{30} - 3\eta_{12})^2 + (3\eta_{21} - \eta_{03})^2},$$ (Eq. 3-10)

$$\boldsymbol{HU_4 = (\eta_{30} + \eta_{12})^2 + (\eta_{21} + \eta_{03})^2},$$ (Eq. 3-11)

$$\boldsymbol{HU_5 = (\eta_{30} - 3\eta_{12})(\eta_{30} + \eta_{12})[(\eta_{30} + 3\eta_{12})^2 - 3(\eta_{21} - \eta_{03})^2] + (3\eta_{21} - \eta_{03})(\eta_{21} + \eta_{03})[3(\eta_{30} + \eta_{12})^2 - (\eta_{21} + \eta_{03})^2]},$$ (Eq. 3-12)

$$\boldsymbol{HU_6 = (\eta_{20} - \eta_{02})[(\eta_{30} + \eta_{12})^2 - (\eta_{21} - \eta_{03})^2] + 4\eta_{11}(\eta_{30} + \eta_{12})(\eta_{21} + \eta_{03})},$$ (Eq. 3-13)

$$\boldsymbol{HU_7 = (3\eta_{21} - \eta_{03})(\eta_{30} + \eta_{12})[(\eta_{30} + \eta_{12})^2 - 3(\eta_{21} + \eta_{03})^2] - (\eta_{30} - 3\eta_{12})(\eta_{21} + \eta_{03})[3(\eta_{30} + \eta_{12})^2 - (\eta_{21} + \eta_{03})^2]},$$ (Eq. 3-14)

As a result, a 7-dimension Hu-moment feature is generated for each ROI, and three of them are successively concatenated into a 21-dimension Hu-moment feature vector.

3.3.2.3. Haralick feature extraction

The Haralick feature is used to quantify an image based on texture, and it is used to extract the avocado texture feature from each ROI in this study (Haralick et al., 1973). Mahotas library of Python (Coelho, 2013) was used to extract Haralick texture features, and this provides the Haralick texture features into four and 13 for 2D and 3D directions, respectively. The 13 Haralick features were extracted from RGB images and are listed in Table 3-1 (Attig and Perner, 2011). The steps involved in feature extraction are as follows. First, images are divided into non-overlapping patches. Second, each patch obtains four sub-bands via redundant discrete wavelet transform decomposition, which consists of approximation, horizontal, vertical, and diagonal. Third, Haralick features are computed over all four sub-bands for all patches. Fourth, Haralick features are computed over the original image patch without wavelet decomposition. Finally, the feature vector of one color channel is the concatenation of Haralick features all four sub-bands of each patch and all original patches. Each color channel (i.e., RGB) separately repeats steps 1–5, and the feature vector obtained in each is concatenated as a 13-dimension Haralick feature (Agarwal et al., 2016). In this study, the three texture features generated from ROIs were successively concatenated into a 39-dimension Haralick feature vector.

Table 3-1. List of thirteen Haralick texture features used in this study.

Feature label	Feature name	Feature label	Feature name
f1	Angular second moment	f8	Sum entropy
f2	Contrast	f9	Entropy
f3	Correlation	f10	Difference variance
f4	Sum of squares: variance	f11	Difference entropy
f5	Inverse difference moment	f12	Information measure of correlation 1
f6	Sum average	f13	Information measure of correlation 2
f7	Sum variance		

3.4. Data analysis

I used an ANN to analyze the collected data. Python 3.7 was used for analysis, and the ANN model was implemented using the Keras library (Gulli and Pal, 2017).

3.4.1. ANN

ANN performance was tested according to the topology shown in Fig. 3-5. The hyperparameter value is used to control the learning process, and it should be tuned so that the ANN can optimally solve the problems. A grid-search method was used to search the optimal hyperparameter for the ANN. Thus, I used a K-fold cross-validation method to validate the ANN for each hyperparameter. Using this method, the original sample was randomly divided into K equal-sized subsamples. Of the K subsamples, a single subsample was retained as the validation data for testing the classification and regression models, and

the remaining K-1 subsamples were used as the training set. The cross-validation process was then repeated K times with each of the K subsamples used exactly once as the testing set. The K results from the folds were then averaged to produce a single estimation (Moreno-Torres et al., 2012). In this study, a five-fold cross-validation function was used.

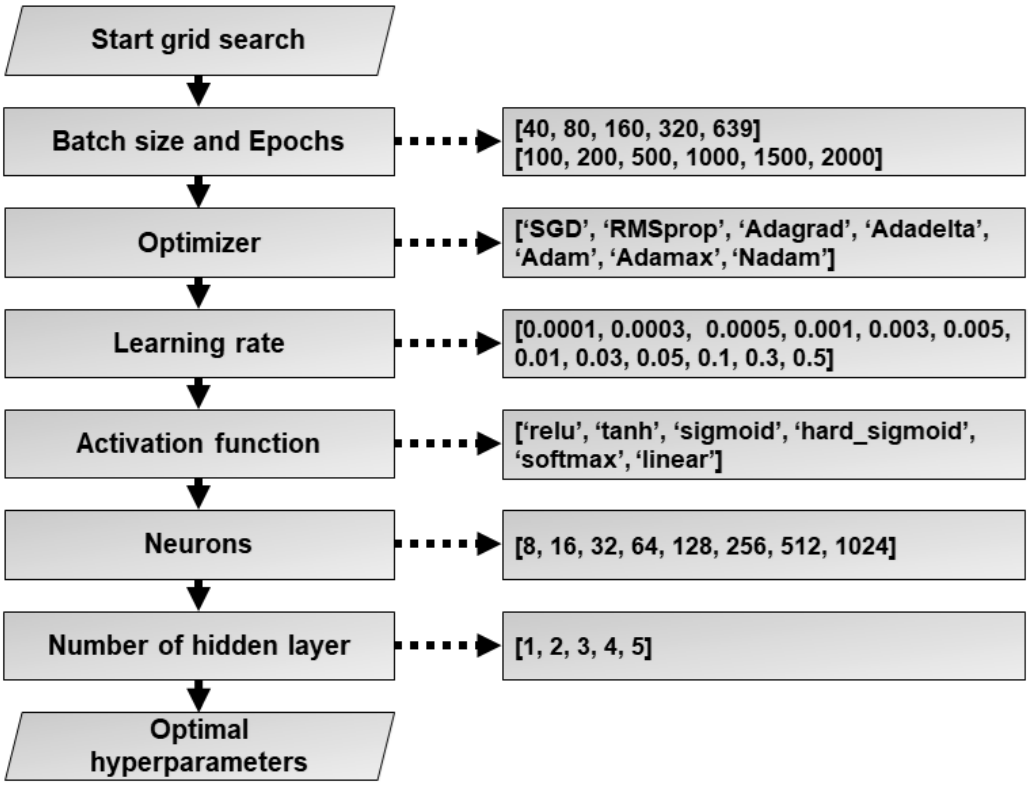

Fig. 3-5. Flow diagram for optimal hyperparameters selection of ANN.

3.4.2. Model evaluation

The entire dataset containing 600 images was randomly divided into two subsets: a training set (90%, 540 images) and a testing set (10%, 60 images). The training set was used to develop an estimation model of avocado-ripening stages, and the testing set was used to validate the developed model. Additionally, the developed ANN models were verified by R^2, RMSE, and the ratio of performance-to-deviation (RPD).

The R^2 value measures the agreement between the measured and predicted values and was calculated using Eq. 3-15. The R^2 value ranged from 0 to 1, where 1 indicates a perfect linear relationship between the measured and predicted values (Porep et al., 2015).

$$\boldsymbol{R^2 = 1 - \frac{\sum_{i=1}^{n}(P_i - M_i)^2}{\sum_{i=1}^{n} M_i^2}}, \qquad \text{(Eq. 3-15)}$$

where $\boldsymbol{P}$ is the predicted value, and $\boldsymbol{M}$ is the measured value.

The RMSE was used to assess the difference between the measured and predicted values, calculated using Eq. 3-16:

$$\boldsymbol{RMSE = \sqrt{\frac{1}{n}\sum_{i=1}^{n}(P_i - M_i)^2}}, \qquad \text{(Eq. 3-16)}$$

Furthermore, the RPD value was used to define the ability of the model to predict future data and was determined with Eq. 3-17. A higher RPD value indicates better predictive ability (Prieto et al., 2017; Díaz et al., 2019).

$$\boldsymbol{RPD = \frac{SD}{RMSE}}, \qquad \text{(Eq. 3-17)}$$

where $\boldsymbol{SD}$ is the standard deviation of measured values.

The F1-score was used to evaluate the classification performance of the ANN model and was calculated using Eq. 3-18. The F1-socre represents the harmonic mean of precision and recall and is useful when the class distribution is uneven. It ranges from zero to one, and high values indicate high classification performance (Tharwat, 2020).

$$\boldsymbol{Precision = \frac{TP}{TP + FP}}, \qquad \text{(Eq. 3-18)}$$

$$\boldsymbol{Recall} = \frac{\boldsymbol{TP}}{\boldsymbol{TP} + \boldsymbol{FN}}, \quad \text{(Eq. 3-19)}$$

$$\boldsymbol{F1\ score} = \frac{\boldsymbol{2} \times (\boldsymbol{Precision} \times \boldsymbol{Recall})}{\boldsymbol{Precision} + \boldsymbol{Recall}}, \quad \text{(Eq. 3-20)}$$

where ***TP***, ***FP***, and ***FN*** is the number of true positives, false positives, and false negatives, respectively.

3.4.3. Statistical analysis

Correlation and statistical analyses were conducted using a bivariate and one-way analyses of variance (ANOVA), respectively. IBM SPSS (v.20.0, IBM, Armonk, USA) was used to analyze the significance in this study.

The correlation coefficient (R) between quality indices and each color feature value was determined using Pearson's test. Differences according to storage period were established using the Tukey–Kramer's multiple-range test with a significance level of $p < 0.05$.

3.5. Results and discussion

3.5.1. Weight loss

The changes in avocado weight during the ripening process at different temperatures are shown in Fig. 3-6 and Table 3-2. Weight loss via transpiration was observed for all storage conditions. In particular, the weight-loss rate according to storage period showed significant differences. However, there were no significant differences related to temperature conditions, and these results are similar to those of a previous study (Yearsly et al., 2002).

Water loss is a major cause of postharvest deterioration and weight loss, which leads to economic loss if the commodity is sold by weight. Moreover, water loss after harvest affects the quality of avocados by influencing ripening and/or rotting. High rates of water loss after harvest decreases the ripening period, but the incidence of rotting can increase 5–15% (Bower and Cutting 1998; Lallu et al., 2003; Lallum et al., 2004). Therefore, water loss should be minimized and managed during storage and ripening to reduce development of physiological disorders (Blakely, 2011). It is desirable to store Hass avocados at 2 or 25℃ to prevent weight loss during ripening.

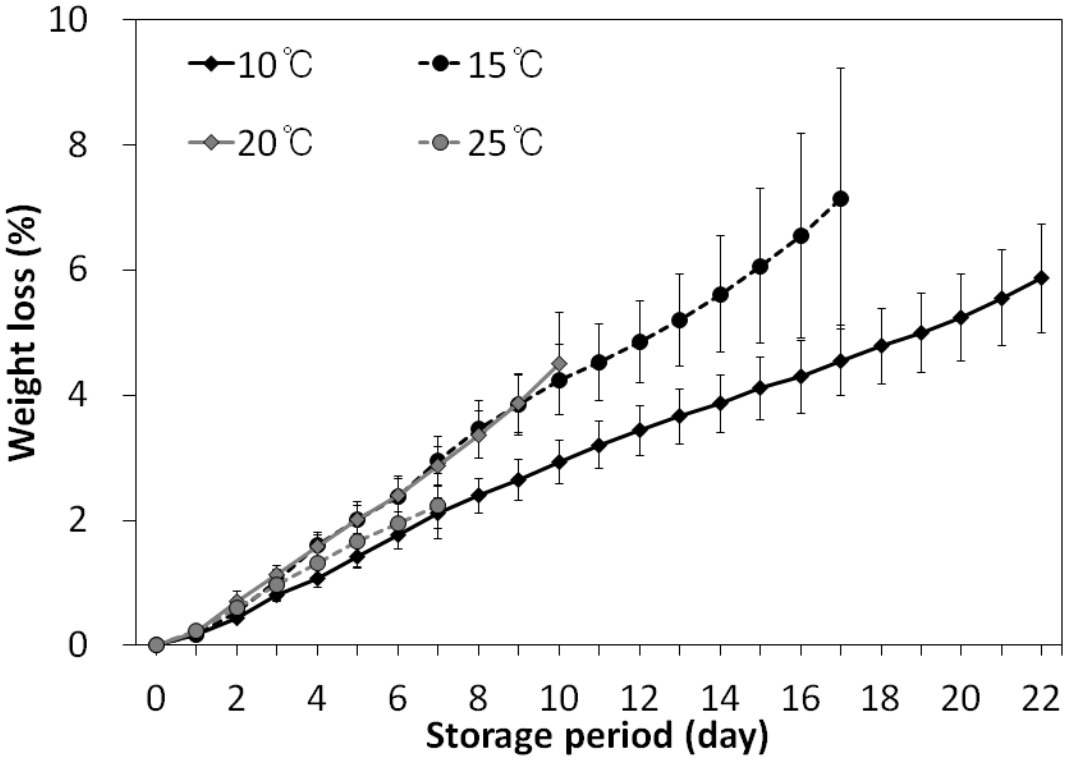

Fig. 3-6. The changes in weight loss of Hass avocado according to temperature conditions. Each value is the mean of 10 fruits assessed at each time, and is the mean ± standard deviation.

Table 3-2. Weight loss of Hass avocado according to temperature conditions.

Storage period	Temperature			
	10℃	15℃	20℃	25℃
0	0.00	0.00	0.00	0.00
1	0.18 ± 0.03^{t}	$0.18 \pm 0.04^{m,n}$	0.21 ± 0.04^{j}	0.24 ± 0.07^{f}
2	$0.45 \pm 0.06^{s,t}$	$0.54 \pm 0.08^{m,n}$	0.70 ± 0.16^{i}	0.61 ± 0.16^{e}
3	$0.82 \pm 0.12^{r,s}$	$1.04 \pm 0.16^{l,m}$	1.13 ± 0.14^{h}	0.97 ± 0.24^{d}
4	$1.07 \pm 0.14^{q,r}$	$1.61 \pm 0.21^{k,l}$	1.58 ± 0.18^{g}	1.31 ± 0.31^{c}
5	$1.41 \pm 0.17^{p,q}$	2.01 ± 0.28^{k}	2.01 ± 0.23^{f}	1.67 ± 0.41^{b}
6	$1.76 \pm 0.22^{o,p}$	$2.38 \pm 0.32^{j,k}$	2.40 ± 0.27^{e}	$1.95 \pm 0.41^{a,b}$
7	$2.11 \pm 0.25^{n,o}$	$2.95 \pm 0.38^{i,j}$	2.86 ± 0.31^{d}	2.23 ± 0.51^{a}
8	$2.40 \pm 0.28^{m,n}$	$3.45 \pm 0.45^{h,i}$	3.37 ± 0.37^{c}	
9	$2.64 \pm 0.32^{l,m}$	$3.85 \pm 0.49^{g-i}$	3.86 ± 0.47^{b}	
10	$2.93 \pm 0.35^{k,l}$	$4.24 \pm 0.56^{f-h}$	4.51 ± 0.81^{a}	
11	$3.20 \pm 0.38^{j,k}$	$4.53 \pm 0.61^{e-g}$		
12	$3.43 \pm 0.41^{i-k}$	$4.85 \pm 0.65^{d-f}$		
13	$3.66 \pm 0.44^{h-j}$	$5.19 \pm 0.74^{c-e}$		
14	$3.86 \pm 0.47^{g-i}$	$5.61 \pm 0.93^{c,d}$		
15	$4.11 \pm 0.50^{f-h}$	$6.06 \pm 1.24^{b,c}$		
16	$4.29 \pm 0.58^{e-g}$	$6.55 \pm 1.64^{a,b}$		
17	$4.55 \pm 0.56^{d-f}$	7.14 ± 2.09^{a}		
18	$4.79 \pm 0.60^{c-e}$			
19	$4.99 \pm 0.64^{c,d}$			
20	$5.24 \pm 0.69^{b,c}$			
21	$5.55 \pm 0.77^{a,b}$			
22	5.87 ± 0.87^{a}			

Each value is the mean of 10 fruits, and is the mean $\pm$ standard deviation.
Means with different letters (a-t) indicate significant differences based on Tukey-Kramer's multiple range test (p<0.05).

3.5.2. Peel color

Figure 3-7 shows the changes in *L*a*b** values, determined using a portable colorimeter. The *L** and *b** values decreased during the ripening process, whereas the a* value increased. These results were probably caused by the progressive changes in peel color of the Hass avocados from green to purplish-black. These color changes were similarly reported in previous studies (Cox et al., 2004; Arzate-Vázquez et al., 2011; Magwaza and Tesfay, 2015). These changes are caused by the chlorophyll content decreasing during ripening followed by an increase in anthocyanin and cyanidin 3-O-glucoside (Cox et al., 2004). These peel-color changes can be used for non-destructive analysis of Hass avocado ripeness.

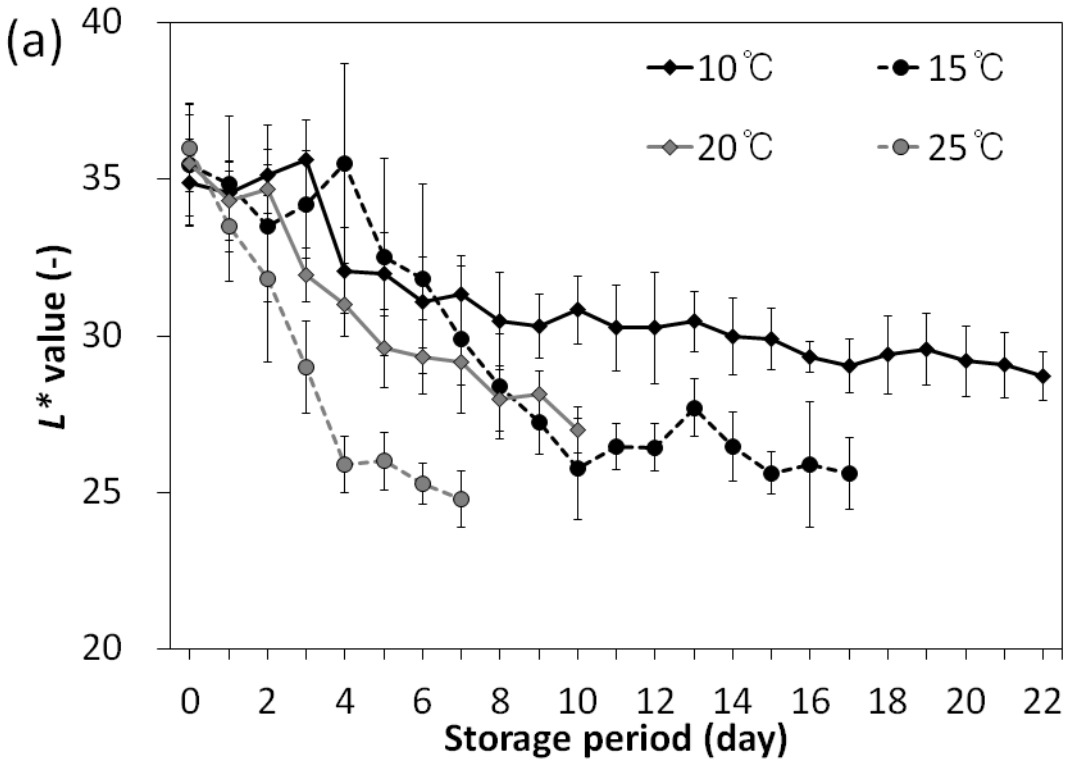

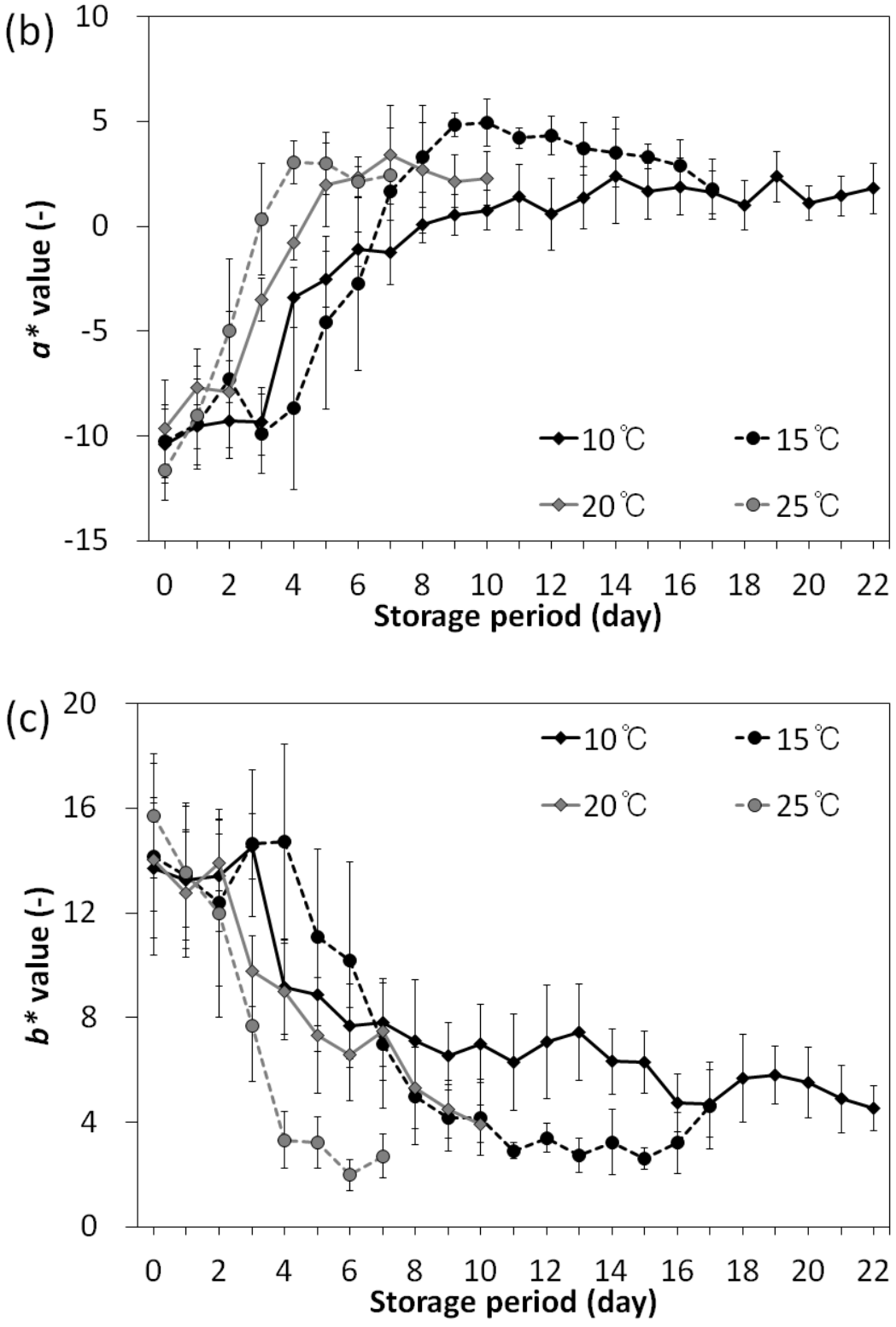

Fig. 3-7. The changes in *L*a*b of Hass avocado according to temperature conditions determined by a portable colorimeter: (a) *L**, (b) *a**, and (c) *b** values. Each value is the mean of 10 fruits assessed at each time, and is the mean ± standard deviation.**

Table 3-3. *L value of Hass avocado according to temperature conditions.**

Storage period	Temperature			
	10℃	15℃	20℃	25℃
0	34.88 ± 1.38[a]	35.45 ± 1.63[a]	35.49 ± 1.94[a]	36.01 ± 1.39[a]
1	34.56 ± 1.04[a]	34.85 ± 2.15[a,b]	34.31 ± 1.24[a]	33.50 ± 1.74[b]
2	35.13 ± 1.59[a]	33.52 ± 2.44[a,b]	34.69 ± 0.78[a]	31.83 ± 2.66[b]
3	35.62 ± 1.26[a]	34.21 ± 1.71[a,b]	31.96 ± 0.85[b]	29.02 ± 1.47[c]
4	32.09 ± 1.37[b]	35.49 ± 3.19[a]	30.99 ± 1.01[b,c]	25.92 ± 0.90[d]
5	31.98 ± 1.33[b,c]	32.54 ± 3.15[a-c]	29.60 ± 1.26[c,d]	26.02 ± 0.92[d]
6	31.08 ± 1.46[b-e]	31.82 ± 3.01[b,c]	29.33 ± 1.18[d]	25.28 ± 0.65[d]
7	31.33 ± 1.25[b-d]	29.89 ± 2.35[c,d]	29.17 ± 0.73[d]	24.79 ± 0.90[d]
8	30.48 ± 1.54[b-g]	28.40 ± 1.67[d,e]	27.99 ± 1.04[d,e]	
9	30.32 ± 1.03[b-g]	27.25 ± 1.04[d,e]	28.13 ± 0.76[d,e]	
10	30.84 ± 1.08[b-f]	25.76 ± 1.61[e]	27.02 ± 0.74[e]	
11	30.26 ± 1.37[b-g]	26.47 ± 0.72[e]		
12	30.27 ± 1.78[b-g]	26.45 ± 0.75[e]		
13	30.46 ± 0.98[b-g]	27.72 ± 0.93[d,e]		
14	29.98 ± 1.23[c-g]	26.48 ± 1.09[e]		
15	29.90 ± 0.99[d-g]	25.63 ± 0.66[e]		
16	29.32 ± 0.49[e-g]	25.91 ± 2.01[e]		
17	29.06 ± 0.87[f,g]	25.62 ± 1.15[e]		
18	29.41 ± 1.25[d-g]			
19	29.59 ± 1.15[d-g]			
20	29.20 ± 1.13[e-g]			
21	29.08 ± 1.05[f,g]			
22	28.74 ± 0.78[g]			

Each value is the mean of 10 fruits, and is the mean ± standard deviation.
Means with different letters (a-g) indicate significant differences based on Tukey-Kramer's multiple range test (p<0.05).

Table 3-4. *a value of Hass avocado according to temperature conditions.**

Storage period	Temperature			
	10℃	15℃	20℃	25℃
0	-10.39 ± 1.86^{g}	-10.26 ± 1.55^{d}	-9.65 ± 2.33^{d}	-11.65 ± 1.41^{c}
1	-9.56 ± 1.07^{g}	-9.44 ± 2.17^{d}	-7.71 ± 1.87^{d}	-9.03 ± 2.34^{c}
2	-9.30 ± 1.76^{g}	-7.31 ± 3.25^{c,d}	-7.89 ± 1.47^{d}	-4.99 ± 3.43^{b}
3	-9.31 ± 1.62^{g}	-9.88 ± 1.89^{d}	-3.50 ± 1.02^{c}	0.33 ± 2.64^{a}
4	-3.40 ± 1.45^{f}	-8.68 ± 3.87^{d}	-0.80 ± 0.83^{b}	3.03 ± 1.02^{a}
5	-2.51 ± 1.34^{e,f}	-4.59 ± 4.11^{b,c}	1.97 ± 2.01^{a}	3.01 ± 1.48^{a}
6	-1.09 ± 0.83^{c-e}	-2.75 ± 4.13^{b}	2.35 ± 0.96^{a}	2.10 ± 0.72^{a}
7	-1.26 ± 1.55^{d-f}	1.67 ± 2.99^{a}	3.38 ± 2.35^{a}	2.43 ± 1.00^{a}
8	0.08 ± 0.84^{b-d}	3.28 ± 1.64^{a}	2.70 ± 3.03^{a}	
9	0.54 ± 0.96^{a-d}	4.84 ± 0.58^{a}	2.14 ± 1.25^{a}	
10	0.76 ± 0.95^{a-d}	4.94 ± 1.14^{a}	2.28 ± 1.27^{a}	
11	1.40 ± 1.57^{a,b}	4.20 ± 0.47^{a}		
12	0.58 ± 1.71^{a-d}	4.32 ± 0.94^{a}		
13	1.38 ± 1.49^{a,b}	3.69 ± 1.27^{a}		
14	2.36 ± 2.26^{a}	3.53 ± 1.68^{a}		
15	1.66 ± 1.32^{a,b}	3.31 ± 0.58^{a}		
16	1.88 ± 1.35^{a,b}	2.92 ± 1.20^{a}		
17	1.61 ± 1.01^{a,b}	1.76 ± 1.44^{a}		
18	1.00 ± 1.18^{a-c}			
19	2.37 ± 1.21^{a}			
20	1.11 ± 0.83^{a-c}			
21	1.44 ± 0.94^{a,b}			
22	1.80 ± 1.20^{a,b}			

Each value is the mean of 10 fruits, and is the mean ± standard deviation.
Means with different letters (a-g) indicate significant differences based on Tukey-Kramer's multiple range test (p<0.05).

Table 3-5. *b value of Hass avocado according to temperature conditions.**

Storage period	Temperature			
	10℃	15℃	20℃	25℃
0	13.71 ± 2.68[a]	14.14 ± 2.07[a,b]	14.04 ± 3.66[a]	15.71 ± 2.37[a]
1	13.27 ± 1.81[a]	13.41 ± 2.79[a-c]	12.75 ± 2.43[a]	13.52 ± 2.57[a,b]
2	13.41 ± 2.12[a]	12.40 ± 3.19[a-c]	13.92 ± 1.10[a]	11.98 ± 3.97[b]
3	14.54 ± 1.24[a]	14.66 ± 2.82[a]	9.77 ± 1.36[b]	7.70 ± 2.14[c]
4	9.15 ± 1.80[b]	14.73 ± 3.72[a]	9.00 ± 1.84[b,c]	3.32 ± 1.08[d]
5	8.89 ± 2.19[b,c]	11.06 ± 3.37[b,c]	7.30 ± 2.21[b-e]	3.23 ± 0.97[d]
6	7.70 ± 1.59[b-d]	10.17 ± 3.75[c,d]	6.59 ± 1.79[c-e]	1.99 ± 0.59[d]
7	7.80 ± 1.67[b-d]	7.00 ± 2.47[d,e]	7.47 ± 1.87[b-d]	2.69 ± 0.84[d]
8	7.12 ± 2.32[b-f]	4.99 ± 1.87[e,f]	5.32 ± 1.57[d-f]	
9	6.52 ± 1.28[b-f]	4.16 ± 1.27[e,f]	4.50 ± 1.09[e,f]	
10	7.01 ± 1.50[b-f]	4.19 ± 1.46[e,f]	3.93 ± 0.72[f]	
11	6.28 ± 1.85[c-f]	2.90 ± 0.30[f]		
12	7.08 ± 2.16[b-f]	3.40 ± 0.55[f]		
13	7.43 ± 1.83[b-e]	2.73 ± 0.65[f]		
14	6.32 ± 1.24[c-f]	3.24 ± 1.24[f]		
15	6.31 ± 1.19[c-f]	2.61 ± 0.41[f]		
16	4.74 ± 1.11[e,f]	3.21 ± 1.18[f]		
17	4.70 ± 1.29[e,f]	4.62 ± 1.66[e,f]		
18	5.68 ± 1.69[d-f]			
19	5.80 ± 1.11[d-f]			
20	5.53 ± 1.36[d-f]			
21	4.89 ± 1.28[e,f]			
22	4.52 ± 0.85[f]			

Each value is the mean of 10 fruits, and is the mean ± standard deviation.
Means with different letters (a-f) indicate significant differences based on Tukey-Kramer's multiple range test (p<0.05).

3.5.3. Firmness

The firmness of fresh fruits is the best indicator of ripening. A previous study showed that avocado firmness correlated well with fruit ripeness and expected storage periods (Lewis, 1978). Firmness can also be used to assess pathological and physiological disorders, which develop rapidly during the latter stages of ripening (Hopkirk et al., 1994).

The firmness of the Hass avocados decreased during ripening under all conditions. Average measured firmness were 1,483–4,453 kPa initially and decreased to 60–95 kPa at full ripeness. The firmness at the initial 20℃ temperature condition was 1,483 kPa, which was found to be approximately 2,423–2,970 kPa lower than other temperature conditions. This is because avocado ripening progresses during distribution. Meanwhile, the decrease of the firmness can also be attributed to the transformation of cellulose (Scott et al., 1963).

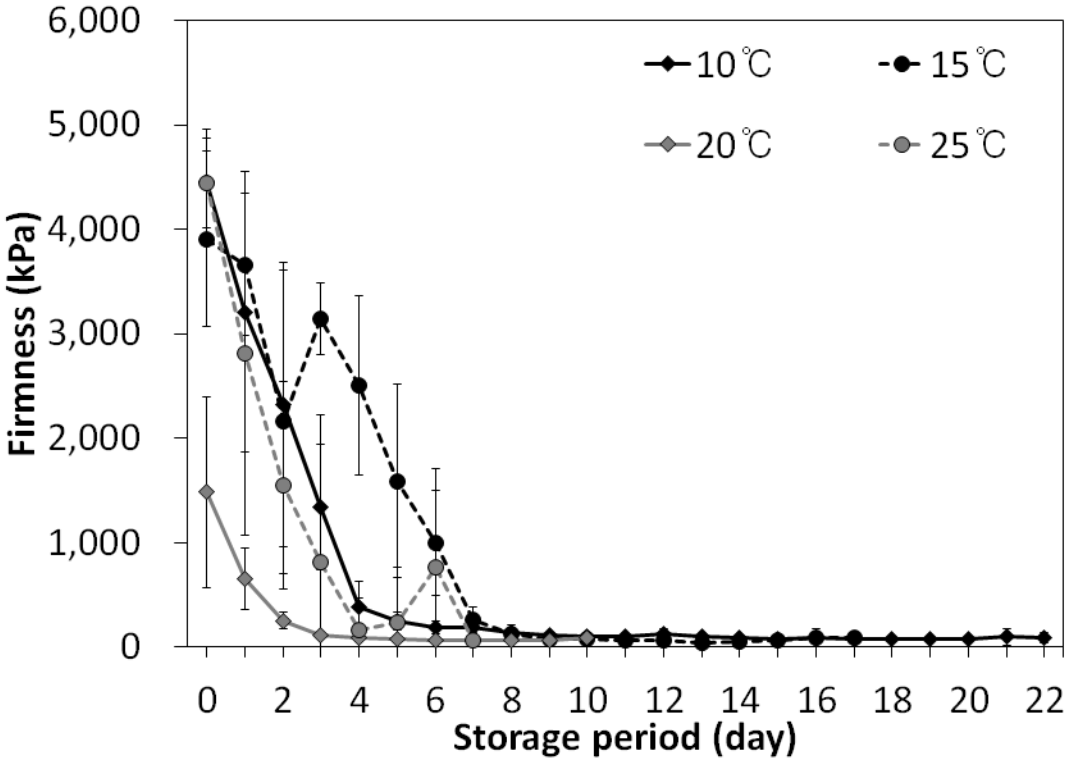

Fig. 3-8. The changes in firmness of Hass avocado according to temperature conditions. Each value is the mean of 10 fruits assessed at each time, and is the mean ± standard deviation.

Table 3-6. Firmness of Hass avocado according to temperature conditions.

Storage period	Temperature			
	10℃	15℃	20℃	25℃
0	4453.66 ± 502.07a	3906.78 ± 840.67^{a}	1483.80 ± 916.44^{a}	4445.79 ± 427.36^{a}
1	3209.57 ± 1341.57^{b}	3662.56 ± 678.62^{a}	652.39 ± 296.43^{b}	2814.14 ± 1743.32^{b}
2	2327.85 ± 1361.40^{c}	2160.97 ± 1453.94^{c,d}	256.32 ± 80.37^{b,c}	1553.03 ± 995.95^{b,c}
3	1345.00 ± 601.96^{d}	3140.79 ± 341.74^{a,b}	120.10 ± 20.13^{c}	817.26 ± 1404.86^{c,d}
4	386.61 ± 238.60^{e}	2505.77 ± 855.93^{d,e}	95.52 ± 8.68^{c}	165.74 ± 305.34^{d}
5	250.95 ± 81.81^{e}	1592.53 ± 923.76^{e,f}	82.92 ± 8.08^{c}	238.61 ± 523.06^{c,d}
6	187.54 ± 63.10^{e}	998.22 ± 504.63^{f,g}	69.03 ± 9.91^{c}	771.17 ± 937.09^{c,d}
7	183.63 ± 59.23^{e}	266.32 ± 125.08^{g}	68.36 ± 11.36^{c}	60.62 ± 38.99^{d}
8	143.42 ± 20.34^{e}	130.33 ± 77.71^{g}	67.25 ± 13.46^{c}	
9	114.25 ± 9.86^{e}	82.38 ± 8.73^{g}	63.23 ± 23.19^{c}	
10	107.10 ± 12.52^{e}	74.46 ± 10.85^{g}	86.25 ± 50.49^{c}	
11	99.48 ± 13.91^{e}	62.54 ± 8.97^{g}		
12	122.55 ± 53.99^{e}	60.86 ± 7.12^{g}		
13	108.20 ± 10.28^{e}	46.87 ± 8.30^{g}		
14	97.19 ± 12.67^{e}	53.60 ± 9.06^{g}		
15	75.39 ± 10.80^{e}	64.54 ± 12.76^{g}		
16	85.17 ± 17.97^{e}	89.78 ± 87.38^{g}		
17	77.56 ± 13.04^{e}	87.79 ± 49.18^{g}		
18	83.24 ± 11.91^{e}			
19	81.60 ± 15.49^{e}			
20	84.49 ± 17.51^{e}			
21	98.07 ± 84.68^{e}			
22	89.79 ± 51.71^{e}			

Each value is the mean of 10 fruits, and is the mean ± standard deviation.
Means with different letters (a-g) indicate significant differences based on Tukey-Kramer's multiple range test (p<0.05).

3.5.4. pH value

The pH value can be used to assess the physico-chemical properties of the avocado (Kassim et al., 2013). These values increase slightly from one to four days of storage, regardless of temperature conditions. The pH values of the avocados studied reached 7.39–7.41, showing a similar trend as one shown in a previous study (Saucedo-Pompa et al., 2009). However, there was no significant difference thereafter. Thus, these results cannot be used as an indicator to determine the ripening stages of avocados.

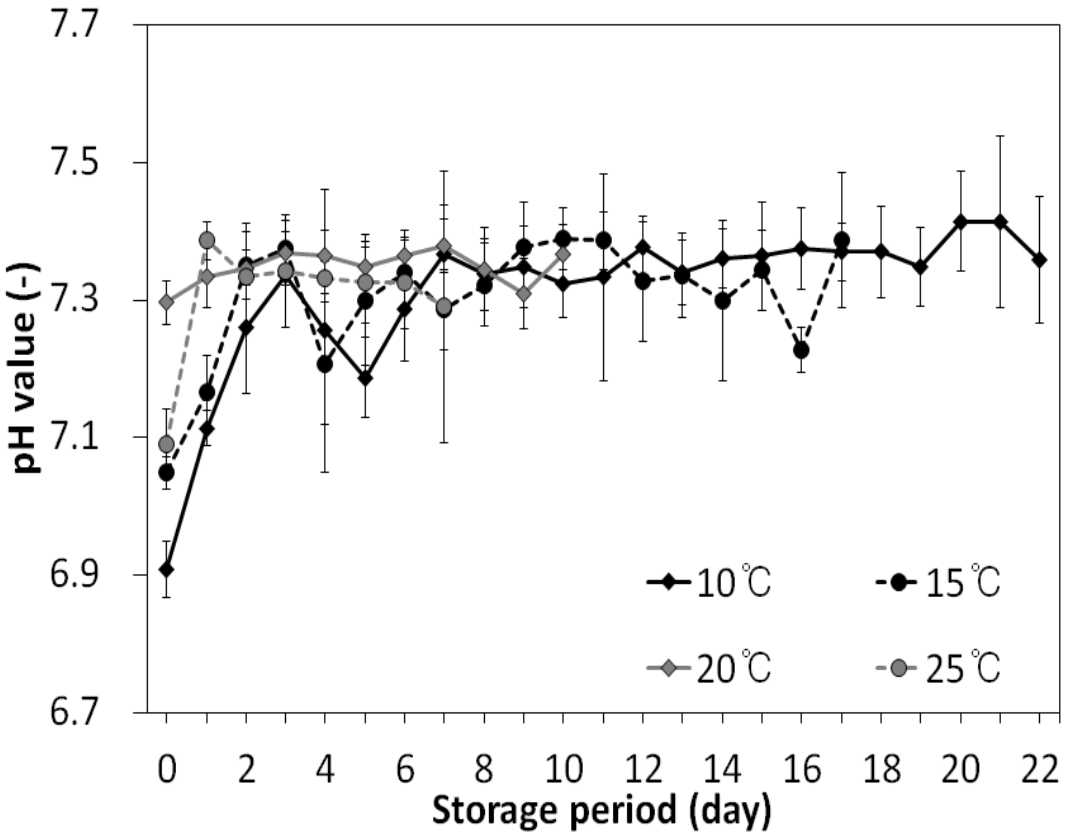

Fig. 3-9. The changes in pH of Hass avocado according to temperature conditions. Each value is the mean of 10 fruits assessed at each time, and is the mean ± standard deviation.

Table 3-7. pH of Hass avocado according to temperature conditions.

Storage period	Temperature			
	10℃	15℃	20℃	25℃
0	6.91 ± 0.04e	7.05 ± 0.02^{d}	7.30 ± 0.03^{c}	7.09 ± 0.05^{c}
1	7.11 ± 0.03^{d}	7.17 ± 0.05^{c,d}	7.33 ± 0.05^{a-c}	7.39 ± 0.03^{a}
2	7.26 ± 0.10^{b,c}	7.35 ± 0.05^{a,b}	7.35 ± 0.03^{a-c}	7.33 ± 0.08^{a,b}
3	7.34 ± 0.02^{a,b}	7.38 ± 0.04^{a}	7.37 ± 0.03^{a}	7.34 ± 0.08^{a,b}
4	7.26 ± 0.21^{b,c}	7.21 ± 0.09^{b-d}	7.37 ± 0.04^{a,b}	7.33 ± 0.02^{a,b}
5	7.19 ± 0.06^{c,d}	7.30 ± 0.09^{a-c}	7.35 ± 0.03^{a-c}	7.33 ± 0.06^{a,b}
6	7.29 ± 0.08^{a-c}	7.34 ± 0.05^{a,b}	7.36 ± 0.04^{a,b}	7.32 ± 0.07^{a,b}
7	7.37 ± 0.07^{a,b}	7.29 ± 0.06^{a-c}	7.38 ± 0.04^{a}	7.29 ± 0.20^{b}
8	7.34 ± 0.05^{a,b}	7.32 ± 0.06^{a-c}	7.34 ± 0.06^{a-c}	
9	7.35 ± 0.06^{a,b}	7.38 ± 0.07^{a}	7.31 ± 0.05^{b,c}	
10	7.32 ± 0.05^{a,b}	7.39 ± 0.05^{a}	7.37 ± 0.04^{a,b}	
11	7.33 ± 0.15^{a,b}	7.39 ± 0.04^{a}		
12	7.38 ± 0.05^{a,b}	7.33 ± 0.09^{a-c}		
13	7.34 ± 0.05^{a,b}	7.34 ± 0.06^{a,b}		
14	7.36 ± 0.04^{a,b}	7.30 ± 0.12^{a-c}		
15	7.36 ± 0.08^{a,b}	7.34 ± 0.06^{a,b}		
16	7.37 ± 0.06^{a,b}	7.23 ± 0.03^{a-c}		
17	7.37 ± 0.04^{a,b}	7.39 ± 0.10^{a}		
18	7.37 ± 0.07^{a,b}			
19	7.35 ± 0.06^{a,b}			
20	7.41 ± 0.07^{a}			
21	7.41 ± 0.12^{a}			
22	7.36 ± 0.09^{a,b}			

Each value is the mean of 10 fruits, and is the mean ± standard deviation.
Means with different letters (a-e) indicate significant differences based on Tukey-Kramer's multiple range test (p<0.05).

3.5.5. DM

The DM content is used commercially as an indicator of ripening in different countries, because is gradually increases during ripening (Magwaza and Tesfay, 2015). However, in this study, there was no significant difference in DM content according to the ripening process and temperature conditions. These results are consistent with those of a previous study (Hofman et al., 2000) that suggested that the percentage DM was not a suitable indicator of avocado ripening in late-harvested Hass avocados, owing to late-harvested fruit undergoing inconsistent changes.

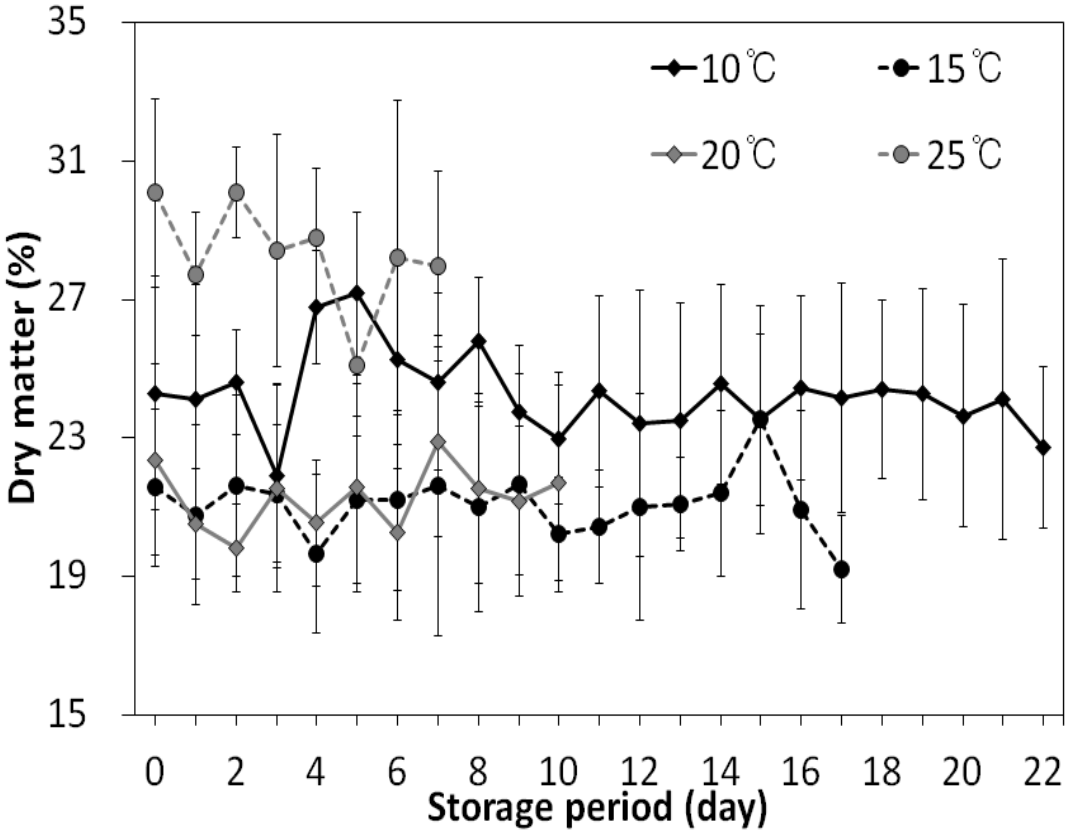

Fig. 3-10. The changes in DM of Hass avocado according to temperature conditions. Each value is the mean of 10 fruits assessed at each time, and is the mean ± standard deviation.

Table 3-8. DM of Hass avocado according to temperature conditions.

Storage period	Temperature			
	10℃	15℃	20℃	25℃
0	24.29 ± 3.39[a,b]	21.56 ± 2.26[a,b]	22.37 ± 2.76[a]	30.08 ± 2.72[a]
1	24.13 ± 3.30[a,b]	20.77 ± 2.59[a,b]	20.53 ± 1.60[a]	27.74 ± 1.79[a,b]
2	24.60 ± 1.50[a,b]	21.62 ± 2.61[a,b]	19.80 ± 1.26[a]	30.10 ± 1.30[a]
3	21.91 ± 2.66[b]	21.39 ± 1.97[a,b]	21.54 ± 2.98[a]	28.41 ± 3.37[a,b]
4	26.79 ± 1.63[a]	19.65 ± 2.29[a,b]	20.55 ± 1.81[a]	28.79 ± 2.00[a,b]
5	27.17 ± 2.35[a]	21.20 ± 2.41[a,b]	21.56 ± 3.01[a]	25.12 ± 2.06[b]
6	25.25 ± 3.14[a,b]	21.20 ± 2.60[a,b]	20.26 ± 2.55[a]	28.20 ± 4.55[a,b]
7	24.62 ± 2.56[a,b]	21.63 ± 4.33[a,b]	22.89 ± 2.74[a]	27.96 ± 2.75[a,b]
8	25.79 ± 1.86[a,b]	21.00 ± 3.03[a,b]	21.54 ± 2.73[a]	
9	23.76 ± 1.89[a,b]	21.64 ± 3.22[a,b]	21.18 ± 2.15[a]	
10	22.99 ± 1.91[a,b]	20.21 ± 1.67[a,b]	21.71 ± 2.83[a]	
11	24.36 ± 2.76[a,b]	20.44 ± 1.64[a,b]		
12	23.41 ± 3.86[a,b]	20.99 ± 3.28[a,b]		
13	23.49 ± 3.40[a,b]	21.07 ± 1.35[a,b]		
14	24.54 ± 2.89[a,b]	21.40 ± 2.39[a,b]		
15	23.53 ± 2.47[a,b]	23.53 ± 3.29[a]		
16	24.45 ± 2.65[a,b]	20.93 ± 2.88[a,b]		
17	24.15 ± 3.31[a,b]	19.20 ± 1.57[b]		
18	24.40 ± 2.58[a,b]			
19	24.27 ± 3.05[a,b]			
20	23.64 ± 3.21[a,b]			
21	24.11 ± 4.06[a,b]			
22	22.71 ± 2.33[a,b]			

Each value is the mean of 10 fruits, and is the mean ± standard deviation.
Means with different letters (a-b) indicate significant differences based on Tukey-Kramer's multiple range test (p<0.05).

3.5.6. Relationship between ripening indices and color features

To obtain the best set of color features for predicting avocado ripening, the relationship between the ripening indices of Hass avocados and color features extracted from RGB images were analyzed, and the results are shown in Table 3-9.

Significant correlations were observed between the ripening indices and color features at 99 and 95%. These results suggest that there were good agreements between quality indices and some of color features. In this study, nine color features (i.e., *L*a*b**, LUV, and YUV) were selected as input data to develop ripening-index estimation models.

Table 3-9. Relationship between color feature values extracted from RGB images and quality indices of Hass avocado.

	R	G	B	H	S	V	*L**	*a**	*b**	L	U	V	Y	U	V
Firmness	0.05	0.48**	0.04	-0.36**	0.66**	0.38**	0.40**	-0.79**	0.69**	0.40**	-0.79**	0.71**	0.34**	-0.66**	-0.80**
pH	0.00	-0.17**	-0.01	0.18**	-0.25**	-0.13**	-0.14**	0.32**	-0.26**	-0.14**	0.32**	-0.27**	-0.12**	0.25**	0.33**
DM	0.00	0.03	0.09*	-0.01	-0.13**	0.01	0.03	-0.02	-0.09*	0.03	-0.07	-0.08	0.03	0.10*	-0.09*

** Correlation is significant at the .01 level (2-tailed).
* Correlation is significant at the .05 level (2-tailed).

3.5.7. Prediction models

Table 3-10 shows the R^2, RMSE, and RPD obtained for each quality index, and Table 3-11 shows the optimal network topology for each ANN model. As can be seen in Table 3-10, the color-feature-based ANN model successfully predicted all quality indices based on features, because the changes in peel color during ripening provided a more significant feature difference in appearance compared with those provided by local shape and texture (Zhuang et al., 2019). When using the color-feature-based ANN model, firmness was predicted with R^2 value of 0.84 and an RMSE of 573.2 kPa. However, the color feature-based ANN model was not suitable for predicting pH and DM. Meanwhile, the RPD values were 2.48, 1.00, and 1.00 for firmness, pH, and DM, respectively. A higher RPD values indicate better predictive ability, and an RPD value of 2.0 or greater is an excellent prediction model (Bellon-Maurel et al., 2010). Thus, the color-feature-based ANN model predicted the firmness of the Hass avocado with high accuracy regardless of ripening conditions. However, it could not predict the pH and DM.

For this reason, I applied the firmness prediction model to clearly classify the ripening stage of Hass avocado into three levels: unripe, ripe, and overripe. The ANN model could classify the ripening stages with an accuracy of 71.67% and an F1-score of 0.716.

Table 3-10. Results of ANN for predicting the quality indices of Hass avocado.

Quality indices	Feature	Train set		Test set		RPD
		R^2	RMSE	R^2	RMSE	
Firmness	Color	0.84	541.1	0.84	573.2	2.48
	Hu moments	0.53	993.5	0.65	923.4	1.54
	Haralick	0.92	464.0	0.75	823.8	1.72
pH	Color	0.34	0.10	0.30	0.09	1.20
	Hu moments	0.19	0.10	0.18	0.10	1.09
	Haralick	0.14	0.15	0.10	0.16	0.71
DM	Color	0.28	3.22	0.05	3.67	0.92
	Hu moments	0.04	3.66	0.02	3.35	1.00
	Haralick	0.27	3.20	0.20	3.04	1.10

R^2: Coefficient of determination, RMSE: Root mean square error, RPD: Ratio of performance to deviation, DM: Dry matter

Table 3-11. Optimal network topology for each ANN model.

Quality indices	Features	Network structure	Batch size	Epochs	Optimizer	Learning rate	Activation function
Firmness	Color	9-64-8-1	40	2000	Nadam	0.003	ReLU
	Hu moments	21-256-32-1	40	2000	Nadam	0.5	ReLU
	Haralick	39-256-8-1	40	1500	Adadelta	0.5	Softplus
pH	Color	9-8-128-64-1	40	2000	Adam	0.01	ReLU
	Hu moments	21-16-64-8-1	80	2000	Adam	0.05	ReLU
	Haralick	39-8-1024-16-1	40	2000	Adam	0.01	ReLU
DM	Color	9-8-256-32-1	40	1500	Adam	0.003	ReLU
	Hu moments	21-64-256-64-1	80	1500	Adam	0.001	ReLU
	Haralick	39-8-64-1	40	1500	Adam	0.001	ReLU

DM: Dry matter

3.6. Conclusion

This study investigated the importance of different external properties (i.e., color, Hu-moments, and Haralick features) for predicting the quality indices and classifying the ripening stages of the Hass avocado. The color-feature-based ANN model successfully predicted the firmness of the Hass avocado with an R^2 value of 0.84 and an RMSE of 573.2 kPa. Furthermore, the firmness prediction model classified the ripening stages of the Hass avocado into three levels (i.e., unripe, ripe, and overripe) with an accuracy of 71.67% and an F1-score of 0.716. Therefore, the smartphone CVS aided by the color-feature-based ANN is a useful tool for predicting the firmness or ripening stage of the Hass avocado in the lab.

Chapter 4 Development of prediction model of Cavendish banana quality indices and ripening stages using ANN

4.1. Introduction

The banana (*Musa* AAA) is one of the most popular fruits in the world and is the main fruit of international trade. Global banana production resulted in approximately 116-million tons transferred in 2018, predominantly produced in Asia, Latin America, and Africa (FAO STAT, 2020). Because the banana is a climacteric fruit, it is typically harvested unripe and is ripened during storage and distribution. Suitable temperature, humidity, and time are all needed for this process, during which, the banana undergoes changes in chemical and physical properties. It softens, starch is converted into sugar, and the peel color changes from green to yellow (Kajuna et al., 1997; Gomes et al., 2013). In particular, temperature considerably affects ripening, and an increase in storage temperature enhances the rate of ripening and softening (Ahmad et al., 2001). However, when ripening at temperatures above 24℃, bananas fail to fully develop their yellow peel and instead retain high levels of chlorophyll (Blackbourn et al., 1990; Yang et al., 2009). RH also has a great effect on banana ripening. When ripening in a low RH, banana peels dry to a black color, negatively affecting consumer choices (Wills et al., 1989). As such, environmental factors, such as temperature and RH, should be controlled during storage and ripening. However, there is no standard storage condition for bananas. However, temperatures of 16–24℃ and an RH of 85–95% are suggested. These variables affect ripening times and banana quality. Therefore, to guarantee high quality, a postharvest management technology is needed to predict the ripening stage and quality indices regardless of ripening conditions.

Over the past few decades extensive studies have been conducted on the development

of non-destructive methods for the quality evaluation of bananas. This has entailed the use of near infrared spectroscopy (Jaiswal et al., 2012; Liew and Lau, 2012; Rajkumar et al., 2012; Chowdhury et al., 2015). Recent studies have attempted to determine fresh banana ripeness using digital images and ML models (El-Bendary et al., 2015; Sanaeifar et al., 2016; Mohapatra et al., 2017; Castro et al., 2019; Maimunah et al., 2019; Zhuang et al., 2019; Cho et al., 2020). Sanaeifar et al. (2016) analyzed the relationship between the color features of a banana peel and the quality indices of the pulp, reporting that the internal quality of banana, including firmness, TSS, pH, and TA, could be predicted with support vector regression. Mohapatra et al. (2017) applied the dielectric-properties measurement technique and image processing to assess the ripening of red bananas. Maimunah et al. (2019) used digital images and ANNs to classify banana ripening stages into three levels with an accuracy of 95.24%. However, because most studies have developed prediction models for banana ripening stages or quality indices based on changes in chemical and physical properties under only one ripening condition, those models are difficult generalize to the full variety of storage/ripening conditions.

Therefore, I investigated the changes in the chemical and physical properties of the Cavendish banana under different temperatures and RH conditions to develop a predictive model that can predict ripening stages and quality indices regardless of storage conditions. I also applied image-processing techniques and an ANN to develop the optimal banana ripening-stage/quality index prediction model.

4.2. Materials and methods

4.2.1. Banana sampling

A total of 710 unripe Cavendish bananas imported from Philippines by a Japanese company were used in this study. Bananas without damage were selected and stored at 20, 25, 27.5, and 30℃ at 90% RH and at RHs of 50, 70, and 90% at 20℃, as suggested previously (Akkaravessapong et al., 1992; Ahmad et al., 2001; Rajkumar et al., 2012; Xie et al., 2018). The changes of bananas at different ripening stages were measured each day, and 10 bananas were used for each experiment.

Fig. 4-1. Cavendish banana used in this study.

4.2.2. Weight loss

Ten bananas were used to determine weight loss, and they were measured each day to compare the initial weight to that after ripening. This provides the percentage loss of initial weight (Eq. 4-1):

$$\boldsymbol{Weight\ loss}\ (\%) = \frac{\boldsymbol{W_i - W_f}}{\boldsymbol{Wi}} \times \mathbf{100}, \qquad \text{(Eq. 4-1)}$$

where $\boldsymbol{W_i}$ and $\boldsymbol{W_f}$ denote initial weight and weight after storage and ripening, respectively.

4.2.3. Peel color

Peel color characteristics of Cavendish bananas were assessed using a portable colorimeter (CR-400, KONICA MINOLTA, Tokyo, Japan), calibrated using a standard white plate (Y = 85.4, x = 0.3173, and y = 0.3240). Each sample was measured three times, and the color values were expressed as *L*a*b** values. Each value ranged from 0 to 100 (*L**) and from -127 to 127 (*a** and *b**) (Cho et al., 2016), and the color values of each sample were averaged.

4.2.4. Firmness

The firmness of the banana pulp was measured until tissue failure using a tabletop universal testing instrument (EZ-SX, SHIMADZU, Kyoto, Japan) employing a cylindrical probe having a diameter of 10 mm and a crosshead loading rate of 50 mm/min (Sanaeifar et al., 2016). Each banana fruit was measured three times and was averaged. The firmness of the banana pulp was expressed as maximum kPa.

4.2.5. TSS

The TSS of bananas pulp was measured by dividing the fruit into three equal parts

lengthwise. 10 g samples were collected fresh and diluted in 50 g distilled water in a homogenizer (HG-92G, TAITEC, Koshigaya, Japan) at 10,000 rpm for 2 min (Soltani et al., 2011). The banana juice was filtered each time through a new piece of experimental tissue to avoid suspended solids. The TSS of the filtered juice was determined using a refractometer (PAL-S, ATAGO, Tokyo, Japan) (Jha and Matsuoka, 2004; Jaiswal et al., 2012), and the TSS values of each sample were averaged.

4.2.6. pH value

The pH value of banana pulp was measured by dividing the fruit into three equal parts lengthwise. 10 g samples were collected from banana pulp and diluted in 50 g distilled water in a homogenizer (HG-92G, TAITEC, Koshigaya, Japan) at 10,000 rpm for 2 min (Soltani et al., 2011). The banana juice was filtered each time through a new piece of experimental tissue to minimize suspended solids (Jha and Matsuoka, 2004; Jaiswal et al., 2012). The pH value of the filtered juice was determined using a pH meter (D-51, HORIBA, Kyoto, Japan), and the pH values of each sample were averaged.

4.2.7. Ratio of pulp to peel

Bananas were peeled, and the pulp and peel portions of each were weighed separately on an electronic scale (BP3100S, Sartorius, Göttingen, Germany). The ratio of the pulp-to-peel of each banana was calculated as pulp weights relative to peel weights and averaged (Srivastava and Dwivedi, 2000).

4.2.8. MC

The moisture content (MC) content of the banana pulp was determined using hot-air oven method (AOAC, 1990). Three equal portions (lengthwise) of each banana were weighed separately on an electronic scale (BP3100S, Sartorius, Göttingen, Germany) of 5±0.5 g and were dried using the dry oven at 70℃ for 24 h. MC is expressed based on the weight of wet matter by the weight change before and after drying using Eq. 4-2. The MC values were then averaged.

$$\boldsymbol{Moisture\ content}\ (\%) = \frac{\boldsymbol{W_f - W_d}}{\boldsymbol{W_f}} \times \mathbf{100}, \qquad \text{(Eq. 4-2)}$$

where $\boldsymbol{W_f}$ is the fresh weight of sample, and $\boldsymbol{W_d}$ is the dry weight of the sample.

4.3. Image processing

Image processing was used to extract features from the banana samples, and Fig. 4-2 shows the related flow diagram. In this study, acquired images were processed using Scikit-image and OpenCV Python libraries (Van der Walt et al., 2014; Mustaffa and Khairul, 2017). Before processing, all images were rescaled to 816×612 pixels while maintaining the aspect ratio using the Scikit-image library.

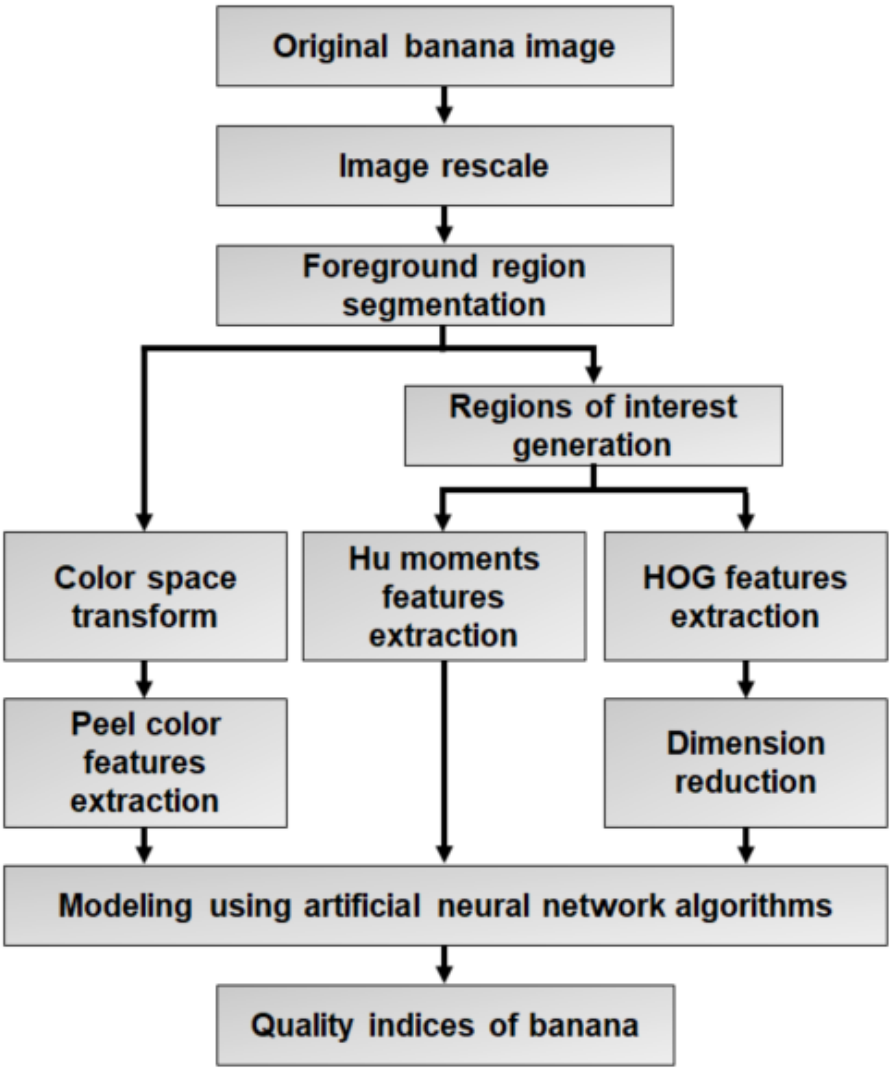

Fig. 4-2. Flow diagram of the image processing for Cavendish banana.

4.3.1. Sample segmentation

The banana samples were separated from the background using K-means clustering (Fig. 4-3). The number of clusters was two, because the banana images were divided into two parts: sample and background. RGB images were transformed to HSV, and the S-channel image was extracted as the initial clustering sample. Thus, the initial clustering centers were determined from the color histogram of the S-channel image using the K-means algorithm (Chen et al., 2008; Aravind et al., 2010). The Euclidean distance was

adopted as the distance criterion, and the clustering centers were constantly updated by minimizing the objective function via multiple iterations. When the cluster centers stop updating, it means that the cluster process has completed (Hu et al., 2014; Li et al., 2015). A color-inverse transition was performed on the binary images obtained from the above process, which made the background and banana sample pixels equal to 0 and 1, respectively, and any holes in sample surface were removed. The binary image without background and original RGB image were overlapped using the logical AND operator. Thus, the background and banana sample formed an RGB image with zeros and color values, respectively.

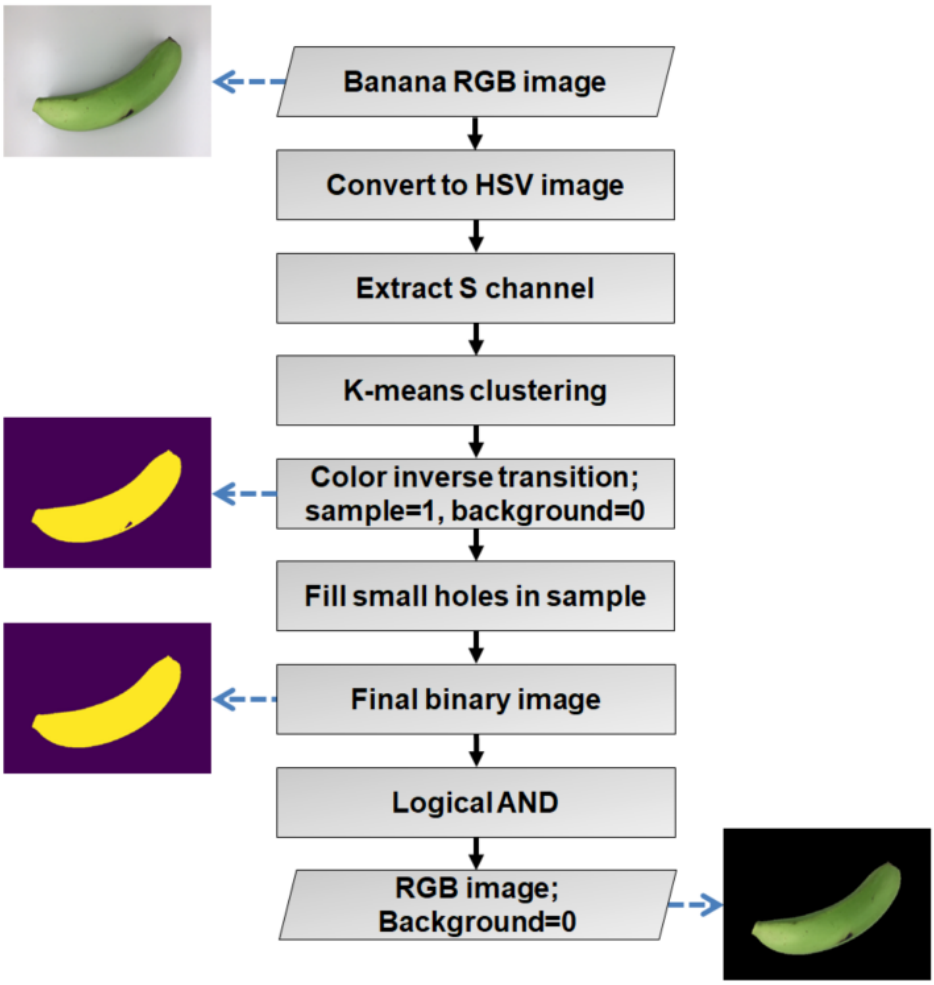

Fig. 4-3. Flow diagram of the algorithm employed for foreground region segmentation for Cavendish banana.

4.3.2. Feature extraction

The external optical characteristics of bananas, including color and shape features that were observed from samples belonging to various ripening stages, were potential criteria for identifying different ripening stages. For example, the shape feature is significantly affected by the distribution of brown spots on the peel at higher ripening stages (Zhuang et al., 2019). Thus, I extracted those features from banana images and used them as input data.

Three ROIs were sampled and extracted from the banana sample using the process shown in Fig. 4-4. The sizes of each ROI were assigned to 48×48 pixels to simplify feature extraction. The location of each ROI was calculated by

$$\boldsymbol{ROI_1 = P_{Center} - \frac{Y_v}{3} - 48_h,} \quad \text{(Eq. 4-3)}$$

$$\boldsymbol{ROI_2 = P_{Center} - 48_h,} \quad \text{(Eq. 4-4)}$$

$$\boldsymbol{ROI_3 = P_{Center} + \frac{Y_v}{3},} \quad \text{(Eq. 4-5)}$$

where $\boldsymbol{P_{center}}$ is the center coordinate of banana sample, and $\boldsymbol{Y_v}$ is the vertical length. $\boldsymbol{48_h}$ means to move 48 pixels horizontally.

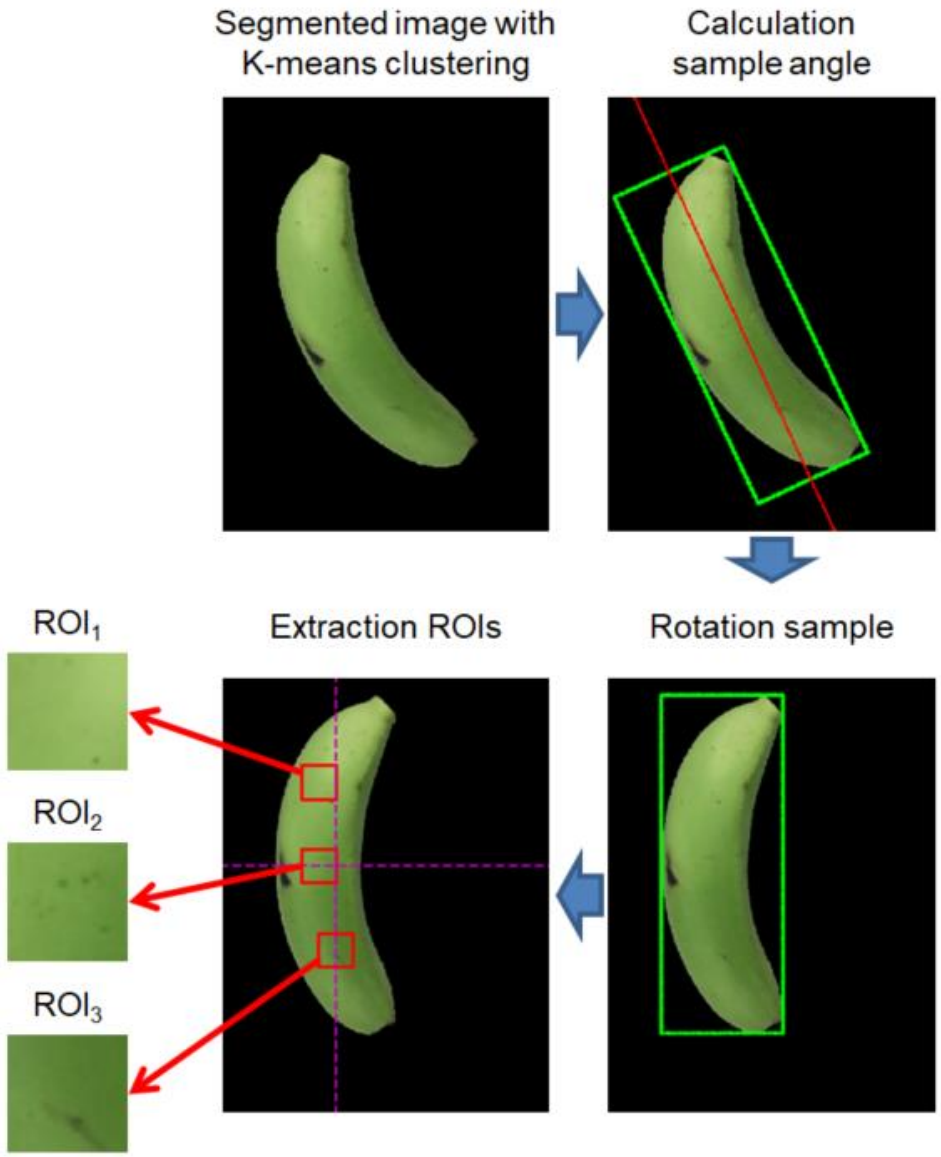

Fig. 4-4. Location of three ROIs from the segmented banana region.

4.3.2.1. Color-feature extraction

All images were converted from RGB to several color spaces (i.e., RGB, *L*a*b**, HSV, YUV, and XYZ) using the Scikit-image library function. RGB images were specified by three values, one each for red, blue, and green components of the pixel scalar (Tumar and Verma, 2010).

In *L*a*b** color space, the *L** value refers to lightness from black (0) to white (100). The *a** and *b** values express the hue of the color from green (−) to red (+), and from blue (−) to yellow (+), respectively (Bell et al., 2009). HSV provides pure color information (Zhuang et al., 2019). In the YUV color space, the Y value describes the intensity of light, and U and V values describe the color information as blue and red, respectively (Podpora et al., 2014). The XYZ color space encompasses all color sensations that are visible to a person having average eyesight and has a linear relationship with non-gamma-corrected RGB (Asmare et al., 2009).

RGB, *L*a*b**, HSV, YUV, and XYZ color features were extracted from the whole banana sample, and the average intensity of all pixels in each color space was calculated. All feature values obtained from the different color spaces were analyzed for correlation to each quality index (e.g., firmness, TSS, pH value, ratio of pulp to peel, and MC).

4.3.2.2. Hu-moment feature extraction

The Hu-moment method was used to characterize the outline or silhouette of an object in an image. ROIs were converted from RGB images to gray-scale, because the Hu-moment method requires a single-channel image. To calculate the Hu moments, the original 24 moments were calculated from each ROI to Hu's seven invariant moments (Eqs. 4-6 to 4-12) after which, the obtained array was flattened to form the shape feature vector (Leiva-Valenzuela and Aguilera, 2013). Therefore, the Hu-moment feature having seven dimensions was extracted from each ROI, and the three shape features generated from the ROIs were successively concatenated into a Hu-moment feature vector having 21-dimension.

$$HU_1 = \eta_{20} - \eta_{02}, \quad \text{(Eq. 4-6)}$$

$$HU_2 = (\eta_{20} - \eta_{02})^2 + (2\eta_{11})^2, \quad \text{(Eq. 4-7)}$$

$$HU_3 = (\eta_{30} - 3\eta_{12})^2 + (3\eta_{21} - \eta_{03})^2, \quad \text{(Eq. 4-8)}$$

$$HU_4 = (\eta_{30} + \eta_{12})^2 + (\eta_{21} + \eta_{03})^2, \quad \text{(Eq. 4-9)}$$

$$HU_5 = (\eta_{30} - 3\eta_{12})(\eta_{30} + \eta_{12})[(\eta_{30} + 3\eta_{12})^2 - 3(\eta_{21} - \eta_{03})^2] + (3\eta_{21} - \eta_{03})(\eta_{21} + \eta_{03})[3(\eta_{30} + \eta_{12})^2 - (\eta_{21} + \eta_{03})^2], \quad \text{(Eq. 4-10)}$$

$$HU_6 = (\eta_{20} - \eta_{02})[(\eta_{30} + \eta_{12})^2 - (\eta_{21} - \eta_{03})^2] + 4\eta_{11}(\eta_{30} + \eta_{12})(\eta_{21} + \eta_{03}), \quad \text{(Eq. 4-11)}$$

$$HU_7 = (3\eta_{21} - \eta_{03})(\eta_{30} + \eta_{12})[(\eta_{30} + \eta_{12})^2 - 3(\eta_{21} + \eta_{03})^2] - (\eta_{30} - 3\eta_{12})(\eta_{21} + \eta_{03})[3(\eta_{30} + \eta_{12})^2 - (\eta_{21} + \eta_{03})^2], \quad \text{(Eq. 4-12)}$$

$$\eta_{ij} = \frac{\mu_{ij}}{\mu_{00}^{(i+j)/2+1}}, \quad \text{(Eq. 4-13)}$$

where η_{ij} and μ_{00} are the central moments, and *i* and *j* describe the pixel position of the segmented image.

4.3.2.3. Histogram of oriented gradients (HOG) feature extraction

The shape of the banana peel can be influenced by the increase in the ripening stage. For example, the change in the gray-level intensity discontinuity across adjacent ripening stages can influence the distribution of local intensity gradients. Thus, the HOG feature was adopted (Dalal and Triggs, 2005; Déniz et al., 2011; Zhuang et al., 2019). The main

idea of HOG is that local shape information can be well-explained by calculating the local edge directions and intensity gradient distributions on dense grids (Dalal and Triggs, 2005; Rybski et al., 2010; Zhuang et al., 2019).

When extracting HOG features, I used the proposed method from a previous study (Zhuang et al., 2019). Fig. 4-5 shows the visualization of the HOG features for each banana ROI. Each ROI was divided into 12×12 cells and 2×2 adjacent cells, forming an image block. Thus, 3×3 blocks were generated. The Prewitt operator was used to calculate the gradients of the pixels within each cell, and the magnitude of the gradients was cumulatively voted into nine uniformly spaced bins from 0 to **π**, depending on the direction of the gradient. Thus, each block generated a 36-dimension histogram that was normalized using the L1-normalization method. Therefore, a 324-dimension HOG feature was extracted from each ROI, and the three shape features generated from three ROIs were successively concatenated into a 972-dimension HOG.

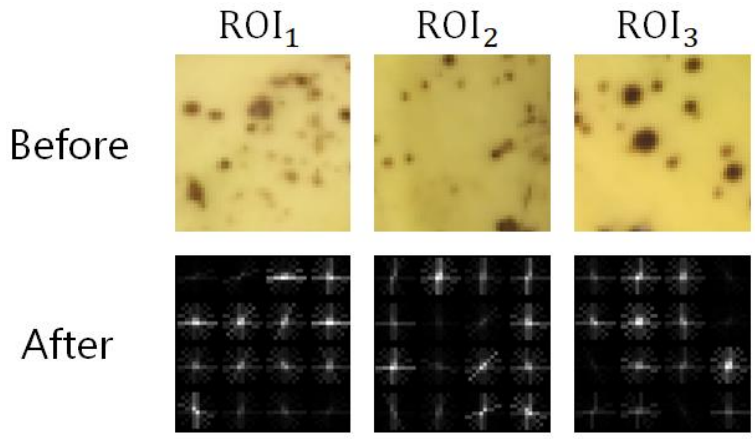

Fig. 4-5. The visualization of the HOG features with ROIs.

4.4. Data analysis

I used the ANN to analyze the collected data. Python 3.7 was used for data analysis, and the ANN model was implemented using the Keras library (Gulli and Pal, 2017).

4.4.1. ANN

ANNs generate batch sizes, epochs, optimizer, and activation hyperparameters during the training process. The hyperparameter's value is used to control the learning process, which must be tuned so that the ANN can optimally solve the problem. A grid search is the traditional method of performing hyperparameter optimization, which involves exhaustive searches through a manually specified subset of the hyperparameter space of a learning algorithm. The grid search must be guided by some performance metric typically measured via cross-validation of the training set (Hsu et al., 2010). The cross-validation is often used to estimate the generalization performance of the ML model (Bergstra and Bengio, 2012). In this study, I applied both the grid-search algorithm and five-fold cross-validation method for developing the optimal ANN model (Fig. 4-6).

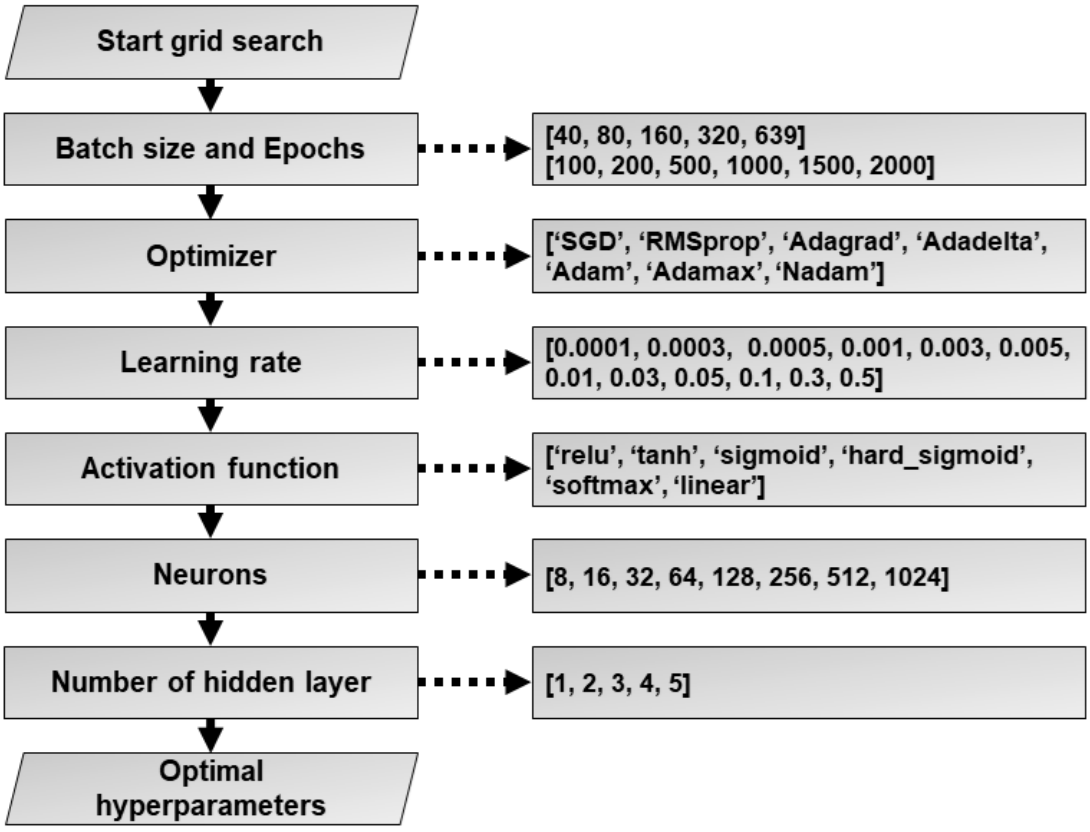

Fig. 4-6. Flow diagram for optimal hyperparameters selection of ANN.

4.4.2. Model evaluation

The entire dataset containing a total of 710 images was randomly divided into two: a training set (90%, 639 images) and a testing set (10%, 71 images). The training set was used to develop an estimation model of banana quality indices, and the testing set was used to validate the developed model. The developed ANN models were verified by several actions, including R^2, RMSE, and RPD.

The R^2 value measures the agreement between the predicted and measured values and was calculated using Eq. 4-6. The R^2 values range from 0 to 1, where 1 of R^2 value indicates a perfect linear relationship between the predicted and measured values (Porep et al., 2015).

$$\boldsymbol{R^2 = 1 - \frac{\sum_{i=1}^{n}(P_i - M_i)^2}{\sum_{i=1}^{n} M_i^2}}, \qquad \text{(Eq. 4-6)}$$

where $\boldsymbol{P}$ is the predicted value, and $\boldsymbol{M}$ is the measured value.

The RMSE was chosen to assess the difference between the measured and predicted values, calculated using Eq. 4-7.

$$\boldsymbol{RMSE = \sqrt{\frac{1}{n}\sum_{i=1}^{n}(P_i - M_i)^2}}, \qquad \text{(Eq. 4-7)}$$

Three RPD values were chosen to define the ability of the model to predict future data and was determined using Eq. 4-8. A higher RPD value indicates better predictive ability (Prieto et al., 2017; Díaz et al., 2019).

$$\boldsymbol{RPD = \frac{SD}{RMSE}}, \qquad \text{(Eq. 4-8)}$$

where $\boldsymbol{SD}$ is the standard deviation of measured values.

An F1-score was also calculated to evaluate the classification performance of the ANN model (Eq. 4-11):

$$\boldsymbol{Precision} = \frac{\boldsymbol{TP}}{\boldsymbol{TP} + \boldsymbol{FP}}, \qquad \text{(Eq. 4-9)}$$

$$\boldsymbol{Recall} = \frac{\boldsymbol{TP}}{\boldsymbol{TP} + \boldsymbol{FN}}, \qquad \text{(Eq. 4-10)}$$

$$\boldsymbol{F1\ score} = \frac{\boldsymbol{2} \times (\boldsymbol{Precision} \times \boldsymbol{Recall})}{\boldsymbol{Precision} + \boldsymbol{Recall}}, \qquad \text{(Eq. 4-11)}$$

where $\boldsymbol{TP}$ is the number of true positives, and $\boldsymbol{FP}$ and $\boldsymbol{FN}$ are the number of false positives and false negatives, respectively.

4.4.3. Statistical analysis

Correlation and statistical analyses were conducted using a bivariate analysis and one-way ANOVA, respectively. IBM SPSS (v.20.0, IBM, Armonk, USA) was used to analyze the significance in this study.

The correlation coefficient (R) between quality indices and color features was determined using the Pearson's test. Differences according to storage period were established using the Tukey–Kramer multiple range test with a significance level of $p < 0.05$.

4.5. Results and discussion

4.5.1. Weight loss

Figures 4-7 shows the changes in weight loss of bananas at different (a) temperatures and (b) RHs, respectively. Weight loss by transpiration during ripening was observed in all storage conditions. The weight-loss rate was increased by the higher temperature and the lower RH. The increase in weight loss at high temperature or low RH was caused by the increase of transpiration (Ding et al., 1998; Jiang and Fu, 1999; Javanmardi and Kubota, 2006).

Postharvest fruits and vegetables are susceptible to water loss, which reduces their quality and marketability (Huang and Jiang, 2012; Silva et al., 2017). Weight loss is caused by the breakdown of cell walls and the increase in permeability of the outer cell layers caused by water vapor. Eventually, the invasion by micro-organisms leads to progressive decay, which can affect the entire fruit (Dadzie and Orchard, 1997). Therefore, the weight loss of bananas should be minimized and managed during ripening and shipping to reduce the development of physiological disorders (Huang and Jiang, 2012). It is desirable to store them at below 25℃ and over 90% RH to prevent weight loss.

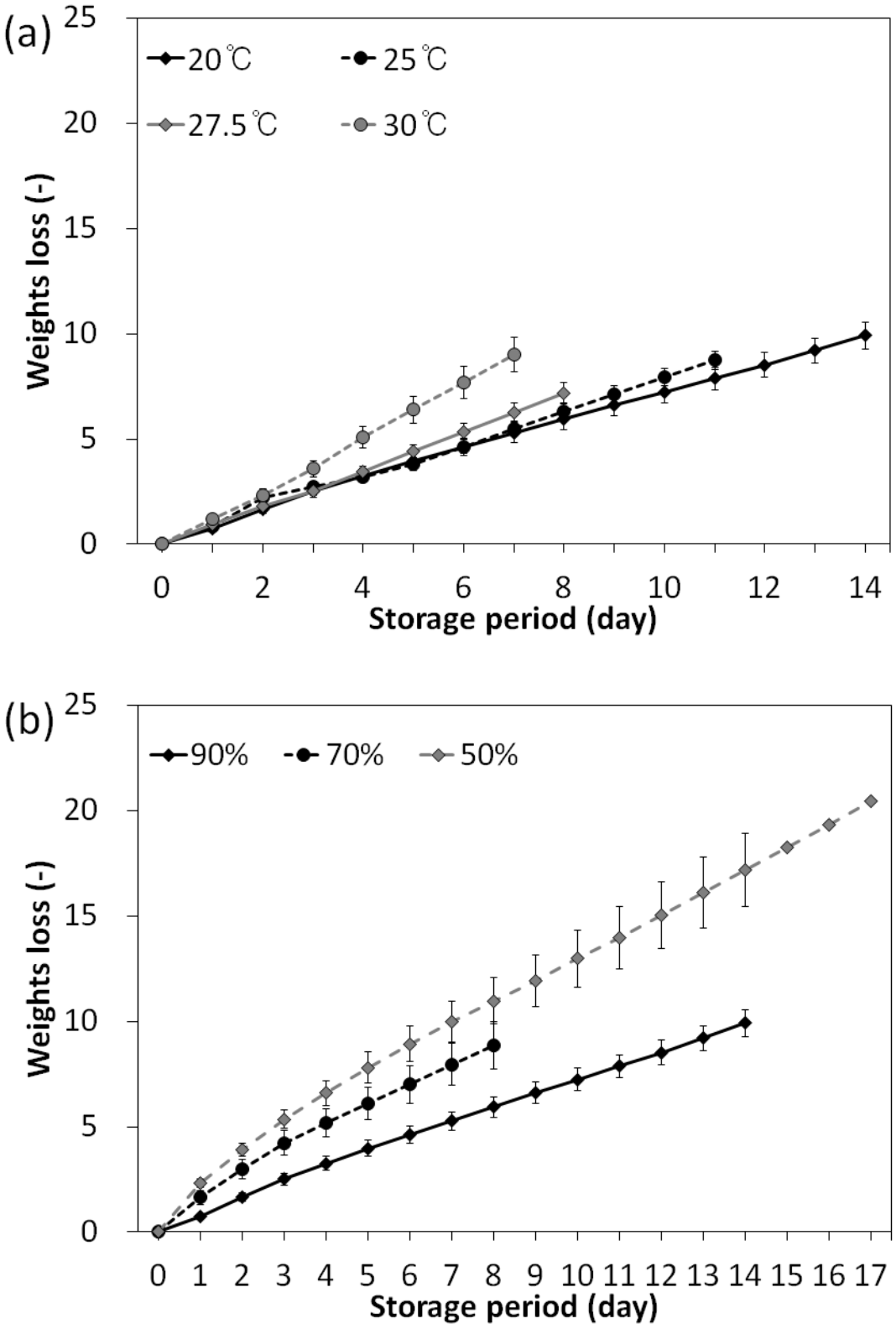

Fig. 4-7. The changes in weight loss of Cavendish banana according to (a) temperature and (b) RH conditions. Each value is the mean of 10 fruits assessed at each time, and is the mean ± standard deviation.

Table 4-1. Weight loss of Cavendish banana according to temperature conditions.

Storage period	Temperature			
	20℃	25℃	27.5℃	30℃
0	0.00	0.00	0.00	0.00
1	0.75 ± 0.08^{m}	0.82 ± 0.10^{j}	0.95 ± 0.09^{h}	1.20 ± 0.17^{g}
2	1.67 ± 0.20^{l}	2.20 ± 0.21^{i}	1.80 ± 0.15^{g}	2.34 ± 0.27^{f}
3	2.51 ± 0.29^{k}	2.72 ± 0.24^{i}	2.54 ± 0.21^{f}	3.59 ± 0.39^{e}
4	3.26 ± 0.35^{j}	3.21 ± 0.28^{h}	3.44 ± 0.28^{e}	5.07 ± 0.51^{d}
5	3.98 ± 0.39^{i}	3.81 ± 0.30^{g}	4.41 ± 033^{d}	6.40 ± 0.64^{c}
6	$4.63 \pm 0.42^{h,i}$	4.64 ± 0.32^{f}	5.35 ± 0.39^{c}	7.68 ± 0.76^{b}
7	$5.27 \pm 0.43^{g,h}$	5.49 ± 0.35^{e}	6.26 ± 0.45^{b}	9.01 ± 0.84^{a}
8	$5.94 \pm 0.47^{f,g}$	6.32 ± 0.38^{d}	7.16 ± 0.51^{a}	
9	$6.60 \pm 0.50^{e,f}$	7.14 ± 0.40^{c}		
10	$7.25 \pm 0.53^{d,e}$	7.94 ± 0.42^{b}		
11	$7.87 \pm 0.56^{c,d}$	8.74 ± 0.44^{a}		
12	$8.52 \pm 0.58^{b,c}$			
13	9.19 ± 0.59^{b}			
14	9.91 ± 0.62^{a}			

Each value is the mean of 10 fruits, and is the mean $\pm$ standard deviation.
Means with different letters (a-m) indicate significant differences based on Tukey-Kramer's multiple range test ($p<0.05$).

Table 4-2. Weight loss of Cavendish banana according to RH conditions.

Storage period	Relative humidity		
	50%	70%	90%
0	0.00	0.00	0.00
1	2.34 ± 0.21^{o}	1.64 ± 0.32^{g}	0.75 ± 0.08^{m}
2	$3.89 \pm 0.31^{n,o}$	2.97 ± 0.46^{f}	1.67 ± 0.20^{l}
3	$5.35 \pm 0.44^{m,n}$	4.22 ± 0.58^{e}	2.51 ± 0.29^{k}
4	$6.60 \pm 0.59^{l,m}$	$5.17 \pm 0.67^{d,e}$	3.26 ± 0.35^{j}
5	$7.81 \pm 0.73^{k,l}$	$6.10 \pm 0.78^{c,d}$	3.98 ± 0.39^{i}
6	$8.93 \pm 0.86^{j,k}$	$7.01 \pm 0.89^{b,c}$	$4.63 \pm 0.42^{h,i}$
7	$9.97 \pm 0.98^{i,j}$	$7.96 \pm 1.01^{a,b}$	$5.27 \pm 0.43^{g,h}$
8	10.96 ± 1.10^{i}	8.85 ± 1.12^{a}	$5.94 \pm 0.47^{f,g}$
9	$11.94 \pm 1.23^{h,i}$		$6.60 \pm 0.50^{e,f}$
10	$12.98 \pm 1.36^{g,h}$		$7.25 \pm 0.53^{d,e}$
11	$13.97 \pm 1.47^{f,g}$		$7.87 \pm 0.56^{c,d}$
12	$15.03 \pm 1.59^{e,f}$		$8.52 \pm 0.58^{b,c}$
13	$16.11 \pm 1.68^{d,e}$		9.19 ± 0.59^{b}
14	$17.19 \pm 1.76^{c,d}$		9.91 ± 0.62^{a}
15	$18.25 \pm 1.83^{b,c}$		
16	$19.36 \pm 1.90^{a,b}$		
17	20.44 ± 1.96^{a}		

Each value is the mean of 10 fruits, and is the mean $\pm$ standard deviation.
Means with different letters (a-o) indicate significant differences based on Tukey-Kramer's multiple range test (p<0.05).

4.5.2. Peel color

Figures 4-8 and 4-9 show the changes in the *L*a*b** values of the banana at different temperatures and RHs, respectively. The *L*a*b** values were determined using a portable colorimeter. Banana-peel colors change from green to yellow during ripening. Under all storage conditions, the *L*a*b** values increased as ripening progressed, but there was a decrease in the *L** and *b** values as senescence continued. The loss of green color was caused by the degradation of the chlorophyll structure in the peel (Dadzie and Orchard, 1997). Additionally, the peel-color change occurred more rapidly at higher temperatures. However, the peel color of bananas stored at 30℃ remained in the green color range, because, during ripening process at temperatures above 24℃, banana failed to develop a fully yellow peel, because the peel retained high levels of chlorophyll (Inaba et al., 1984; Blackbourn et al., 1990; Yang et al., 2009). Meanwhile, there was no significant difference during ripening under different RH conditions. In particular, under the 70% RH condition, the *L*a*b** value changed faster than in other conditions, caused by the ripening of bananas during distribution.

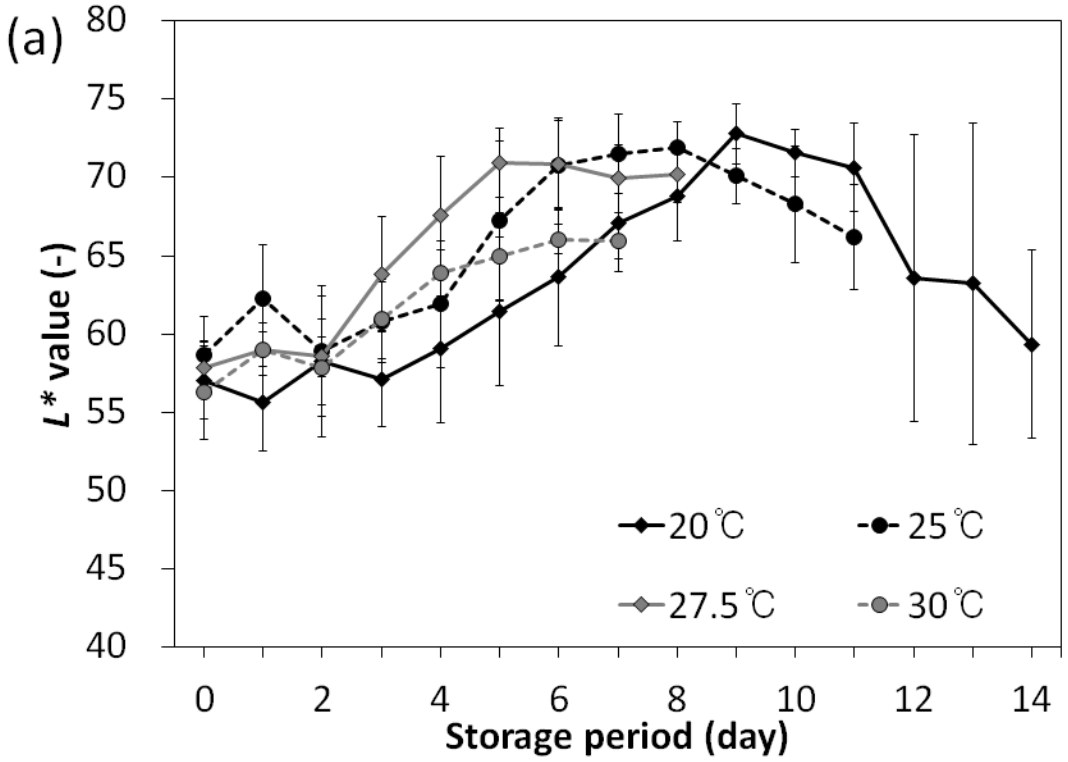
(a)
80
75
70
65
60
55
50
45
40
L* value (-)
20℃
25℃
27.5℃
30℃
0
2
4
6
8
10
12
14
Storage period (day)

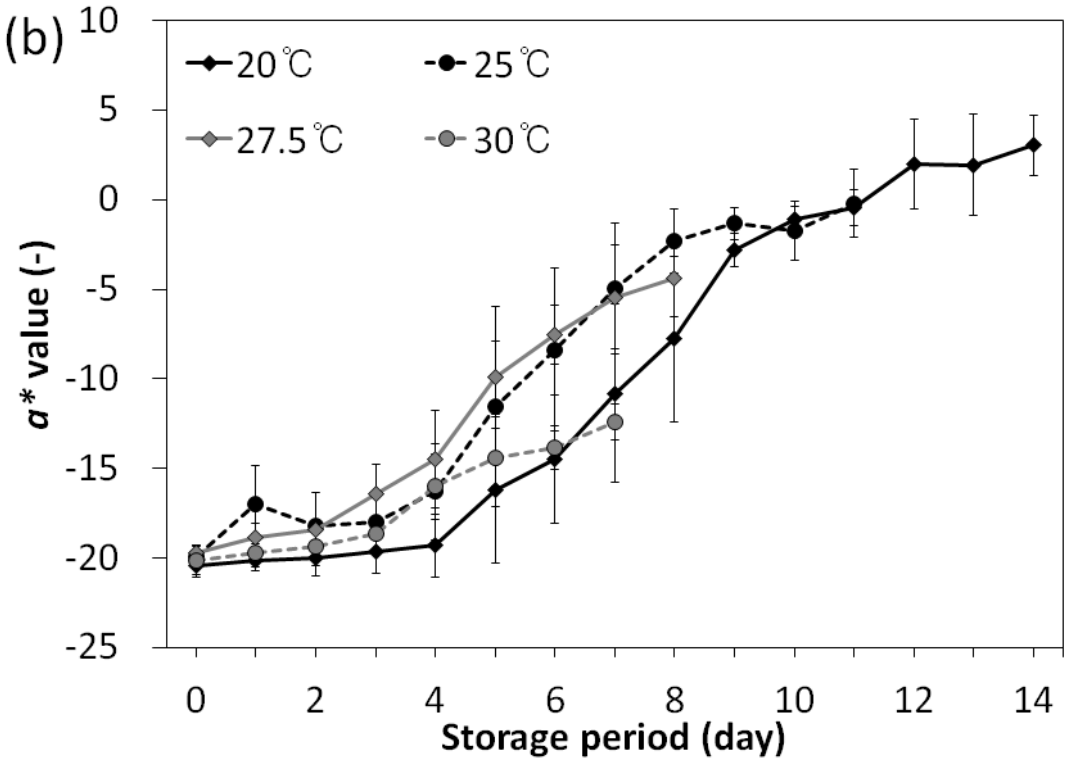
(b)
10
5
0
-5
-10
-15
-20
-25
a* value (-)
20℃
25℃
27.5℃
30℃
0
2
4
6
8
10
12
14
Storage period (day)

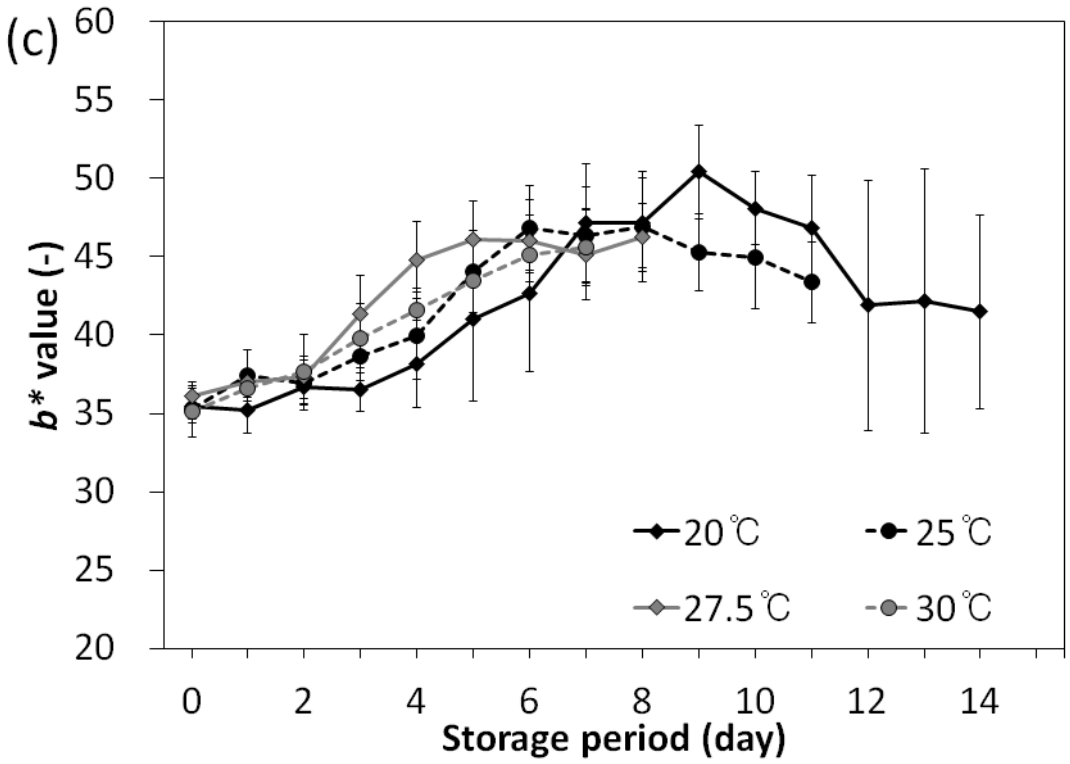

Fig. 4-8. The changes in *L*a*b of Cavendish banana according to temperature conditions determined by a portable colorimeter: (a) *L**, (b) *a**, and (c) *b** values. Each value is the mean of 10 fruits assessed at each time, and is the mean ± standard deviation.**

Table 4-3. *L value of Cavendish banana according to temperature conditions.**

Storage period	Temperature			
	20℃	25℃	27.5℃	30℃
0	57.06 ± 2.51^{d,e}	58.68 ± 2.46^{d}	57.85 ± 1.62^{c}	56.28 ± 2.96^{d}
1	55.63 ± 3.13^{e}	62.25 ± 3.46^{c,d}	59.03 ± 1.11^{c}	59.04 ± 1.68^{c,d}
2	58.26 ± 4.85^{d,e}	58.94 ± 3.48^{d}	58.56 ± 1.27^{c}	57.85 ± 3.13^{c,d}
3	57.09 ± 3.02^{d,e}	60.78 ± 2.56^{d}	63.86 ± 3.65^{b}	60.94 ± 2.52^{b,c}
4	59.06 ± 4.71^{d,e}	61.91 ± 4.07^{b,d}	67.60 ± 3.71^{a}	63.93 ± 1.46^{a,b}
5	61.43 ± 4.74^{c-e}	67.23 ± 5.11^{a,b}	70.93 ± 2.18^{a}	64.99 ± 2.79^{a}
6	63.63 ± 4.41^{b-d}	70.78 ± 2.84^{a,b}	70.87 ± 2.91^{a}	66.04 ± 0.94^{a}
7	67.10 ± 3.10^{a-c}	71.51 ± 2.51^{a}	69.92 ± 2.18^{a}	65.92 ± 1.13^{a}
8	68.78 ± 2.79^{a-c}	71.94 ± 1.65^{a}	70.22 ± 1.80^{a}	
9	72.78 ± 1.92^{a}	70.08 ± 1.77^{a,b}		
10	71.55 ± 1.53^{a}	68.29 ± 3.73^{a,b}		
11	70.64 ± 2.82^{a,b}	66.21 ± 3.36^{b,c}		
12	63.58 ± 9.12^{b-d}			
13	63.23 ± 10.25^{b-e}			
14	59.35 ± 5.98^{d,e}			

Each value is the mean of 10 fruits, and is the mean ± standard deviation.
Means with different letters (a-e) indicate significant differences based on Tukey-Kramer's multiple range test (p<0.05).

Table 4-4. *a value of Cavendish banana according to temperature conditions.**

Storage period	Temperature			
	20℃	25℃	27.5℃	30℃
0	-20.41 ± 0.65^{h}	-19.95 ± 0.57^{e}	-19.70 ± 0.45^{f}	-20.11 ± 0.82^{d}
1	-20.17 ± 0.59^{g,h}	-17.01 ± 2.17^{e}	-18.87 ± 0.80^{e,f}	-19.70 ± 0.83^{d}
2	-20.00 ± 1.03^{g,h}	-18.20 ± 1.82^{e}	-18.44 ± 0.55^{e,f}	-19.34 ± 1.11^{d}
3	-19.66 ± 1.22^{g,h}	-18.00 ± 1.68^{e}	-16.44 ± 1.66^{d,e}	-18.62 ± 0.90^{d}
4	-19.30 ± 1.74^{g,h}	-16.29 ± 2.69^{e}	-14.48 ± 2.70^{d}	-16.03 ± 1.85^{c}
5	-16.22 ± 4.08^{f,g}	-11.56 ± 5.57^{d}	-9.92 ± 2.05^{c}	-14.38 ± 1.60^{b,c}
6	-14.48 ± 3.60^{e,f}	-8.37 ± 4.53^{c,d}	-7.57 ± 1.65^{b,c}	-13.85 ± 1.19^{a,b}
7	-10.81 ± 4.99^{d,e}	-4.96 ± 3.68^{b,c}	-5.43 ± 2.90^{a,b}	-12.39 ± 1.02^{a}
8	-7.78 ± 4.61^{d}	-2.31 ± 1.79^{a,b}	-4.42 ± 2.14^{a}	
9	-2.80 ± 0.92^{c}	-1.34 ± 0.89^{a,b}		
10	-1.06 ± 0.71^{b,c}	-1.72 ± 1.64^{a,b}		
11	-0.43 ± 1.01^{a-c}	-0.21 ± 1.89^{a}		
12	1.96 ± 2.51^{a,b}			
13	1.93 ± 2.83^{a,b}			
14	3.03 ± 1.67^{a}			

Each value is the mean of 10 fruits, and is the mean ± standard deviation.
Means with different letters (a-h) indicate significant differences based on Tukey-Kramer's multiple range test (p<0.05).

Table 4-5. *b value of Cavendish banana according to temperature conditions.**

Storage period	Temperature			
	20℃	25℃	27.5℃	30℃
0	35.49 ± 1.11^{e,f}	35.28 ± 0.62^{d}	36.11 ± 0.90^{c}	35.14 ± 1.62^{e}
1	35.18 ± 1.48^{e}	37.42 ± 1.60^{c,d}	36.98 ± 0.81^{c}	36.63 ± 0.59^{e}
2	36.70 ± 1.05^{d-f}	36.93 ± 1.44^{c,d}	37.30 ± 1.32^{c}	37.65 ± 2.42^{d,e}
3	36.54 ± 1.40^{d-f}	38.63 ± 1.52^{c,d}	41.32 ± 2.46^{b}	39.82 ± 2.21^{c,d}
4	38.18 ± 2.79^{d-f}	39.94 ± 2.81^{b,c}	44.81 ± 2.44^{a}	41.55 ± 1.39^{b,c}
5	41.05 ± 5.28^{c-f}	44.07 ± 2.62^{a}	46.11 ± 2.43^{a}	43.46 ± 2.56^{a,b}
6	42.63 ± 4.99^{b-d}	46.83 ± 2.69^{a}	46.02 ± 2.65^{a}	45.14 ± 1.22^{a}
7	47.15 ± 3.78^{a-c}	46.37 ± 3.05^{a}	45.11 ± 2.88^{a}	45.58 ± 2.46^{a}
8	47.13 ± 2.85^{a-c}	46.92 ± 3.51^{a}	46.21 ± 2.18^{a}	
9	50.40 ± 3.00^{a}	45.28 ± 2.46^{a}		
10	48.10 ± 2.30^{a,b}	44.97 ± 3.33^{a}		
11	46.83 ± 3.34^{a-c}	43.36 ± 2.60^{a,b}		
12	41.88 ± 7.96^{b-f}			
13	42.14 ± 8.42^{b-e}			
14	41.49 ± 6.18^{b-f}			

Each value is the mean of 10 fruits, and is the mean ± standard deviation.
Means with different letters (a-f) indicate significant differences based on Tukey-Kramer's multiple range test (p<0.05).

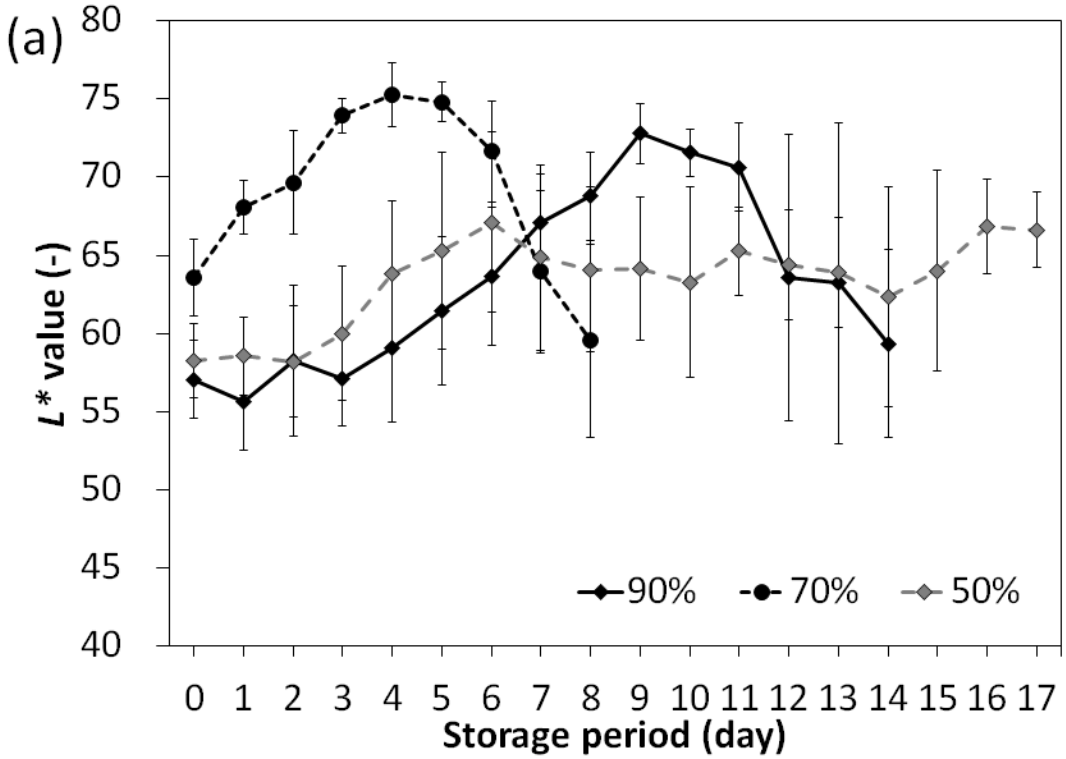
(a)
L* value (-)
80
75
70
65
60
55
50
45
40
90%
70%
50%
0 1 2 3 4 5 6 7 8 9 10 11 12 13 14 15 16 17
Storage period (day)

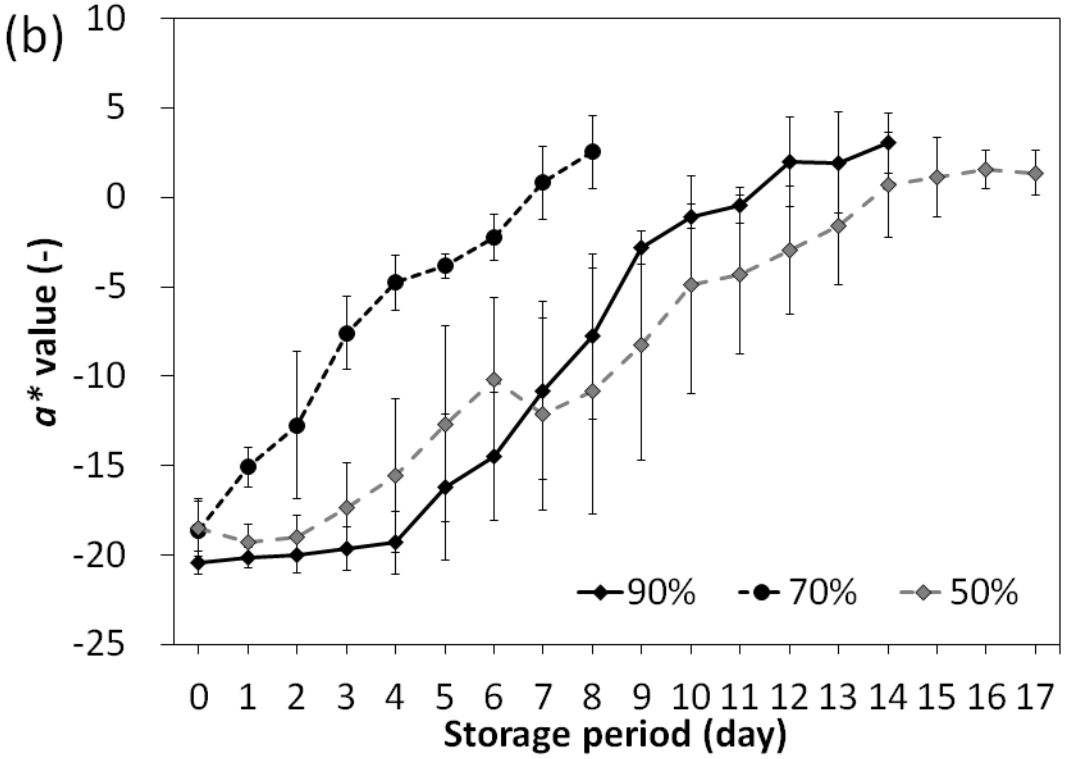
(b)
a* value (-)
10
5
0
-5
-10
-15
-20
-25
90%
70%
50%
0 1 2 3 4 5 6 7 8 9 10 11 12 13 14 15 16 17
Storage period (day)

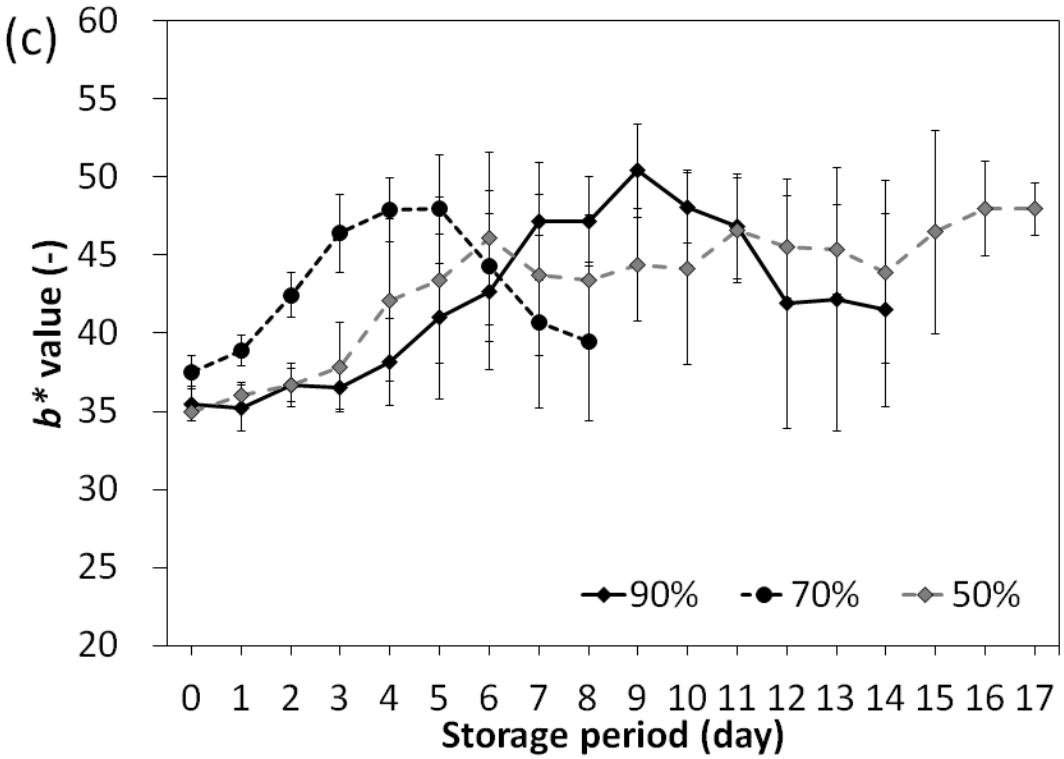

Fig. 4-9. The changes in *L*a*b of Cavendish banana according to RH conditions determined by a portable colorimeter: (a) *L**, (b) *a**, and (c) *b** values. Each value is the mean of 10 fruits assessed at each time, and is the mean ± standard deviation.**

Table 4-6. *L value of Cavendish banana according to RH conditions.**

Storage period	Relative humidity		
	50%	70%	90%
0	58.26 ± 2.41[b]	63.56 ± 2.48[d,e]	57.06 ± 2.51[d,e]
1	58.55 ± 2.52[b]	68.08 ± 1.71[c,d]	55.63 ± 3.13[e]
2	58.22 ± 3.55[b]	69.63 ± 3.31[b,c]	58.26 ± 4.85[d,e]
3	60.00 ± 4.30[a,b]	73.92 ± 1.13[a,b]	57.09 ± 3.02[d,e]
4	63.86 ± 4.64[a,b]	75.24 ± 2.06[a]	59.06 ± 4.71[d,e]
5	65.32 ± 6.28[a,b]	74.80 ± 1.28[a]	61.43 ± 4.74[c-e]
6	67.11 ± 5.75[a]	71.66 ± 3.24[a-c]	63.63 ± 4.41[b-d]
7	64.87 ± 5.92[a,b]	63.97 ± 5.18[d,e]	67.10 ± 3.10[a-c]
8	64.10 ± 5.26[a,b]	59.55 ± 6.16[e]	68.78 ± 2.79[a-c]
9	64.14 ± 4.59[a,b]		72.78 ± 1.92[a]
10	63.28 ± 6.11[a,b]		71.55 ± 1.53[a]
11	65.26 ± 2.82[a,b]		70.64 ± 2.82[a,b]
12	64.37 ± 3.52[a,b]		63.58 ± 9.12[b-d]
13	63.88 ± 3.52[a,b]		63.23 ± 10.25[b-e]
14	62.34 ± 7.05[a,b]		59.35 ± 5.98[d,e]
15	64.00 ± 6.41[a,b]		
16	66.84 ± 3.05[a]		
17	66.63 ± 2.40[a]		

Each value is the mean of 10 fruits, and is the mean ± standard deviation.
Means with different letters (a-e) indicate significant differences based on Tukey-Kramer's multiple range test (p<0.05).

Table 4-7. *a value of Cavendish banana according to RH conditions.**

Storage period	Relative humidity		
	50%	70%	90%
0	-18.52 ± 1.52^{h-j}	-18.66 ± 1.79^{e}	-20.41 ± 0.65^{h}
1	-19.32 ± 1.07^{j}	-15.06 ± 1.11^{d}	-20.17 ± 0.59^{g,h}
2	-19.00 ± 1.22^{i,j}	-12.75 ± 4.11^{d}	-20.00 ± 1.03^{g,h}
3	-17.35 ± 2.49^{h-j}	-7.60 ± 2.04^{c}	-19.66 ± 1.22^{g,h}
4	-15.54 ± 4.30^{g-j}	-4.77 ± 1.53^{b,c}	-19.30 ± 1.74^{g,h}
5	-12.68 ± 5.47^{f-i}	-3.85 ± 0.68^{b}	-16.22 ± 4.08^{f,g}
6	-10.17 ± 4.55^{d-g}	-2.26 ± 1.30^{b}	-14.48 ± 3.60^{e,f}
7	-12.14 ± 5.37^{f-h}	0.81 ± 2.02^{a}	-10.81 ± 4.99^{d,e}
8	-10.82 ± 6.89^{e-g}	2.52 ± 2.06^{a}	-7.78 ± 4.61^{d}
9	-8.28 ± 6.41^{c-f}		-2.80 ± 0.92^{c}
10	-4.87 ± 6.09^{b-e}		-1.06 ± 0.71^{b,c}
11	-4.32 ± 4.44^{a-d}		-0.43 ± 1.01^{a-c}
12	-2.96 ± 3.57^{a-c}		1.96 ± 2.51^{a,b}
13	-1.60 ± 3.29^{a,b}		1.93 ± 2.83^{a,b}
14	0.69 ± 2.92^{a,b}		3.03 ± 1.67^{a}
15	1.15 ± 2.23^{a,b}		
16	1.55 ± 1.10^{a}		
17	1.35 ± 1.27^{a,b}		

Each value is the mean of 10 fruits, and is the mean ± standard deviation.
Means with different letters (a-j) indicate significant differences based on Tukey-Kramer's multiple range test (p<0.05).

Table 4-8. *b value of Cavendish banana according to RH conditions.**

Storage period	Relative humidity		
	50%	70%	90%
0	34.97 ± 0.56^{d}	37.50 ± 1.08^{e}	$35.49 \pm 1.11^{e,f}$
1	$36.04 \pm 0.78^{c,d}$	$38.89 \pm 0.95^{d,e}$	35.18 ± 1.48^{e}
2	$36.67 \pm 1.42^{c,d}$	$42.44 \pm 1.46^{b-d}$	$36.70 \pm 1.05^{d-f}$
3	$37.83 \pm 2.84^{b-d}$	$46.39 \pm 2.47^{a,b}$	$36.54 \pm 1.40^{d-f}$
4	$42.12 \pm 5.18^{a-c}$	47.88 ± 2.07^{a}	$38.18 \pm 2.79^{d-f}$
5	$43.41 \pm 5.31^{a,b}$	47.95 ± 3.47^{a}	$41.05 \pm 5.28^{c-f}$
6	46.07 ± 5.52^{a}	$44.28 \pm 4.81^{a-c}$	$42.63 \pm 4.99^{b-d}$
7	$43.71 \pm 5.14^{a,b}$	$40.70 \pm 5.53^{c-e}$	$47.15 \pm 3.78^{a-c}$
8	$43.35 \pm 4.23^{a,b}$	$39.48 \pm 5.06^{c-e}$	$47.13 \pm 2.85^{a-c}$
9	$44.37 \pm 3.58^{a,b}$		50.40 ± 3.00^{a}
10	$44.13 \pm 6.15^{a,b}$		$48.10 \pm 2.30^{a,b}$
11	46.55 ± 3.37^{a}		$46.83 \pm 3.34^{a-c}$
12	45.51 ± 3.29^{a}		$41.88 \pm 7.96^{b-f}$
13	45.33 ± 2.87^{a}		$42.14 \pm 8.42^{b-e}$
14	$43.91 \pm 5.83^{a,b}$		$41.49 \pm 6.18^{b-f}$
15	46.46 ± 6.48^{a}		
16	47.97 ± 3.02^{a}		
17	47.96 ± 1.69^{a}		

Each value is the mean of 10 fruits, and is the mean $\pm$ standard deviation.
Means with different letters (a-f) indicate significant differences based on Tukey-Kramer's multiple range test (p<0.05).

4.5.3. Firmness

The firmness of the banana pulp is an important postharvest quality attribute, and it can be used as a maturity/ripening measure (Dadzie and Orchard, 1997). The firmness of the Cavendish bananas decreased during ripening under all conditions. It also decreased with the increase in temperature, similar to the results found by previous studies (Inaba et al., 1984; Ahmad et al., 2001; Chen and Ramaswamy, 2002). There was also a significant difference in the firmness according to the storage period from the zero stage to the ripe stage. However, after the ripe stage, the firmness was similar across storage periods. However, there was no significant change according to RH conditions.

Softening of bananas during the ripening process has been associated with two or three factors (Smith et al., 1989; Dadzie and Orchard, 1997; Soltani et al., 2011). The first is the breakdown of starch to form sugar. The second is the breakdown of the cell wall structure or the reduction of the middle lamella cohesion caused by the solubilization of pectic substances. The third is the movement of water from the peel to the pulp during ripening, owing to osmosis.

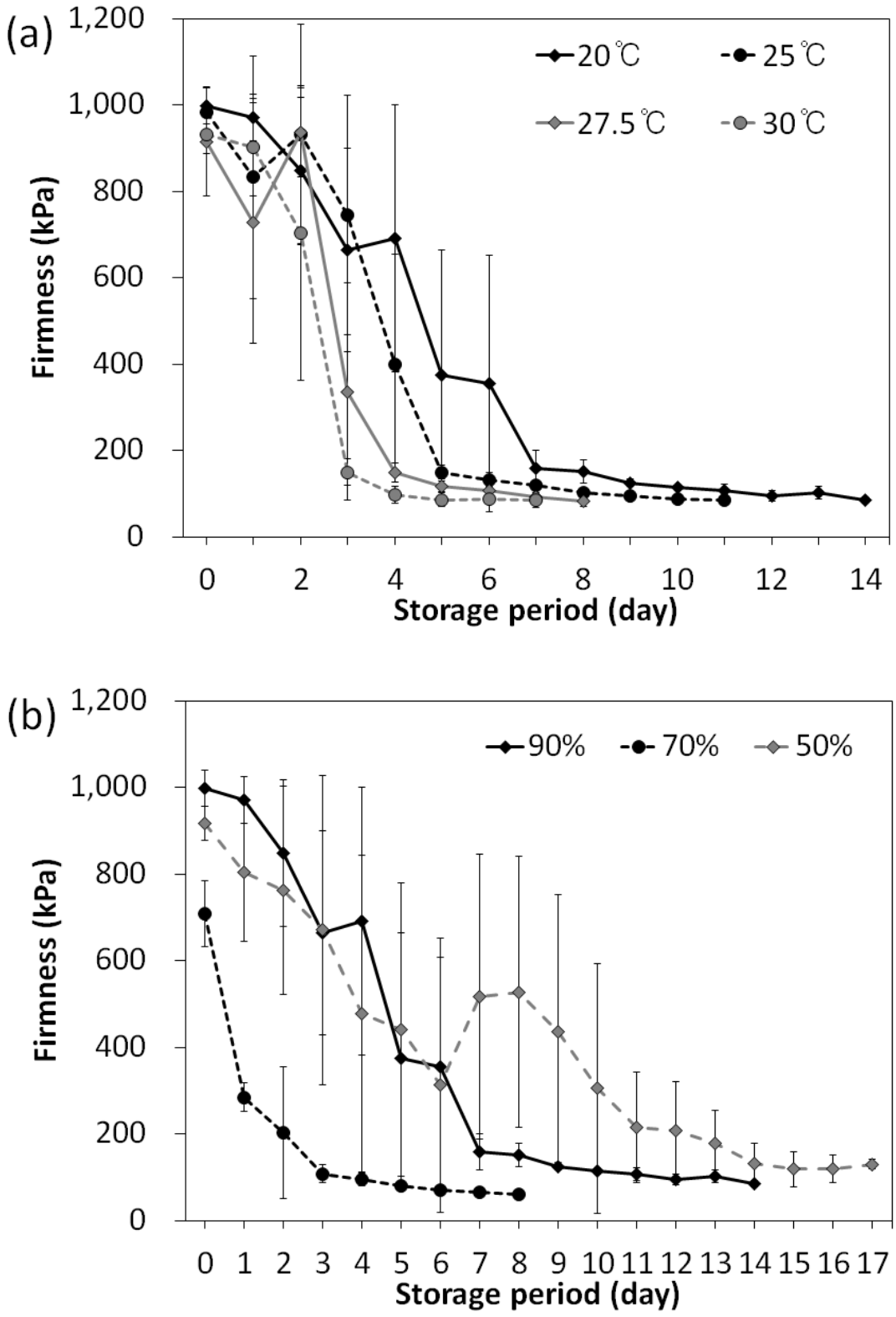

Fig. 4-10. The changes in firmness of Cavendish banana according to (a) temperature and (b) RH conditions. Each value is the mean of 10 fruits assessed at each time, and is the mean ± standard deviation.

Table 4-9. Firmness of Cavendish banana according to temperature conditions.

Storage period	Temperature			
	20℃	25℃	27.5℃	30℃
0	999.19 ± 41.46^{a}	983.89 ± 59.84^{a}	914.86 ± 125.85^{a,b}	932.80 ± 45.65^{a}
1	972.28 ± 53.71^{a}	833.13 ± 280.65^{a,b}	727.99 ± 279.24^{b}	903.08 ± 113.23^{a}
2	848.89 ± 170.16^{a,b}	932.64 ± 255.70^{a,b}	938.12 ± 102.84^{a}	703.19 ± 340.98^{b}
3	665.31 ± 236.14^{b}	745.54 ± 278.04^{b}	335.74 ± 251.71^{c}	150.25 ± 30.15^{c}
4	691.63 ± 309.61^{b}	398.98 ± 256.52^{c}	149.01 ± 22.66^{c,d}	97.14 ± 18.88^{c}
5	374.25 ± 290.40^{c}	149.63 ± 16.37^{d}	117.67 ± 11.94^{d}	85.95 ± 15.71^{c}
6	354.86 ± 296.54^{c,d}	131.34 ± 16.56^{d}	108.52 ± 9.85^{d}	88.16 ± 9.69^{c}
7	159.24 ± 41.49^{c-e}	118.91 ± 8.63^{d}	93.34 ± 8.63^{d}	85.01 ± 16.55^{c}
8	151.02 ± 26.38^{c-e}	103.33 ± 7.08^{d}	82.56 ± 11.53^{d}	
9	125.66 ± 9.35^{d,e}	95.54 ± 7.16^{d}		
10	114.22 ± 6.23^{e}	88.12 ± 5.41^{d}		
11	106.88 ± 15.13^{e}	84.75 ± 5.28^{d}		
12	95.51 ± 11.79^{e}			
13	102.85 ± 14.13^{e}			
14	85.27 ± 8.16^{e}			

Each value is the mean of 10 fruits, and is the mean ± standard deviation.
Means with different letters (a-e) indicate significant differences based on Tukey-Kramer's multiple range test (p<0.05).

Table 4-10. Firmness of Cavendish banana according to RH conditions.

Storage period	Relative humidity		
	50%	70%	90%
0	918.11 ± 38.53[a]	708.84 ± 76.41[a]	999.19 ± 41.46[a]
1	804.02 ± 159.27[a,b]	284.91 ± 32.60[b]	972.28 ± 53.71[a]
2	762.95 ± 240.67[a,b]	203.00 ± 152.17[b]	848.89 ± 170.16[a,b]
3	670.99 ± 357.52[a-c]	108.43 ± 20.29[c]	665.31 ± 236.14[b]
4	478.13 ± 366.53[b-e]	94.93 ± 14.48[c]	691.63 ± 309.61[b]
5	440.30 ± 339.00[b-e]	80.55 ± 5.01[c]	374.25 ± 290.40[c]
6	313.55 ± 293.57[c-e]	71.07 ± 4.64[c]	354.86 ± 296.54[c,d]
7	517.14 ± 329.29[b-d]	66.09 ± 5.89[c]	159.24 ± 41.49[c-e]
8	527.56 ± 312.93[b-d]	59.80 ± 5.98[c]	151.02 ± 26.38[c-e]
9	436.84 ± 316.52[b-e]		125.66 ± 9.35[d,e]
10	305.15 ± 289.12[c-e]		114.22 ± 6.23[e]
11	215.85 ± 127.76[d,e]		106.88 ± 15.13[e]
12	208.21 ± 113.00[d,e]		95.51 ± 11.79[e]
13	179.00 ± 75.99[d,e]		102.85 ± 14.13[e]
14	131.07 ± 47.45[e]		85.27 ± 8.16[e]
15	119.32 ± 40.25[e]		
16	119.54 ± 32.97[e]		
17	130.47 ± 11.85[e]		

Each value is the mean of 10 fruits, and is the mean ± standard deviation.
Means with different letters (a-e) indicate significant differences based on Tukey-Kramer's multiple range test (p<0.05).

4.5.4. TSS

Bananas contain many compounds that are soluble in water, such as sugars, acids, vitamin C, amino acids, and some pectins. Sugars forms the main component of soluble solids in a ripe banana. TSSs comprise an important postharvest quality characteristic. Because the TSSs of fruits usually increase as they mature and ripen, the soluble solids content of bananas can be a useful index of maturity or stage of ripeness (Dadzie and Orchard, 1997). Banana TSSs increase, because their starch content is hydrolyzed into soluble sugars (e.g., sucrose, glucose, and fructose) during ripening (Marriott et al., 1981).

Under temperature conditions, the TSS was 1.95–2.41% Brix at all green stages (unripe), and increased to 17.65–19.08% Brix at the ripe stage, regardless of temperature conditions. The TSS increased more rapidly at higher temperature conditions, similar to the results shown in a previous study (Inaba et al., 1984). There was also no significant difference during the green stage. However, there was a significant difference during the ripe stage. After ripening, the TSS was similar among storage periods. However, there was no significant difference according to RH conditions. The TSS at a 70% RH condition changed faster than in other conditions, which was caused by the ripening of bananas starting during distribution.

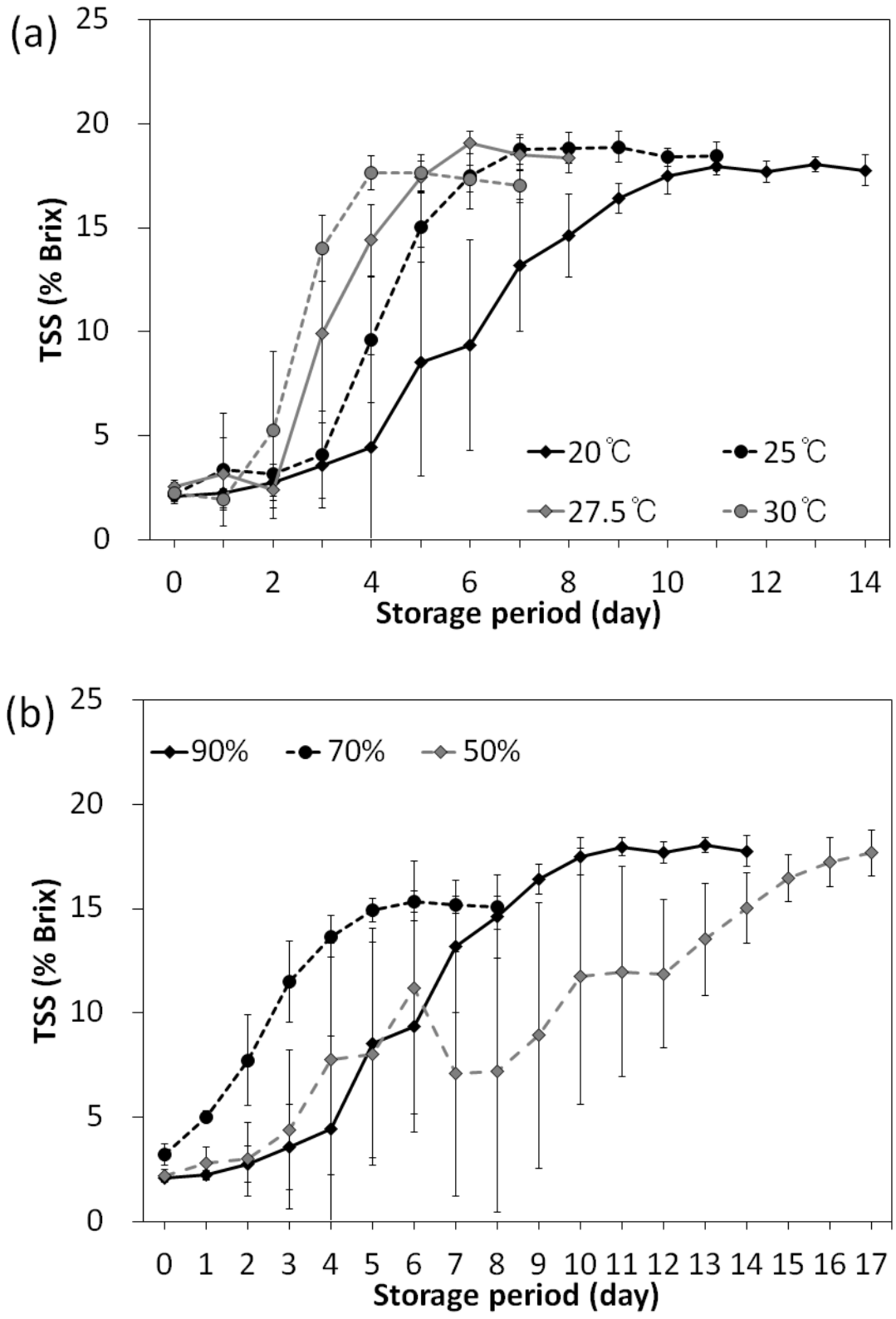

Fig. 4-11. The changes in TSS of Cavendish banana according to (a) temperature and (b) RH conditions. Each value is the mean of 10 fruits assessed at each time, and is the mean ± standard deviation.

Table 4-11. TSS of Cavendish banana according to temperature conditions.

Storage period	Temperature			
	20℃	25℃	27.5℃	30℃
0	2.10 ± 0.21^{e}	2.20 ± 0.36^{d}	2.53 ± 0.30^{d}	2.25 ± 0.51^{d}
1	2.25 ± 0.21^{e}	3.36 ± 2.72^{d}	3.15 ± 1.73^{d}	1.95 ± 0.42^{d}
2	2.77 ± 0.87^{e}	3.17 ± 2.16^{d}	2.41 ± 0.32^{d}	5.28 ± 3.74^{c}
3	3.55 ± 2.05^{e}	4.07 ± 2.11^{d}	9.91 ± 4.30^{c}	13.99 ± 1.59^{b}
4	4.46 ± 4.45^{e}	9.60 ± 3.02^{c}	14.40 ± 1.70^{b}	17.65 ± 0.81^{a}
5	8.55 ± 5.51^{d}	15.04 ± 1.68^{b}	17.44 ± 0.77^{a}	17.64 ± 0.87^{a}
6	$9.36 \pm 5.06^{c,d}$	$17.49 \pm 1.57^{a,b}$	19.08 ± 0.53^{a}	17.34 ± 0.64^{a}
7	$13.19 \pm 3.19^{b,c}$	18.76 ± 0.72^{a}	18.53 ± 0.77^{a}	17.01 ± 0.78^{a}
8	$14.62 \pm 2.00^{a,b}$	18.82 ± 0.73^{a}	18.36 ± 0.72^{a}	
9	$16.42 \pm 0.72^{a,b}$	18.88 ± 0.72^{a}		
10	17.50 ± 0.91^{a}	18.38 ± 0.44^{a}		
11	17.96 ± 0.42^{a}	18.45 ± 0.69^{a}		
12	17.70 ± 0.50^{a}			
13	18.03 ± 0.36^{a}			
14	17.76 ± 0.75^{a}			

Each value is the mean of 10 fruits, and is the mean ± standard deviation.
Means with different letters (a-e) indicate significant differences based on Tukey-Kramer's multiple range test ($p<0.05$).

Table 4-12. TSS of Cavendish banana according to RH conditions.

Storage period	Relative humidity		
	50%	70%	90%
0	2.20 ± 0.28^{d}	3.23 ± 0.51^{e}	2.10 ± 0.21^{e}
1	2.78 ± 0.81^{d}	5.02 ± 0.30^{f}	2.25 ± 0.21^{e}
2	2.98 ± 1.77^{d}	7.73 ± 2.16^{d}	2.77 ± 0.87^{e}
3	4.41 ± 3.79^{d}	11.49 ± 1.94^{c}	3.55 ± 2.05^{e}
4	$7.78 \pm 5.54^{c,d}$	13.66 ± 1.00^{b}	4.46 ± 4.45^{e}
5	$8.04 \pm 5.36^{c,d}$	$14.92 \pm 0.58^{a,b}$	8.55 ± 5.51^{d}
6	$11.21 \pm 6.04^{a-c}$	15.33 ± 0.50^{a}	$9.36 \pm 5.06^{c,d}$
7	$7.09 \pm 5.86^{c,d}$	$15.19 \pm 0.40^{a,b}$	$13.19 \pm 3.19^{b,c}$
8	$7.22 \pm 6.76^{c,d}$	$15.07 \pm 0.53^{a,b}$	$14.62 \pm 2.00^{a,b}$
9	$8.92 \pm 6.37^{b-d}$		$16.42 \pm 0.72^{a,b}$
10	$11.76 \pm 6.13^{a-c}$		17.50 ± 0.91^{a}
11	$11.98 \pm 5.03^{a-c}$		17.96 ± 0.42^{a}
12	$11.86 \pm 3.55^{a-c}$		17.70 ± 0.50^{a}
13	$13.52 \pm 2.69^{a-c}$		18.03 ± 0.36^{a}
14	$15.01 \pm 1.68^{a,b}$		17.76 ± 0.75^{a}
15	16.45 ± 1.13^{a}		
16	17.22 ± 1.16^{a}		
17	17.66 ± 1.11^{a}		

Each value is the mean of 10 fruits, and is the mean $\pm$ standard deviation.
Means with different letters (a-e) indicate significant differences based on Tukey-Kramer's multiple range test (p<0.05).

4.5.5. pH value

Figure 4-12 shows the changes in pH value of the bananas at different temperatures (a) and RH (b) conditions. The pH value is used primarily to estimate consumption quality and hidden attributes and can be used as an indicator of banana maturity or ripeness (Dadzie and Orchard, 1997).

Under all temperature conditions, the pH value of the bananas was 5.26–5.75 at the unripe stage (all green), and it decreased to 4.72–5.08 during the ripe stage. As senescence continued, the pH value increased, finally reaching 5.21–5.85 under all temperature conditions. However, there was no significant difference according to temperature conditions. The change of the pH value at RH conditions was similar to those of the temperature conditions, but there was no significant difference according to RH conditions. Thus, regardless of storage conditions, the pH value at the green stage was high. However, as ripening progressed, the pH value decreased. This change was mainly caused by changes in the content of malic acid (John and Marchal, 1995; Dadzie and Orchard, 1997).

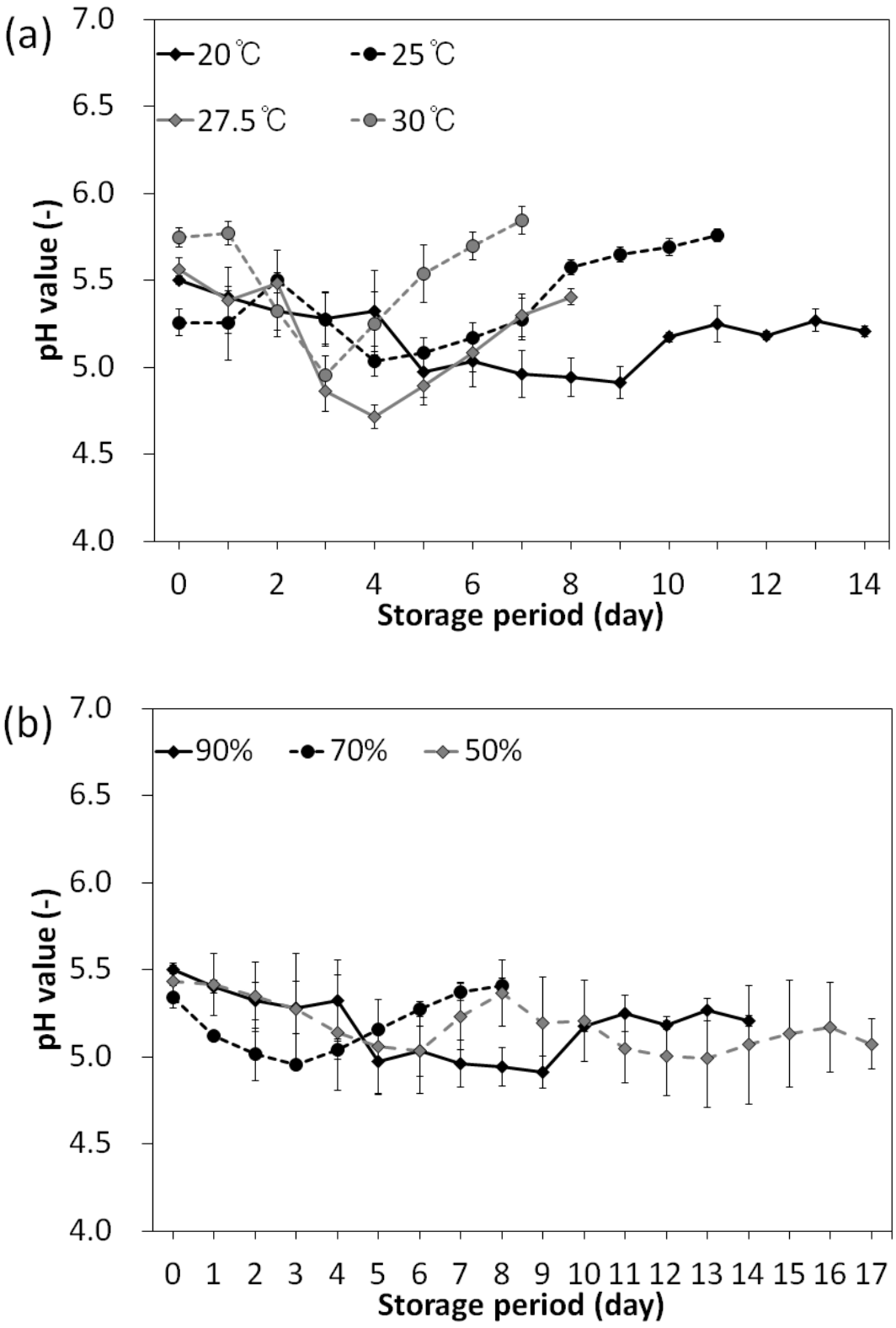

Fig. 4-12. The changes in pH value of Cavendish banana according to (a) temperature and (b) RH conditions. Each value is the mean of 10 fruits assessed at each time, and is the mean ± standard deviation.

Table 4-13. pH of Cavendish banana according to temperature conditions.

Storage period	Temperature			
	20℃	25℃	27.5℃	30℃
0	5.50 ± 0.03^{a}	5.26 ± 0.08^{d}	5.56 ± 0.07^{a}	5.75 ± 0.06^{a}
1	$5.40 \pm 0.04^{a,b}$	5.25 ± 0.21^{d}	$5.39 \pm 0.19^{b,c}$	5.77 ± 0.07^{a}
2	$5.32 \pm 0.11^{a-c}$	5.50 ± 0.17^{c}	$5.49 \pm 0.06^{a,b}$	5.32 ± 0.15^{c}
3	$5.28 \pm 0.15^{b,c}$	5.27 ± 0.15^{d}	$4.86 \pm 0.12^{e,f}$	4.96 ± 0.11^{d}
4	$5.32 \pm 0.23^{a-c}$	5.04 ± 0.09^{e}	4.72 ± 0.07^{f}	5.25 ± 0.18^{c}
5	4.98 ± 0.19^{e}	5.08 ± 0.09^{e}	4.90 ± 0.07^{e}	5.54 ± 0.16^{b}
6	$5.03 \pm 0.14^{d,e}$	$5.17 \pm 0.09^{d,e}$	5.09 ± 0.11^{d}	$5.70 \pm 0.08^{a,b}$
7	4.96 ± 0.13^{e}	5.28 ± 0.12^{d}	5.30 ± 0.12^{c}	5.85 ± 0.08^{a}
8	4.94 ± 0.11^{e}	$5.58 \pm 0.04^{b,c}$	$5.41 \pm 0.05^{b,c}$	
9	4.91 ± 0.09^{e}	$5.65 \pm 0.04^{a-c}$		
10	$5.17 \pm 0.03^{c,d}$	$5.69 \pm 0.05^{a,b}$		
11	$5.25 \pm 0.11^{b,c}$	5.76 ± 0.04^{a}		
12	$5.18 \pm 0.02^{c,d}$			
13	$5.27 \pm 0.07^{b,c}$			
14	$5.21 \pm 0.03^{c,d}$			

Each value is the mean of 10 fruits, and is the mean ± standard deviation.
Means with different letters (a-d) indicate significant differences based on Tukey-Kramer's multiple range test ($p<0.05$).

Table 4-14. pH of Cavendish banana according to RH conditions.

Storage period	Relative humidity		
	50%	70%	90%
0	5.43 ± 0.10^{a}	$5.34 \pm 0.07^{a,b}$	5.50 ± 0.03^{a}
1	$5.42 \pm 0.18^{a,b}$	$5.12 \pm 0.02^{c,d}$	$5.40 \pm 0.04^{a,b}$
2	$5.35 \pm 0.20^{a-c}$	5.02 ± 0.15^{e}	$5.32 \pm 0.11^{a-c}$
3	$5.27 \pm 0.32^{a-c}$	4.96 ± 0.02^{e}	$5.28 \pm 0.15^{b,c}$
4	$5.14 \pm 0.33^{a-c}$	$5.04 \pm 0.06^{d,e}$	$5.32 \pm 0.23^{a-c}$
5	$5.06 \pm 0.27^{a-c}$	5.16 ± 0.03^{c}	4.98 ± 0.19^{e}
6	$5.04 \pm 0.25^{a-c}$	5.28 ± 0.04^{b}	$5.03 \pm 0.14^{d,e}$
7	$5.23 \pm 0.19^{a-c}$	5.37 ± 0.05^{a}	4.96 ± 0.13^{e}
8	$5.37 \pm 0.19^{b,c}$	5.41 ± 0.04^{a}	4.94 ± 0.11^{e}
9	$5.20 \pm 0.26^{a-c}$		4.91 ± 0.09^{e}
10	$5.21 \pm 0.23^{a-c}$		$5.17 \pm 0.03^{c,d}$
11	$5.05 \pm 0.20^{a-c}$		$5.25 \pm 0.11^{b,c}$
12	$5.01 \pm 0.23^{a-c}$		$5.18 \pm 0.02^{c,d}$
13	5.00 ± 0.29^{c}		$5.27 \pm 0.07^{b,c}$
14	5.07 ± 0.34^{c}		$5.21 \pm 0.03^{c,d}$
15	$5.13 \pm 0.31^{a-c}$		
16	$5.17 \pm 0.26^{a-c}$		
17	$5.08 \pm 0.14^{a-c}$		

Each value is the mean of 10 fruits, and is the mean $\pm$ standard deviation.
Means with different letters (a-e) indicate significant differences based on Tukey-Kramer's multiple range test (p<0.05).

4.5.6. Ratio of pulp to peel

Figure 4-13 shows the changes in the pulp-to-peel ratio of the banana at different temperatures (a) and RHs (b). The ratio of the Cavendish bananas decreased during ripening at all conditions. Under all temperature conditions, the ratio was 1.12–1.28 at the zero stage, and it finally reached a value of 1.59–1.94. Under all RH conditions, the ratio of pulp to peel was 1.15–1.62 at the zero stage, and it finally reached a value of 1.59–2.56. The reason why the ratio at the 70% RH condition was higher than others is that the bananas started to ripen during distribution.

The ratio of pulp to peel is a good index of banana ripening, and it increases in response to ripeness. Changes in ratio during ripening indicates differential changes in moisture content of the peel and pulp. The increase in the ratio during ripening is also related to sugar concentration. During ripening, the sugar concentration in the pulp increases rapidly compared with the peel, thus contributing to a differential changes in osmotic pressure. The peel loses water both by transpiration to the atmosphere and to the pulp via osmosis. Therefore, it contributes to the increase of the fresh weight of the pulp as the fruit ripens. As a result, the ratio increases during ripening (Stover and Simmonds, 1987; Dadzie and Orchard, 1997).

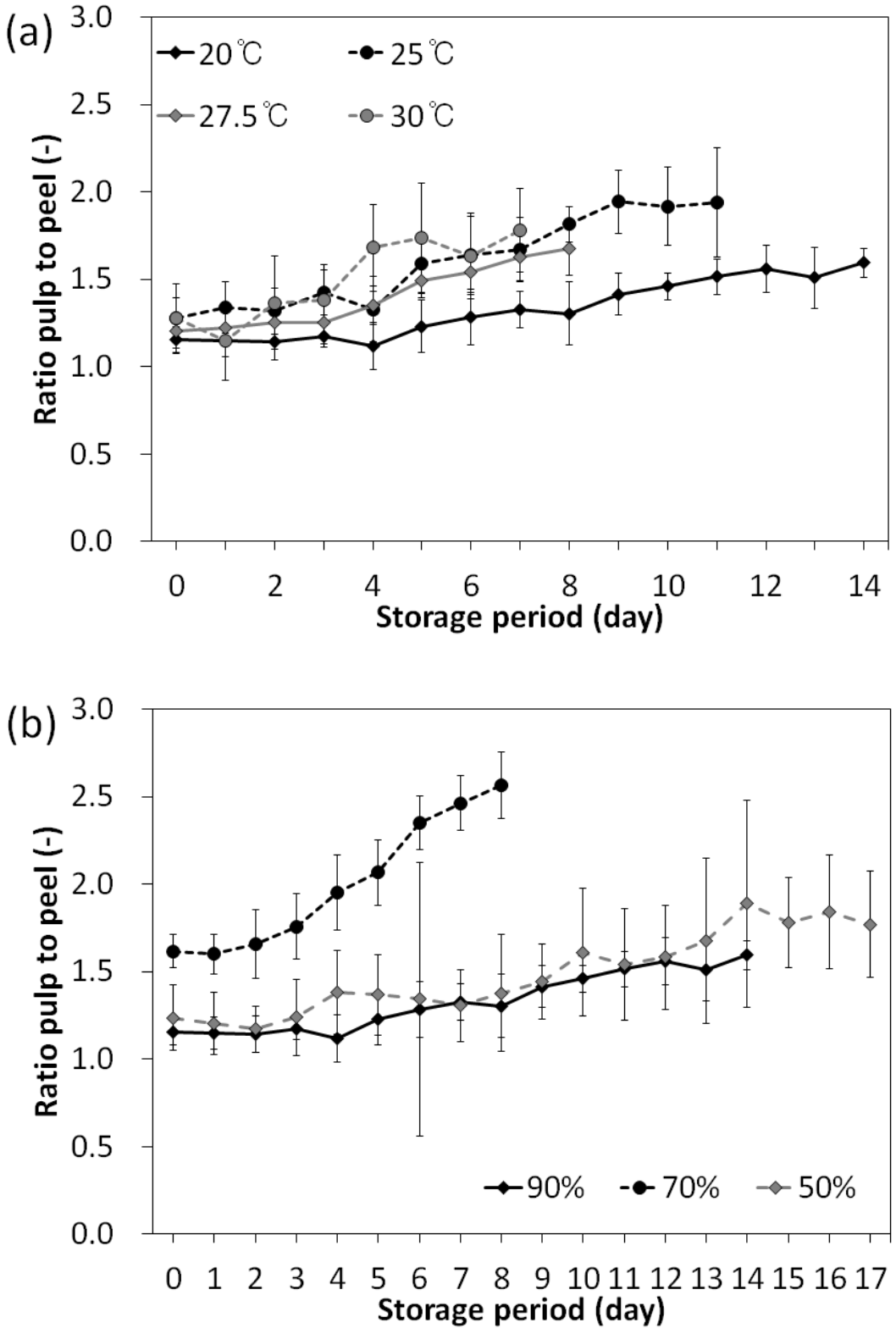

Fig. 4-13. The changes in ratio pulp to peel of Cavendish banana according to (a) temperature and (b) RH conditions. Each value is the mean of 10 fruits assessed at each time, and is the mean ± standard deviation.

Table 4-15. Ratio pulp to peel of Cavendish banana according to temperature conditions.

Storage period	Temperature			
	20℃	25℃	27.5℃	30℃
0	$1.15 \pm 0.07^{e,f}$	1.28 ± 0.12^{e}	1.20 ± 0.10^{d}	1.28 ± 0.20^{c}
1	$1.15 \pm 0.09^{e,f}$	$1.34 \pm 0.15^{d,e}$	1.22 ± 0.10^{d}	1.15 ± 0.22^{c}
2	$1.14 \pm 0.10^{e,f}$	$1.32 \pm 0.13^{d,e}$	1.25 ± 0.12^{d}	$1.37 \pm 0.27^{b,c}$
3	$1.17 \pm 0.06^{e,f}$	$1.43 \pm 0.13^{c-e}$	1.25 ± 0.12^{d}	$1.38 \pm 0.20^{b,c}$
4	1.12 ± 0.13^{f}	$1.33 \pm 0.19^{d,e}$	$1.35 \pm 0.11^{c,d}$	$1.68 \pm 0.25^{a,b}$
5	$1.23 \pm 0.15^{d-f}$	$1.59 \pm 0.17^{b-d}$	$1.49 \pm 0.10^{b,c}$	1.74 ± 0.31^{a}
6	$1.29 \pm 0.16^{c-f}$	$1.64 \pm 0.22^{b,c}$	$1.54 \pm 0.12^{a,b}$	$1.63 \pm 0.24^{a,b}$
7	$1.33 \pm 0.10^{b-e}$	$1.67 \pm 0.18^{a-c}$	$1.63 \pm 0.14^{a,b}$	1.78 ± 0.24^{a}
8	$1.31 \pm 0.18^{c-f}$	$1.82 \pm 0.10^{a,b}$	1.67 ± 0.15^{a}	
9	$1.41 \pm 0.12^{a-d}$	1.94 ± 0.18^{a}		
10	$1.46 \pm 0.08^{a-c}$	1.92 ± 0.22^{a}		
11	1.51 ± 0.10^{a}	1.94 ± 0.31^{a}		
12	1.56 ± 0.13^{a}			
13	$1.51 \pm 0.17^{a,b}$			
14	1.59 ± 0.08^{a}			

Each value is the mean of 10 fruits, and is the mean ± standard deviation.
Means with different letters (a-f) indicate significant differences based on Tukey-Kramer's multiple range test (p<0.05).

Table 4-16. Ratio pulp to peel of Cavendish banana according to RH conditions.

Storage period	Relative humidity		
	50%	70%	90%
0	$1.24 \pm 0.19^{d,e}$	1.62 ± 0.10^{d}	$1.15 \pm 0.07^{e,f}$
1	$1.20 \pm 0.18^{d,e}$	1.60 ± 0.11^{d}	$1.15 \pm 0.09^{e,f}$
2	1.17 ± 0.13^{e}	1.66 ± 0.20^{d}	$1.14 \pm 0.10^{e,f}$
3	$1.24 \pm 0.22^{d,e}$	$1.76 \pm 0.19^{c,d}$	$1.17 \pm 0.06^{e,f}$
4	$1.38 \pm 0.24^{b-e}$	$1.95 \pm 0.21^{b,c}$	1.12 ± 0.13^{f}
5	$1.37 \pm 0.23^{b-e}$	2.07 ± 0.19^{b}	$1.23 \pm 0.15^{d-f}$
6	$1.34 \pm 0.78^{a-e}$	2.35 ± 0.15^{a}	$1.29 \pm 0.16^{c-f}$
7	$1.31 \pm 0.21^{c-e}$	2.46 ± 0.15^{a}	$1.33 \pm 0.10^{b-e}$
8	$1.38 \pm 0.33^{b-e}$	2.56 ± 0.19^{a}	$1.31 \pm 0.18^{c-f}$
9	$1.44 \pm 0.21^{a-e}$		$1.41 \pm 0.12^{a-d}$
10	$1.61 \pm 0.36^{a-e}$		$1.46 \pm 0.08^{a-c}$
11	$1.54 \pm 0.32^{a-e}$		1.51 ± 0.10^{a}
12	$1.58 \pm 0.30^{a-e}$		1.56 ± 0.13^{a}
13	$1.68 \pm 0.47^{a-d}$		$1.51 \pm 0.17^{a,b}$
14	1.89 ± 0.59^{a}		1.59 ± 0.08^{a}
15	$1.78 \pm 0.26^{a-c}$		
16	$1.84 \pm 0.33^{a,b}$		
17	$1.77 \pm 0.30^{a-c}$		

Each value is the mean of 10 fruits, and is the mean $\pm$ standard deviation.
Means with different letters (a-f) indicate significant differences based on Tukey-Kramer's multiple range test (p<0.05).

4.5.7. MC

Pulp MC is an important postharvest parameter used for the evaluation of the ripening quality of bananas. During ripening, the MC of the peel decreases, whereas the MC of the pulp increases. This is because the peel loses water both to the pulp and to the atmosphere (Dadzie and Orchard, 1997).

Figure 4-14 shows the changes of MC of the bananas at different temperatures (a) and RH (b) conditions. The pulp MC of the bananas increased during ripening under all conditions. The MC significantly increased with the increase of temperature, which is also similar to the findings of previous studies (Rajkumar et al., 2012). However, there was no significant changes according to the RH conditions. Moreover, the MC in the 70% RH condition was found to be high compared with other conditions, caused by the harvest time (Ahmad et al., 2001; Nguyen and Price, 2007).

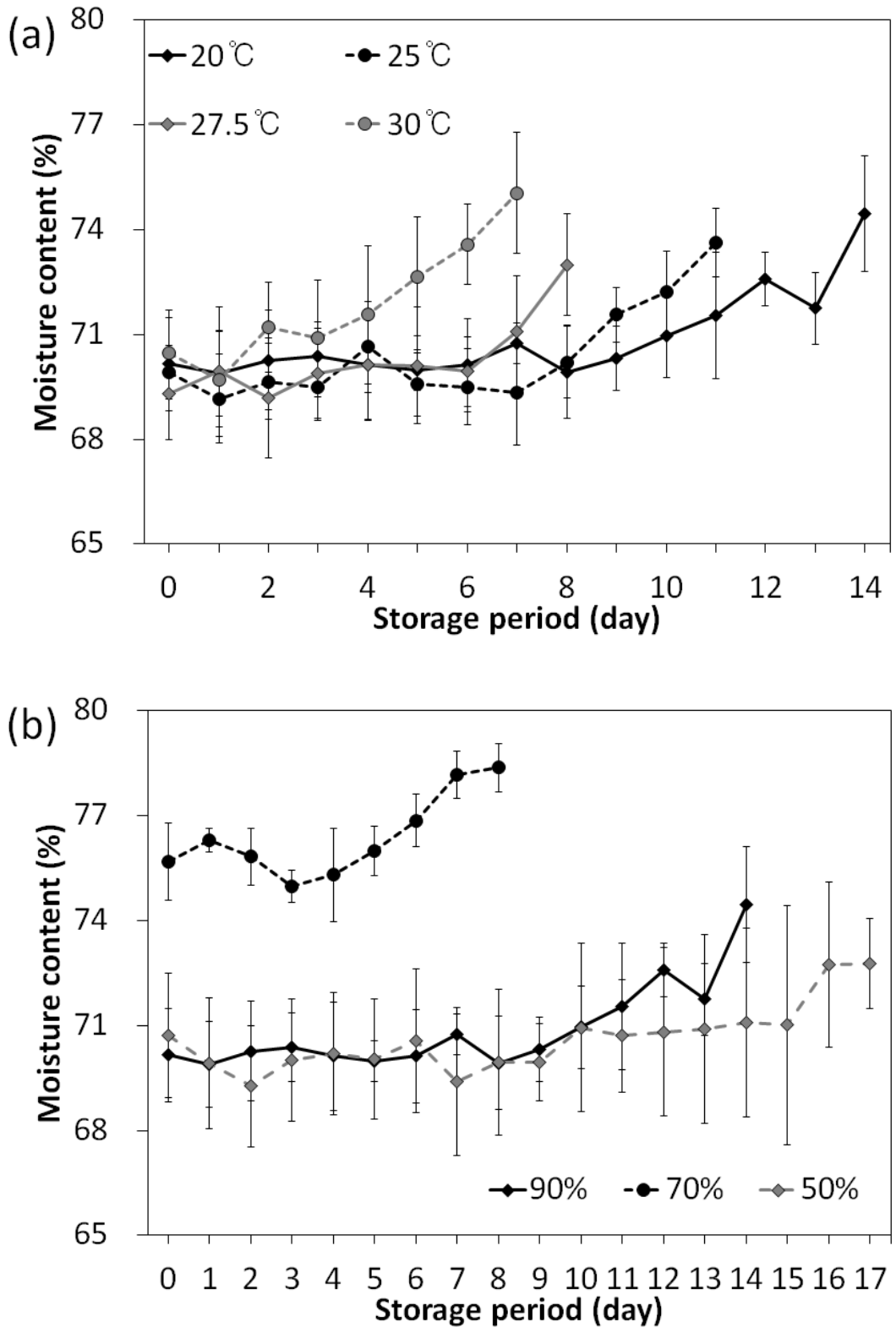

Fig. 4-14. The changes in MC of Cavendish banana according to (a) temperature and (b) RH conditions. Each value is the mean of 10 fruits assessed at each time, and is the mean ± standard deviation.

Table 4-17. MC of Cavendish banana according to temperature conditions.

Storage period	Temperature			
	20℃	25℃	27.5℃	30℃
0	70.15 ± 1.34^{c}	69.92 ± 0.78^{e}	69.30 ± 1.30^{b}	70.46 ± 1.24^{d}
1	69.89 ± 1.23^{c}	69.16 ± 1.27^{e}	69.94 ± 1.86^{b}	69.72 ± 1.36^{d}
2	70.27 ± 1.44^{c}	69.66 ± 1.08^{e}	69.17 ± 1.72^{b}	$71.22 \pm 1.29^{c,d}$
3	70.37 ± 0.98^{c}	$69.50 \pm 0.97^{d,e}$	69.89 ± 1.29^{b}	$70.88 \pm 1.68^{c,d}$
4	70.12 ± 1.54^{c}	70.65 ± 1.30^{e}	70.13 ± 1.60^{b}	$71.57 \pm 1.97^{b-d}$
5	69.97 ± 0.58^{c}	69.58 ± 0.91^{e}	70.11 ± 1.67^{b}	$72.65 \pm 1.70^{b,c}$
6	70.12 ± 1.33^{c}	69.49 ± 1.09^{e}	69.93 ± 0.99^{b}	$73.57 \pm 1.15^{a,b}$
7	$70.75 \pm 0.58^{b,c}$	$69.33 \pm 1.49^{d,e}$	$71.09 \pm 1.60^{a,b}$	75.05 ± 1.73^{a}
8	69.92 ± 1.33^{c}	$70.21 \pm 1.01^{c,d}$	73.00 ± 1.45^{a}	
9	70.32 ± 0.91^{c}	$71.57 \pm 0.79^{b,c}$		
10	$70.95 \pm 1.17^{b,c}$	$72.21 \pm 1.16^{a,b}$		
11	$71.54 \pm 1.82^{b,c}$	73.63 ± 0.98^{a}		
12	$72.58 \pm 0.77^{a,b}$			
13	$71.74 \pm 1.01^{b,c}$			
14	74.44 ± 1.66^{a}			

Each value is the mean of 10 fruits, and is the mean ± standard deviation.
Means with different letters (a-e) indicate significant differences based on Tukey-Kramer's multiple range test ($p<0.05$).

Table 4-18. MC of Cavendish banana according to RH conditions.

Storage period	Relative humidity		
	50%	70%	90%
0	$70.72 \pm 1.79^{a,b}$	$75.67 \pm 1.10^{c,d}$	70.15 ± 1.34^{c}
1	$69.92 \pm 1.88^{a,b}$	$76.29 \pm 0.34^{b,c}$	69.89 ± 1.23^{c}
2	69.27 ± 1.73^{b}	$75.82 \pm 0.81^{b-d}$	70.27 ± 1.44^{c}
3	$70.01 \pm 1.73^{a,b}$	74.98 ± 0.46^{d}	70.37 ± 0.98^{c}
4	$70.19 \pm 1.76^{a,b}$	$75.30 \pm 1.33^{c,d}$	70.12 ± 1.54^{c}
5	$70.04 \pm 1.72^{a,b}$	$75.98 \pm 0.70^{b-d}$	69.97 ± 0.58^{c}
6	$70.57 \pm 2.05^{a,b}$	76.85 ± 0.75^{b}	70.12 ± 1.33^{c}
7	69.40 ± 2.12^{b}	78.15 ± 0.68^{a}	$70.75 \pm 0.58^{b,c}$
8	$69.94 \pm 2.09^{a,b}$	78.36 ± 0.69^{a}	69.92 ± 1.33^{c}
9	$69.96 \pm 1.11^{a,b}$		70.32 ± 0.91^{c}
10	$70.94 \pm 2.40^{a,b}$		$70.95 \pm 1.17^{b,c}$
11	$70.70 \pm 1.61^{a,b}$		$71.54 \pm 1.82^{b,c}$
12	$70.82 \pm 2.41^{a,b}$		$72.58 \pm 0.77^{a,b}$
13	$70.90 \pm 2.69^{a,b}$		$71.74 \pm 1.01^{b,c}$
14	$71.08 \pm 2.70^{a,b}$		74.44 ± 1.66^{a}
15	$71.01 \pm 3.40^{a,b}$		
16	72.74 ± 2.37^{a}		
17	72.77 ± 1.30^{a}		

Each value is the mean of 10 fruits, and is the mean $\pm$ standard deviation.
Means with different letters (a-d) indicate significant differences based on Tukey-Kramer's multiple range test (p<0.05).

4.5.8. Relationship between ripening indices and color features

To obtain the best set of color features for predicting the quality indices of bananas, the relationship between their quality indices and color features extracted from RGB images were analyzed, and the results are shown in Table 4-19.

Significant correlations were observed between the ripening indices and most color features at 99%. These results suggest that there were good agreements between quality indices and some of the color features. In this study, nine color features (i.e., *L*a*b**, HSV, and YUV) were selected as input data to develop the ripening-index estimation model for bananas.

Table 4-19. Relationship between color feature values extracted from RGB images and quality indices of Cavendish banana.

	R	G	B	H	S	V	*L**	*a**	*b**	Y	U	V	X	Y	Z
Firmness	-0.84**	-0.55**	-0.23**	0.83**	-0.64**	-0.76**	-0.72**	-0.75**	-0.78**	-0.76**	0.81**	-0.80**	-0.80**	-0.75**	-0.47**
TSS	0.85**	0.48**	0.22**	-0.86**	0.65**	0.77**	0.69**	0.81**	0.74**	0.74**	-0.78**	0.85**	0.80**	0.72**	0.45**
Ratio pulp to peel	0.64**	0.28**	0.30**	-0.69**	0.39**	0.60**	0.47**	0.68**	0.43**	0.53**	-0.48**	0.67**	0.62**	0.54**	0.44**
pH	-0.27**	-0.34**	0.00	0.20**	-0.29**	-0.27**	-0.33**	-0.14**	-0.41**	-0.32**	0.39**	-0.20**	-0.27**	-0.31**	-0.13**
MC	0.41**	0.27**	0.32**	-0.41**	0.18**	0.42**	0.36**	0.39**	0.27**	0.39**	-0.30**	0.39**	0.44**	0.42**	0.40**

** Correlation is significant at the .01 level (2-tailed).

4.5.9. Prediction models

Table 4-20 shows the R^2, RMSE, and RPD obtained for each quality index, and Table 4-21 shows the optimal network topology for each model. As can be seen in Table 4-20, when using the color-feature-based ANN model, all quality indices were predicted with high accuracy compared with other features. The changes in the peel color during ripening of the Cavendish banana involved a more significant feature difference in appearance than did those of the appearance of local shape features (Zhuang et al., 2019). Additionally, the color-feature-based ANN model accurately predicted the firmness and TSS of bananas with R^2 values higher than 0.87 and RMSE values less than 131 kPa and 2.2 % Brix for firmness and TSS, respectively. However, the color-feature-based ANN models were not suitable for predicting pH, pulp-to-peel ratio, or MC. The RPD values were as low as 2.75, 2.44, 1.21, 1.44, and 1.00 for firmness, TSS, pH, ratio of pulp to peel, and MC, respectively. Higher RPD values indicated better predictive ability, and an RPD of 2.0 or higher gave an excellent prediction model (Bellon-Maurel et al., 2010). Consequently, when using the ANN model based on the color feature, the firmness and TSS of Cavendish bananas were predicted with high accuracy, regardless ripening conditions. However, the color-feature-based ANN model could not predict the pH, ratio of pulp to peel, or MC.

To clearly distinguish the ripening stage of the Cavendish banana, I applied the firmness and TSS prediction models according to the results described above, and Cavendish bananas were classified into three levels of unripe, ripe, and overripe. Among the 71 samples used to test the classification of ripening stages, 14 samples were misclassified. The ANN model succeeded in classifying the ripening stages of Cavendish bananas with accuracy of 80.28% and an F1-score of 0.734.

Table 4-20. Results of ANN for predicting the quality indices of Cavendish banana.

Quality indices	Feature	Train set		Test set		RPD
		R^2	RMSE	R^2	RMSE	
Firmness	Color	0.87	130.98	0.87	131.46	2.75
	Hu moments	0.71	193.54	0.49	265.20	1.36
	HOG	0.19	334.49	0.19	339.14	1.06
TSS	Color	0.89	2.19	0.83	2.73	2.44
	Hu moments	0.72	3.49	0.46	5.01	1.33
	HOG	0.31	5.63	0.15	6.12	1.09
pH	Color	0.36	0.23	0.36	0.23	1.21
	Hu moments	0.12	0.26	0.13	0.26	1.08
	HOG	0.33	0.24	0.09	0.27	1.05
Ratio pulp to peel	Color	0.56	0.25	0.54	0.27	1.44
	Hu moments	0.55	0.25	0.51	0.78	1.39
	HOG	0.36	0.31	0.08	0.37	1.04
MC	Color	0.27	2.33	0.25	2.51	1.13
	Hu moments	0.25	2.32	0.12	2.66	1.07
	HOG	0.09	2.65	0.03	2.82	1.00

R^2: Coefficient of determination, RMSE: Root mean square error, RPD: Ratio of performance to deviation, TSS: Total soluble solids, MC: Moisture content, HOG: Histogram of oriented gradients

Table 4-21. Optimal network topology for each ANN model.

Quality indices	Features	Network structure	Batch size	Epochs	Optimizer	Learning rate	Activation function
Firmness	Color	9-32-64-512-1	160	1500	Adam	0.03	ReLU
	Hu moments	21-64-256-1024-1	80	1500	Adadelta	0.5	ReLU
	HOG	972-16-128-1	40	100	Adam	0.1	ReLU
TSS	Color	9-16-32-128-512-1	160	2000	Nadam	0.003	Softplus
	Hu moments	21-16-32-16-8-1	80	2000	Nadam	0.005	Softsign
	HOG	972-8-32-64-1	80	200	Adam	0.001	ReLU
pH	Color	9-16-64-128-1	40	2000	Adamax	0.003	Softsign
	Hu moments	21-32-128-128-1	80	1000	Adamax	0.001	Tanh
	HOG	972-32-64-64-1	40	100	Adamax	0.001	ReLU
Ratio pulp to peel	Color	9-8-128-1	639	1000	Nadam	0.01	ReLU
	Hu moments	21-8-256-1	40	2000	Adam	0.003	ReLU
	HOG	972-8-1	160	200	Adam	0.001	ReLU
MC	Color	9-8-64-1	40	2000	Adam	0.01	ReLU
	Hu moments	21-128-256-1	40	2000	Adam	0.003	ReLU
	HOG	972-16-1	639	1000	Adam	0.03	ReLU

TSS: Total soluble solids, MC: Moisture content, HOG: Histogram of oriented gradients

4.6. Conclusion

This study investigated the relationship between the quality indices of Cavendish bananas and several external properties (i.e., color, Hu-moments, and HOG features) to develop a prediction model of quality indices and ripening stages of the Cavendish banana. The color-feature-based ANN model successfully predicted the firmness and TSS of Cavendish bananas with high accuracy, regardless of ripening conditions. Furthermore, the ripening stages were classified into three levels (i.e., unripe, ripe, and overripe) with a high accuracy of 80.28% and an F1-score of 0.734 using firmness and TSS prediction models. Therefore, the smartphone CVS aided by the color-feature-based ANN model successfully predicted the quality indices and ripening stages of Cavendish bananas during ripening, regardless of ripening conditions.

Chapter 5 Summary

This study investigated smartphone-camera technologies for the CVS prediction of quality indices and ripening stages of agricultural products (e.g., avocados and bananas) based on digital images and a color-feature-based ANN.

To develop the smartphone-based CVS, several color values (i.e., *L**, *a**, *b**, chroma, hue angle, ΔE, ΔL, ΔC, and ΔH) were obtained using a smartphone camera and a colorimeter and were compared. The RMSE of most color values ranged from 0.06 to 2.62. Thus, smartphone camera was found to be a capable imaging system for CVS.

The changes in chemical and physical properties of Hass avocados and Cavendish bananas during their ripening processes under different ripening conditions were investigated, and digital images were collected using the smartphone CVS to develop the prediction model of quality indices and ripening stages. Additionally, different external properties (i.e., color, shape, and texture features) were compared to support the development of the new prediction model. Consequently, the color-feature-based ANN model successfully predicted their quality indices and ripening processes regardless ripening conditions.

In conclusion, this study demonstrated the potential of a smartphone CVS when used in combination with a color-feature-based ANN as an alternative to the conventional expensive nondestructive analysis devices. The developed CVS exhibited high applicability for the management of agricultural products. However, for portability, the image-capturing procedure should be simplified, such as by using a gray color chart adjacent to the agricultural products so that the variable ambient light can be corrected.

References

Agarwal, A., Singh, R., & Vatsa, M. (2016). Face anti-spoofing using Haralick features. 2016 IEEE 8th International Conference on Biometrics Theory, Applications and Systems (BTAS), Niagara Falls, NY, pp. 1-6.

Ahmad, S., Thompson, A.K., Hafiz, I.A., & Asi, A.A. (2001). Effect of temperature on the ripening behavior and quality of banana fruit. International Journal of Agriculture and Biology, 3(2), 224-227.

Ahmad, S., Chatha, Z.A., Nasir, M.A., Aziz, A., & Mohson, M. (2006). Effect of relative humidity on the ripening behaviour and quality of ethylene treated banana fruit. Journal of Agriculture and Social Sciences, 2(1), 54-56.

Akkaravessapong, P., Joyce, D.C., & Turner, D.W. (1992). The relative humidity at which bananas are stored or ripened does not influence their susceptibility to mechanical damage. Scientia Horticulturae, 52(3), 265-268.

Alden, K.M., Omid, M., Rajabipour, A., Tajeddin, B., & Firouz, M.S. (2019). Quality and shelf-life prediction of cauliflower under modified atmosphere packaging by using artificial neural networks and image processing. Computers and Electronics in Agriculture, 163(6), 104861.

AOAC (1990). Official methods of analysis. (14^{th} den), Association of Official Analytical chemists, Washington, DC.

Aravind, H., Rajgopal, C., & Soman, K.P. (2010). A simple approach to clustering in excel. International Journal of Computer Applications, 11(7), 19-25.

Arakeri, M.P., & Lakshmana (2016). Computer vision based fruit grading system for quality evaluation of tomato in agriculture industry. Procedia Computer Science, 79(4), 426-433.

Arpaia, M.L., Collin, S., Sievert, J., & Obenland, D. (2018). ‘Hass’ avocado quality as influenced by temperatrue and ethylene prior to and during final ripening. Postharvest Biology and Technology, 140, 76-84.

References

Arzate-Vázquez, I., Chanona-Pérez, J.J., Perea-Flores, M.J., Calderón-Domínguez, G., Moreno-Armendáriz, M.A., Calvo, H., et al. (2011). Image processing applied to classification of avocado variety hass (*Persea americana* Mill.) during the ripening process. Food and Bioprocess Technology, 4(5), 1307-1313.

Asmare, M.H., Asirvadam, V.S., & Iznita, L. (2009). Color space selection for color image enhancement applications. 2009 International Conference on Signal Acquisition and Processing, Kuala Lumpur, pp. 208-212.

Asiche, W.O., Mitalo, O.W., Kasahara, Y., Tosa, Y., Mworia, E.G., Ushijima, K., et al. (2017). Effect of storage temperatrue on fruit ripening in three kiwifruit cultivars. The Horticulture Journal, 86(3), 403-410.

Attig, A., & Perner, P. (2011). A comparison between Haralick's texture descriptor and the texture descriptor based on random sets for biological images. Proceedings of 7th International Conference on Machine Learning and Data Mining in Pattern Recognition, Springer-Verlag, Berlin, Heidelberg, pp. 524-538.

Azizi, A., Abbaspour-Gilandeh, Y., Nooshyar, M., & Afkari-Sayah, A. (2016). Identifying potato varieties using machine vision and artificial neural networks. International Journal of Food Properties, 19(3), 618-635.

Barman, U., & Choudhury, R.D. (2020). Smartphone image based digital chlorophyll meter to estimate the value of citrus leaves chlorophyll using Linear Regression, LMBP-ANN and SCGBP-ANN. Journal of King Saud University-Computer and Information Sciences, 2020, 1-13.

Basheer, I.A., & Hajmeer, M. (2000). Artificial neural networks: fundamentals, computing, design, and application. Journal of Microbiological Methods, 43(1), 3-31.

Bell, S.C., Nawrocki, H.D., & Morris, K.B. (2009). Forensic discrimination of glass using cathodoluminescence and CIE LAB color coordinates: a feasibility study. Forensic Science International, 189(1-3), 93-99.

Bellon-Maurel, V., Fernandez-Ahumada, E., Palagos, B., Roger, J.-M., & McBratney, A. (2010). Critical review of chemometric indicators commonly used for assessing the quality of the prediction of soil attributes by NIR spectroscopy. TrAC Trends in

Analytical Chemistry, 29(9), 1073-1081.

Bergstra, J., & Bengio, Y. (2012). Random search for hyper-parameter optimization. Journal of Machine Learning Research, 13(2), 281-305.

Bhargava, A., & Bansal, A. (2018). Fruits and vegetables quality evaluation using computer vision: a review. Journal of King Saud University-Computer and Information Sciences, 2018, 1-15.

Blackbourn, H.D., Jeger, M.J., John, P., & Thompson, A.K. (1990). Inhibition of degreening in the peel of bananas ripened at tropical temperatures. Annals of Applied Biology, 117(1), 147-161.

Blakey, R.J. (2011). Management of avocado post-harvest physiology. Horticultural Science, School of Agricultural Sciences and Agribusiness. University of Kwa Zulu, Pietermaritzburg, PhD Thesis.

Blakey, R.J. (2016). Evaluation of avocado fruit maturity with a portable near-infrared spectrometer. Postharvest Biology and Technology, 121(7), 101-105.

Brosnan, T., & Sun, D.-W. (2002). Inspection and grading of agricultural and food products by computer vision systems-a review. Computers and Electronics in Agriculture, 36(2-3), 193-213.

Castro, W., Oblitas, J., De-La-Torre, M., Cotrina, C., Bazán, K., & Avila-George, H. (2019). Classification of cape gooseberry fruit according to its level of ripeness using machine learning techniques and different color spaces. IEEE Access, 7, 27389-27400.

Chen, C.R., & Ramaswamy, H.S. (2002). Color and texture change kinetics in ripening bananas. LWT-Food Science and Technology, 35(5), 415-419.

Chen, T.-W., Chen, Y.-L., & Chien, S.-Y. (2008). Fast image segmentation based on k-means clustering with histograms in HSV color space. 2008 IEEE 10 th Workshop on Multimedia Signal Processing, Cairns, Qld, 322-325.

Cho, B.-H., Koyama, K., Díaz, E.O., & Koseki, S. (2020). Determination of 'Hass' avocado ripeness during storage based on smartphone image and machine learning model. Food and Bioprocess Technology, 13(7), 1579-1587.

References

Cho, J.-S., Lee, H.-J., Park, J.-H., Sung, J.-H., Choi, J.-Y., & Moon, K.-D. (2016). Image analysis to evaluate the browning degree of banana (*Musa* spp.) peel. Food Chemistry, 194(1), 1028-1033.

Chowdhury, A., Bera, T.K., Ghoshal, D., & Chakraborty, B. (2015). Studying the electrical impedance variations in banana ripening using electrical impedance spectroscopy (EIS). Proceedings of the 2015 Third International Conference on Computer, Communication, Control and Information Technology (C3IT), Hooghly, pp. 1-4.

Coelho, L. (2013). Mahotas: open source software for scriptable computer vision. Journal of open research software, 1(1), e3.

Cox, K.A., McGhie, T.K., White, A., & Woolf, A.B. (2004). Skin colour and pigment changes during ripening of 'hass' avocado fruit. Postharvest Biology and Technology, 31(3), 287-294.

Cruz-Fernandez, M., Luque-Cobija, M.J., Cervera, M.L., Morales-Rubio, A., & de la Guardia, M. (2017). Smartphone determination of fat in cured meat products. Microchemical Journal, 132(12), 8-14.

Cubero, S., Aleixos, N., Moltó, E., Gómez-Sanchis, J., & Blasco, J. (2011). Advances in machine vision applications for automatic inspection and quality evaluation of fruits and vegetables. Food and Bioprocess Technology, 4(7), 487-504.

Cubero, S., Albert, F., Prats-Moltalbán, J.M., Fernández-Pacheco, D.G., Blasco, J., & Aleixos, N. (2018). Application for the estimation of the standard citrus colour index (CCI) using image processing in mobile devices. Biosystems Engineering, 167(1), 63-74.

Dadzie, B.K., & Orchard, J.E. (1997). Routine post-harvest screening of banana/plantain hybrids: criteria and methods. INIBAP Technical Guidelines No. 2, pp. 43-46.

Dalal, N., & Triggs, B. (2005). Histograms of oriented gradients for human detection. 2005 IEEE Computer Society Conference on Computer Vision and Pattern Recognition (CVPR'05), San Diego, CA, USA, pp. 886-893.

Déiz, O., Bueno, G., Salido, J., & De la Torre, F. (2011). Face recognition using histograms

of oriented gradients. Pattern Recognition Letters, 32(12), 1598-1603.

Díaz, E.O., Kawamura, S., Matsuo, M., Kato, M., & Koseki, S. (2019). Combined analysis of near-infrared spectra, colour, and physicochemical information of brown rice to develop accurate calibration models for determining amylose content. Food Chemistry, 286(15), 297-306.

Ding, C.-K., Chachin, K., Hamauzu, Y., Ueda, Y., & Imahori, Y. (1998). Effects of storage temperatures on physiology and quality of loquat fruit. Postharvest Biology and Technology, 14(3), 309-315.

Ding, H., Chin, Y.-W., Kinghorn, A.D., & D'Ambrosio, S.M. (2007). Chemopreventive characteristics of avocado fruit. Seminars in Cancer Biology, 17(5), 386-394.

Ding, H., Han, C., Guo, D., Chin, Y.-W., Ding, Y., Kinghorn, A.D., et al. (2009). Selective induction of apoptosis of human oral cancer cell lines by avocado extracts via a ROS-mediated mechanism. Nutrition and Cancer, 61(3), 348-356.

Dowlati, M., Mohtasebi, S.S., Omid, M., Razavi, S.H., Jamzad, M., & de la Guardia, M. (2013). Freshness assessment of gilthead sea bream (*Sparus aurata*) by machine vision based on gill and eye color changes. Journal of Food Engineering, 119(2), 277-287.

Du, C.-J., & Sun, D.-W. (2006). Learning techniques used in computer vision for food quality evaluation: a review. Journal of Food Engineering, 72(1), 39-55.

El-Bendary, N., Hariri, E.E., Hassanien, A.E., & Badr, A. (2015). Using machine learning techniques for evaluating tomato ripeness. Expert Systems with Applications, 42(4), 1892-1905.

FAO STAT. (2020). Food and agriculture organization of the united nations. http://www.fao.org/faostat/en/#data/QC. Access data: October 21, 2020.

Fernández-Vázquez, R., Stinco, C.M., Hernanz, D., Heredia, F.J., & Vicario, I.M. (2013). Colour training and colour differences thresholds in orange juice. Food Quality and Preference, 30(2), 320-327.

Galindo-Tovar, M.E., Ogata-Aguilar, N., & Arzate-Fernández, A.M. (2008). Some aspects

of avocado (*Persea americana* Mill.) diversity and domestication in mesoamerica. Genetic Resources and Crop Evolution, 55(6), 441-450.

Girolami, A., Napolitano, F., Faraone, D., & Braghieri, A. (2013). Measurement of meat color using a computer vision system. Meat Science, 93(1), 111-118.

Gomes, J.F.S., Vieira, R.R., & Leta, F.R. (2013). Colorimetric indicator for classification of bananas during ripening. Scientia Horticulturae, 150(12), 201-205.

Goñi, S.M., & Salvadori, V.O. (2017). Color measurement: comparison of colorimeter vs. computer vision system. Journal of Food Measurement and Characterization, 11(10), 538-547.

Gulli, A., & Pal, S. (2017). Deep learning with Keras. Packt Publishing Ltd., Brimingham, UK.

Haralick, R.M., Shanmugam, K., & Dinstein, I. (1973). Textural features for image classification. In IEEE Transactions on Systems, Man, and Cybernetics, 3(6), 610-621.

Hewett, E.W. (1999). Fruit and vegetable storage requirements. Agricultural Engineering Handbook, ASAE, Michigan, Section Ⅳ.3.2.

Hopkirk, G., White, A., Beever, D.J., & Forbes, S.K. (1994). Influence of postharvest temperatures and the rate of fruit ripening on internal postharvest rots and disorders of New Zealand 'hass' avocado fruit. New Zealand Journal of Crop and Horticultural Science, 22(3), 305-311.

Hsu, C.W., Chang, C.C., & Lin, C.J. (2010). A practical guide to support vector classification. Technical Report, National Taiwan University.

Hu, M., Dong, Q., Liu, B., & Malakar, P.K. (2014). The potential of double K-meas clustering for banana image segmentation. Journal of Food Process Engineering, 37(1), 10-18.

Huang, H., & Jiang, Y. (2012). Effect of plant growth regulators on banana fruit and broccoli during storage. Scientia Horticulturae, 145(8), 62-67.

Inaba, A., Okamoto., I., Ito, T., & Nakamura, R. (1984). Ripening characteristics of

commercial ‘Cavendish’ bananas attached on the plant in the Philippines, and those harvested at different maturities and transported to Japan. Journal of the Japanese Society for Horticultural Science, 53(1), 66-78.

Intaravanne, Y., Sumriddetchkajorn, S., & Nukeaw, J. (2012). Cell phone-based two-dimensional spectral analysis for banana ripeness estimation. Sensors and Actuators B: Chemical, 168(4), 390-394.

Jaiswal, P., Jha, S.N., & Bharadwaj, R. (2012). Non-destructive prediction of quality of intact banana using spectroscopy. Scientia Horticulturae, 135(12), 14-22.

Jaramillo-Acevedo, C.A., Choque-Valderrama, W.E., Guerrero-Alvarez, G.E., & Meneses-Escobar, C.A. (2020). Hass avocado ripeness classification by mobile devices using digital image processing and ann methods. International Journal of Food Engineering, published online ahead of print 2020, 20190161.

Javanmardi, J., & Kubota, C. (2006). Variation of lycopene, antioxidant activity, total soluble solids and weight loss of tomato during postharvest storage. Postharvest Biology and Technology, 41(2), 151-155.

Jha, S.N., & Matsuoka, T. (2004). Non-destructive determination of acid-brix ratio of tomato juice using near infrared spectroscopy. International Journal of Food Science and Technology, 39(4), 425-430.

Jiang, Y.M., & Fu, J.R. (1999). Postharvest browning of litchi fruit by water loss and its prevention by controlled atmosphere storage a high relative humidity. LWT-Food Science and Technology, 32(5), 278-283.

John, P., & Marchal, J. (1995). Ripening and biochemistry of the fruit. In: S. Gowen (Ed.), Bananas and Plantains, Chapman & Hall, London, pp. 434-467.

Kassim, A., Workneh, T.S., & Bezuidenhout, C.N. (2013). A review on postharvest handling of avocado fruit. African Journal of Agricultural Research, 8(21), 2385-2402.

Kajuna, S.T.A.R., Bilanski, W.K., & Mittal, G.S. (1997). Textural changes of banana and plantain pulp during ripening. Journal of the Science of Food Agriculture, 75(2), 244-250.

References

Kekre, H.B., & Thepade, S.D. (2009). Improving ‘color to gray and back’ using Kekre’s LUV color space. 2009 IEEE International Advance Computing Conference, Patiala, pp. 1218-1223.

Kılıç, K., Boyacı, İ.H., Köksel, H., & Küsmenoğlu, İ. (2007). A classification system for beans using computer vision system and artificial neural networks. Journal of Food Engineering, 78(3), 897-904.

Kumar, T., & Verma, K. (2010). A theory based on conversion of RGB image to gray image. International Journal of Computer Applications, 7(2), 7-10.

Lallu, N., Yearsley, C., Punter, M., Billing, D., Francis, K., & Pidakala, P. (2003). Effects of prepacking holding temperatures on shelf life of ‘Hass’ avocados. New Zealand Avocado Growers’ Association Annual Research Report, 3, 108-117.

Lallum, N., Punter, M., Haynes, G., Pidakala, P., & Burdon, J. (2004). Role of water loss in ripening of ‘Hass’ avocados. New Zealand Avocado Growers’ Association Annual Research Report, 4, 70-79.

Lan, H., Wang, Z., Niu, H., Zhang, H., Zhang, Y., Tang, Y., et al. (2020). A nondestructive testing method for soluble solid content in Korla fragrant pears based on electrical properties and artificial neural network. Food Science and Nutrition, 8(9), 5172-5181.

Lee, J. (2018). Development of maillard reaction based time temperature indicator/integrator for application of agricultural and food process engineering. Ph. D. thesis, Hokkaido University, Japan.

Leiva-Valenzuela, G.A., & Aguilera, J.M. (2013). Automatic detection of orientation and diseases in blueberries using image analysis to improve their postharvest storage quality. Food Control, 33(1), 166-173.

Lewis, C.E. (1978). The maturity of avocados-a general review. Journal of the Science of Food and Agriculture, 29(10), 866-875.

Li, C., Adhikari, R., Yao, Y., Miller, A.G., Kalbaugh, K., Li, D., et al. (2020). Measuring plant growth characteristics using smartphone based image nalysis technique in controlled environment agriculture. Computers and Electronics in Agriculture,

168(12), 105123.

Li, H., He, H., & Wen, Y. (2015). Dynamic particle swarm optimization and K-means clustering algorithm for image segmentation. Optik, 126(24), 4817-4822.

Li, J., & Zhang, Y. (2010). Design and accomplishment of the real-time tracking system of agricultural products logistics process. 2010 International Conference on E-Product E-Service and E-Entertainment, Henan, China, pp. 1-4.

Liakos, K.G., Busato, P., Moshou, D., Pearson, S., & Bochtis, D. (2018). Machine learning in agriculture: a review. Sensor, 18(8), 2674.

Liew, C.Y., & Lau, C.Y. (2012). Determination of quality parameters in Cavendish banana during ripening by NIR spectroscopy. International Food Research Journal, 19(2), 751-758.

Maftoonazad, M., & Ramaswamy, H.S. (2005). Postharvest shelf-life extension of avocados using methyl cellulose-based coating. LWT-Food Science and Technology, 38(6), 617-624.

Magwaza, L.S., & Tesfay, S.Z. (2015). A review of destructive and non-destructive methods for determining avocado fruit maturity. Food and Bioprocess Technology, 8(8), 1995-2011.

Maimunah, R.T., Handayanto, & Herlawati (2019). Nondestructive banana ripeness classification using neural network. 2019 Fourth International Conference on Informatics and Computing (ICIC), Semarang, Indonesia, pp. 1-4.

Marriott, J., Robinson, M., & Karikari, S.K. (1981). Starch and sugar transformation during the ripening of plantains and bananas. Journal of the Science of Food Agriculture, 32(10), 1021-1026.

Menlik, T., Özdemir, M.B., & Kirmaci, V. (2010). Determination of freeze-drying behaviors of apples by artificial neural network. Expert Systems with Applications, 37(12), 7669-7677.

Mizrach, A., & Flitsanov, U. (1999). Nondestructive ultrasonic determination of avocado softening process. Journal of Food Engineering, 40(3), 139-144.

References

Mizrach, A. (2000). Determination of avocado and mango fruit properties by ultrasonic technique. Ultrasonics, 38(1-8), 717-722.

Mohapatra, A., Shanmugasundaram, S., & Malmathanraj, R. (2017). Grading of ripening stages of red banana using dielectric properties changes and image processing approach. Computers and Electronics in Agriculture, 143(10), 100-110.

Mohebbi, M., Fathi, M., & Shahidi, F. (2011). Genetic algorithm-artificial neural network modeling of moisture and oil content of pretreated fried mushroom. Food and Bioprocess Technology, 4(7), 603-609.

Moreno-Torres, J.G., Sáez, J.A., & Herrera, F. (2012). Study on the impact of partition-induced dataset shift on k-fold cross-validation. IEEE Transactions On Neural Networks and Learning Systems, 23(8), pp. 1304-1312.

Muñoz-Rodríguez, J.A., Asundi, A., & Rodriguez-Vera, R. (2005). Recognition of a light line pattern by Hu moments for 3-D reconstruction of a rotated object. Optics & Laser Technology, 37(2), 131-138.

Mustaffa, I.B., & Khairul, S.F.B.M. (2017). Identification of fruit size and maturity through fruit images using OpenCV-Python and Rasberry Pi. 2017 International Conference on Robotics, Automation and Sciences (ICORAS), Melaka, pp. 1-3.

Nasiri, A., Taheri-Garavand, A., & Zhang, Y.-D. (2019). Image-based deep learning automated sorting of date fruit. Postharvest Biology and Technology, 153(4), 133-141.

Nguyen, M.-H., & Price, W.E. (2007). Air-drying of banana: influence of experimental parameters, slab thickness, banana maturity and harvesting season. Journal of Food Engineering, 79(1), 200-207.

Niazian, M., Sadat-Noori, S.A., & Abdipour, M. (2018a). Artificial neural network and multiple regression analysis models to predict essential oil content of ajowan (*Carum copticum* L.). Journal of Applied Research on Medicinal and Aromatic Plants, 9(4), 124-131.

Niazian, M., Sadat-Noori, S.A., & Abdipour, M. (2018b). Modeling the seed yield of Ajowan (*Trachyspermum ammi* L.) using artificial neural network and multiple linear

regression models. Industrial Crops and Products, 117(3), 224-234.

Ohali, Y.A. (2011). Computer vision based date fruit grading system: design and implementation. Journal of King Saud University-computer and Information Sciences, 23(1), 29-36.

Oliveira, J.A., Salomão, L.C.C., Siqueira, D.L., & Cecon, P.R. (2016). Cold tolerance of banana fruits of different cultivars. Revista Caatinga, 29(3), 629-641.

Pereira, L.F.S., Barbon Jr, S., Valous, N.A., & Barbin, D.F. (2018). Predicting the ripening of papaya fruit with digital imaging and random forests. Computers and Electronics in Agriculture, 145(1), 76-82.

Pinto, J., Rueda-Chacón, H., & Arguello, H. (2019). Classification of hass avocado (Persea americana Mill.) in terms of its ripening via hyperspectral images. TecnoLógicas, 22(45), 109-128.

Podpora, M., Korbaś, G.P., & Kawala-Janik, A. (2014). YUV vs RGB-choosing a color space for human-machine interaction. Position papers of the 2014 Federated Conference on Computer Scinece and Information Systems, 3, pp.29-34.

Polder, G., van der Heijden, G.W.A.M., Young, I.T. (2000). Hyperspectral image analysis for measuring ripeness of tomatoes. Transactions of the ASAE, 45(4), 1155-1161.

Prieto, N., Pawluczyk, O., Dugan, M.E.R., & Aalhus, J.L. (2017). A review of the principles and applications of near-infrared spectroscopy to characterize meat, fat, and meat products. Applied Spectroscopy, 71(7), 1403-1426.

Quiñones-Islas, N., Meza-Márquez, O.G., Osorio-Revilla, G., & Gallardo-Velazquez, T. (2013). Detection of adulterants in avocado oil by Mid-FTIR spectroscopy and multivariate analysis. Food Research International, 51(1), 148-154.

Rajkumar, P., Wang, N., Elmasry, G., Raghavan, G.S.V., & Gariepy, Y. (2012). Studies on banana fruit quality and maturity stages using hyperspectral imaging. Journal of Food Engineering, 108(1), 194-200.

Rybski, P.E., Huber, D., Morris, D.D., & Hoffman, R. (2010). Visual classification of coarse vehicle orientation using histogram of oriented gradients features. 2010 IEEE

Intelligent Vehicles Symposium, San Diego, CA, pp. 921-928.

Sanaeifar, A., Bakhshipour, A., de la Guardia, M. (2016). Prediction of banana quality indices from color features using support vector regression. Talanta, 148(10), 54-61.

Saldaña, E., Siche, R., Luján, M., & Quevedo, R. (2013). Review: computer vision applied to the inspection and quality control of fruits and vegetables. Brazilian Journal of Food Technology, 16(4), 254-272.

Sant'Anna, I.C., Tomaz, R.S., Silva, G.N., Nascimento, M., Bhering, L.L., & Cruz, C.D. (2015). Superiority of artificial neural networks for a genetic classification procedure. Genetics and Molecular Research, 14(8), 9898-9906.

Sargent, D.J. (2001). Comparison of artificial neural networks with other statistical approaches: results from medical data sets. Cancer, 91(S8), 1636-1642.

Satish, S., & Setty, Y.P. (2005). Modeling of a continuous fluidized bed dryer using artificial neural networks. International Communications in Heat and Mass Transfer, 32(3-4), 539-547.

Saucedo-Pompa, S., Rojas-Molina, R., Aguilera-Carbó, A.F., Saenz-Galindo, A., Garza, H.L., Jasso-Cantú, D., et al. (2009). Edible film based on candelilla wax to improve the shelf life and quality of avocado. Food Research International, 42(4), 511-515.

Scott, F.M., Bystrom, B.G., & Bowler, E. (1963). Persea americana, mesocarp cell structure, light and electron microscope study. Botanical Gazette, 124(6), 423-428.

Sharma, A.K., Sharma, R.K., & Kasana, H.S. (2007). Prediction of first lactation 305-day milk yield in Karan Fries dairy cattle using ANN modeling. Applied Soft Computing, 7(3), 1112-1120.

Sidehabi, S.W., Suyuti, A., Areni, I.S., & Nurtanio, I. (2018). Classification on passion fruit's ripeness using K-means clustering and artificial neural network. 2018 International Conference on Information and Communications Technology (ICOIACT)m Yogyakarta, pp. 304-309.

Silva, G.M.C., Silva, W.B., Medeiros, D.B., Salvador, A.R., Cordeiro, M.H.M., Silva, N.M., et al. (2017). The chitosan affects severely the carbon metabolism in mango

(*Mangifera indica* L. cv. Palmer) fruit during storage. Food Chemistry, 237(5), 372-378.

Smith, N.J.S., Tucker, G.A., & Jeger, J. (1989). Softening and cell wall changes in bananas and plantains. Aspects of Applied Biology, 20, 57-65.

Soltani, M., Alimardani, R., & Omid, M. (2011). Evaluating banana ripening status from measuring dielectric properties. Journal of Food Engineering, 105(4), 625-631.

Song, W., Jiang, N., Wang, H., & Vincent, J. (2020). Use of msartphone videos and pattern recognition for food authentication. Sensors and Actuators B: Chemical, 304(10), 127247.

Srivastava, M.K., & Dwivedi, U.N. (2000). Delayed ripening of banana fruit by salicylic acid. Plant Science, 158(1-2), 87-96.

Stover, R.H., & Simmonds, N.W. (1987). Bananas (3rd Ed.), Longman, London, pp. 468.

Studman, C.J. (2001). Computers and electronics in postharvest technology-a review. Computers and Electronics in Agriculture, 30(1-3), 109-124.

Sun, X., Gong, H.J., Zhang, F., & Chen, K.J. (2009). A digital image method for measuring and analyzing color characteristics of various color scores of beef. 2009 2nd International Congress on Image and Signal Processing, Tianjin, pp. 1-6.

Sylla, C. (2002). Experimental investigation of human and machine-vision arrangements in inspection tasks. Control Engineering Practice, 10(3), 347-361.

Tesfay, S.Z., Magwaza, L.S., Mbili, N., & Mditshwa, A. (2017). Carboxyl methylcellulose (CMC) containing moringa plant extracts as new postharvest organic edible coating for avocado (*Persea americana* Mill.) fruit. Scientia Horticulturae, 226(9), 201-207.

Tharwat, A. (2020). Classification assessment methods. Applied computing and Informatics, Ahead-of-print.

Tomasevic, I., Tomovic, V., Milovanovic, B., Lorenzo, J., Đorđević, V., Karabasil, N., et al. (2019). Comparison of a computer vision system vs. traditional colorimeter for color evaluation of meat products with various physical properties. Meat Science, 148, 5-12.

References

Tran, V.-L. (2020). Development of empirical formulas for predicting the strength of structural components using ANN approach. Department of Civil and Environmental Engineering. Sejong University, Seoul, PhD Thesis.

Tran, V.-L., Thai, D.-K., & Nguyen, D.-D. (2020). Practical artificial neural network tool for predicting the axial compression capacity of circular concrete-filled steel tube columns with ultra-high-strength concrete. Thin-Walled Structures, 151(4), 106720.

van der Walt, S., Schönberger, J.L., Nunez-Iglesias, J., Boulogne, F., Warner, J.D., Yager, N., et al. (2014). Scikit-image: image processing in Python. PeerJ, 2, e453.

Wang, C.Y., & Wang, S.Y. (2009). Effect of storage temperature on fruit quality of various cranberry cultivars. ISHS Acta Horticulturae, 810, 853-861.

Wang, S., Liu, X., Yang, M., Zhang, Y., Xiang, K., & Tang, R. (2015). Review of time temperature indicators as quality monitors in food packaging. Packaging Technology and Science, 28(1), 839-867.

Wedding, B.B., Wright, C., Grauf, S., White, R.D., Tilse, B., & Gadek, P. (2013). Effects of seasonal variability on FT-NIR prediction of dry matter content for while hass avocado fruit. Postharvest Biology and Technology, 75(9), 9-16.

Wills, R., McGlasson, B., Graham, D., & Joyce, D. (1998). Postharvest: an introduction to the physiology and handling of fruit, vegetables and ornamentals. (4th Ed.), University of New South Wales Press,Sydney, Australia.

Woolf, A.B., Cox, K.A., White, A., & Ferguson, I.B. (2003). Low temperature conditioning treatments reduce external chilling injury of ‘hass’ avocados. Postharvest Biology and Technology, 28(1), 113-122.

Xie, C., Chu, B., & He, Y. (2018). Prediction of banana color and firmness using a novel wavelengths selection method of hyperspectral imaging. Food Chemistry, 245(10), 132-142.

Xie, C., Sun, Y., & Luo, H. (2017). Secured data storage scheme based on block chain for agricultural products tracking. 2017 3rd International Conference on Big Data Computing and Communications (BIGCOM), Chengdu, China, pp. 45-50.

References

Yahaya, O.K.M., Jafri, M.Z.M., Aziz, A.A., & Omar, A.F. (2014). Non-destructive quality evaluation of fruit by color based on RGB LEDs system. 2014 2nd International Conference on Electronic Design (ICED), Penang, Malaysia, pp. 230-233.

Yahaya, O.K.M., Jafri, M.Z.M., Aziz, A.A., & Omar, A.F. (2015). Determining Sala mango qualites with the use of RGB images captured by a mobile phone camera. AIP Conference Proceedings, 1657(1), 060003.

Yakushev, V.P., Kanash, E.V., Evaluation of wheat nitrogen status by colorimetric characteristics of crop canopy presented in digital images. Journal of Agricultural Informatics, 7(1), 65-74.

Yang, X., Zhang, Z., Joyce, D., Huang, X., Xu, L., & Pang, X. (2009). Characterization of chlorophyll degradation in banana and plantain during ripening at high temperature. Food Chemistry, 114(2), 383-390.

Yearsley, C., Lallu, N., Burdon, J., Billing, D., Punter, M., & Osman, S. (2002). Effect of prepacking holding temperatrues on shelf life quality of hass avocados. New Zealand Avocado Growers' Association Annual Research Report, 2, 75-82.

Yossy, E.H., Pranata, J., Wijaya, T., Hermawan, H., & Budiharto, W. (2017). Mango fruit sortation system using neural network and computer vision. Procedia Computer Science, 116(10), 596-603.

Zhang, B., Huang, W., Li, J., Zhao, C., Fan, S., Wu, J., et al. (2014). Principles, developments and applications of computer vision for external quality inspection of fruits and vegetables: a review. Food Research International, 62(3), 326-343.

Zhang, Y., Wang, S., Ji, G., & Philips, P. (2014). Fruit classification using computer vision and feedforward neural network. Journal of Food Engineering, 143(7), 167-177.

Zheng, X., Lei, Q., Yao, R., Gong, Y., & Yin, Q. (2018). Image segmentation based on adaptive K-means algorithm. EURASIP Journal on Image and Video Processing, 2018, 68.

Zhuang, J., Hou, C., Tang, Y., He, Y., Guo, Q., Miao, A., et al. (2019). Assessment of external properties for identifying banana fruit maturity stages using optical imaging

techniques. Sensors, 19(13), 2910.

Zude-Sasse, M., Fountas, S., Gemtos, T.A., & Abu-Khalaf, N. (2016). Applications of precision agriculture in horticultural crops. European Journal of Horticultural Science, 81(2), 78-90.

Development of computer vision system based on smartphone image and artificial neural network for postharvest management of agricultural products

March, 2021

Byeong-Hyo Cho

Laboratory of Agricultural and Food Process Engineering
Division of Bio-systems Sustainability
Graduate School of Agricultural Science, Hokkaido University
Kita-9, Nishi-9, Kita-ku, Sapporo, Hokkaido, Japan
Tel. and Fax.: +81-11-706-2552